JOINT TRANSPORTATION
RESEARCH PROGRAM

INDIANA DEPARTMENT OF TRANSPORTATION
AND PURDUE UNIVERSITY

Pile Stability Analysis in Soft or Loose Soils: Guidance on Foundation Design Assumptions with Respect to Loose or Soft Soil Effects on Pile Lateral Capacity and Stability

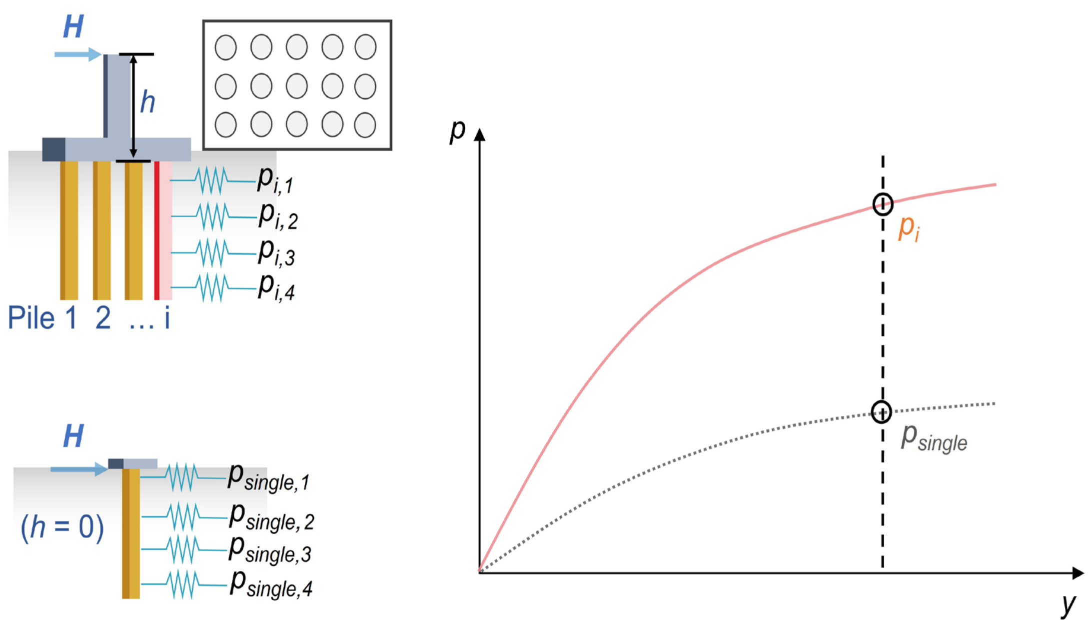

Yao Wang, Jeehee Lim, Rodrigo Salgado,
Monica Prezzi, Jeremy Hunter

SPR-4512 • Report Number: FHWA/IN/JTRP-2022/24 • DOI: 10.5703/1288284317387

RECOMMENDED CITATION

Wang, Y., Lim, J., Salgado, R., Prezzi, M., & Hunter, J. (2022). *Pile stability analysis in soft or loose soils: Guidance on foundation design assumptions with respect to loose or soft soil effects on pile lateral capacity and stability* (Joint Transportation Research Program Publication No. FHWA/IN/JTRP-2022/24). West Lafayette, IN: Purdue University. https://doi.org/10.5703/1288284317387

AUTHORS

Yao Wang
Graduate Research Assistant
Lyles School of Civil Engineering
Purdue University

Jeehee Lim
Graduate Research Assistant
Lyles School of Civil Engineering
Purdue University

Rodrigo Salgado, PhD
Charles Pankow Professor of Civil Engineering
Lyles School of Civil Engineering
Purdue University
(765) 494-5030
rodrigo@ecn.purdue.edu
Corresponding Author

Monica Prezzi, PhD
Professor of Civil Engineering
Lyles School of Civil Engineering
Purdue University

Jeremy Hunter, PE
Managing Director of Engineering,
Chief Engineer
Indiana Department of Transportation

JOINT TRANSPORTATION RESEARCH PROGRAM

The Joint Transportation Research Program serves as a vehicle for INDOT collaboration with higher education institutions and industry in Indiana to facilitate innovation that results in continuous improvement in the planning, design, construction, operation, management and economic efficiency of the Indiana transportation infrastructure. https://engineering.purdue.edu/JTRP/index_html

Published reports of the Joint Transportation Research Program are available at http://docs.lib.purdue.edu/jtrp/.

NOTICE

ACKNOWLEDGMENTS

The work presented in this report was funded by the Joint Transportation Research Program (JTRP) administered by the Indiana Department of Transportation (INDOT) and Purdue University through contract SPR-4512. The support of the Indiana Department of Transportation (INDOT) and the Federal Highway Administration (FHWA) are gratefully acknowledged. Qian Hu and Fei Han assisted with analyses at early stages of the project. The continuous support received from the JTRP director, Darcy Bullock, the director of INDOT Research and Development, Barry Partridge. The assistance of the JTRP staff and, in particular, the support received from the Study Advisory Committee members (Jeremy Hunter, Athar Khan, Mir Zaheer, Peter Becker, Boonam Shin, Mahmoud Hailat, Pete White, Min Sang Lee, and Martha Chernet) is much appreciated.

TECHNICAL REPORT DOCUMENTATION PAGE

1. Report No.	2. Government Accession No.	3. Recipient's Catalog No.
FHWA/IN/JTRP-2022/24		

4. Title and Subtitle Pile Stability Analysis in Soft or Loose Soils: Guidance on Foundation Design Assumptions with Respect to Loose or Soft Soil Effects on Pile Lateral Capacity and Stability and Rating Criteria	**5. Report Date** October 2022 **6. Performing Organization Code**
7. Author(s) Yao Wang, Jeehee Lim, Rodrigo Salgado, Monica Prezzi, and Jeremy Hunter	**8. Performing Organization Report No.** FHWA/IN/JTRP-2020/24
9. Performing Organization Name and Address Joint Transportation Research Program Hall for Discovery and Learning Research (DLR), Suite 204 207 S. Martin Jischke Drive West Lafayette, IN 47907	**10. Work Unit No.** **11. Contract or Grant No.** SPR-4512
12. Sponsoring Agency Name and Address Indiana Department of Transportation (SPR) State Office Building 100 North Senate Avenue Indianapolis, IN 46204	**13. Type of Report and Period Covered** Final Report **14. Sponsoring Agency Code**

15. Supplementary Notes

Conducted in cooperation with the U.S. Department of Transportation, Federal Highway Administration.

16. Abstract

The design of laterally loaded piles is often done in practice using the *p-y* method with API *p-y* curves representing the behavior of soil at discretized points along the pile length. To account for pile-soil-pile interaction in pile groups, AASHTO (2020) proposes the use of *p*-multipliers to modify the *p-y* curves. In this research, we explored, in depth, the design of lateral loaded piles and pile groups using both the Finite Element (FE) method and the *p-y* method to determine under what conditions pile stability problems were likely to occur. The analyses considered a wide range of design scenarios, including pile diameters ranging from 0.36 m (14.17 inches) to 1.0 m (39.37 inches), pile lengths ranging from 10 m (32.81 ft) to 20 m (65.62 ft), uniform and multilayered soil profiles containing weak soil layers of loose sand or normally consolidated (NC) clay, lateral load eccentricity ranging from 0 m to 10 m (32.81 ft), combined axial and lateral loads, three different pile group configurations (1×5, 2×5, and 3×5), pile spacings ranging from 3 to 5 times the pile diameter, two different load directions ("strong" direction and "weak" direction), and two different pile cap types (free-standing and soil-supported pile caps). Based on the FEA results, we proposed new *p-y* curve equations for clay and sand. We also examined the behavior of the individual piles in the pile groups and found that the moment applied to the pile cap is partly transferred to the individual piles as moments, which is contrary to the assumption often made that moments are fully absorbed by axial loads on the group piles. This weakens the response of the piles to lateral loading because a smaller lateral pressure is required to produce a given deflection when moments are transferred to the head of the piles as moments. When the *p-y* method is used without consideration of the transferred moments, unconservative designs result. Based on the FEA results, we proposed both a new set of *p*-multipliers and a new method to use when moment distribution between piles is not known, using pile efficiency instead to calculate the total capacity of pile groups.

17. Key Words	18. Distribution Statement
lateral loading, pile buckling, pile stability, p-y method, p-y curves API, laterally loaded piles, pile groups, p-multipliers, pile efficiency	No restrictions. This document is available through the National Technical Information Service, Springfield, VA 22161.

19. Security Classif. (of this report)	20. Security Classif. (of this page)	21. No. of Pages	22. Price
Unclassified	Unclassified	63 including appendices	

Form DOT F 1700.7 (8-72) Reproduction of completed page authorized

EXECUTIVE SUMMARY

Introduction

INDOT has expressed an interest in investigating the lateral capacity of piles that support bridge piers. Of particular interest are pile caps supported by single rows of piles—the most critical foundation arrangement for lateral resistance. Piles crossing soft clay, organic soil, and very loose sand could all potentially lead to vulnerabilities. In addition to soil vulnerabilities, piles may reach a limit state due to excessive lateral deflection under design loads, and they can be susceptible to buckling instability when subjected to both vertical and lateral bridge loads with very little lateral support provided by the weak, compliant soil in the vicinity of the pile cap.

The design of laterally loaded piles has traditionally been done using the *p-y* method. The results of a *p-y* analysis are highly dependent on the *p-y* curves used in the analysis. Since the *p-y* curves routinely used in *p-y* analyses have been derived empirically using data obtained either from a limited number of lateral pile load tests or from *in situ* test data, the *p-y* method cannot accurately predict the response of all pile groups.

The interactions between piles in a group make the lateral response of the individual piles in that group different from an isolated single pile of the same size that is installed in the same soil profile. This group effect can be quantified by using either the concept of the *p*-multiplier or the concept of pile efficiency. Even though the values of *p*-multipliers depend on the position of the individual piles in the group, the load eccentricity, the lateral deflection level, the soil profile, and the pile group configuration, the research on *p*-multipliers (and the values proposed in the literature) has not accounted for the effects of load eccentricity, deflection level, soil profile, and pile group configuration. In addition, research considering the use of the pile efficiency concept for laterally loaded pile groups is limited.

The critical bucking load of a pile can be calculated by using the Euler column formula, in which the bending stiffness and length of the pile appear as variables. In this approach, a pile partially embedded in soil is modeled as an equivalent fixed-ended Bernoulli beam that reaches the same lateral deflection as the pile under the same loading.

The length of the equivalent Bernoulli beam is determined by summing up the free length of the pile above the ground and the *depth to fixity,* which is calculated as the difference between the free length of the pile and the length of the beam. Thus, the correct estimation of the depth to fixity is very important for accurate buckling stability analysis. However, AASHTO (2020) only provides simple equations for the calculation of the depth to fixity for sand and clay, which were derived with the assumptions that the piles are only subjected to axial loads, the pile bases are fixed, the stiffness of sand increases linearly with depth, and the stiffness of clay is uniform with depth. AASHTO (2020) also uses the term *depth to fixity* to refer to the distance from the pile head to a zero-deflection point for a laterally loaded pile. These two different definitions for the depth to fixity concept are a source of some confusion when buckling stability analysis for laterally loaded piles are done.

In this study, we performed a series of three-dimensional (3D) finite element (FE) analyses for single piles and piles groups. We considered a wide range of design scenarios, with pile diameters ranging from 0.36 m (14.17 inches) to 1.0 m (39.37 inches), pile lengths ranging from 10 m (32.81 ft) to 20 m (65.62 ft), uniform and multilayered soil profiles containing weak soil layers of loose sand or normally consolidated (NC) clay, lateral load eccentricity ranging from 0 m to 10 m (32.81 ft), combined axial and lateral loads, three different pile group configurations (1×5, 2×5, and 3×5), pile spacings ranging from 3 to 5 times the pile diameter, two different load directions (strong direction and weak direction), and two different pile cap types (free-standing and soil-supported pile caps). From the FE simulation results, we propose new sets of *p-y* curves for sand and NC clay, respectively, and new sets of *p*-multipliers and equations for pile efficiencies, which can be directly used in our proposed design methods to accurately estimate the lateral capacity of pile groups. Moreover, based on our findings, we propose general design guidelines for laterally loaded pile groups in soft soils by identifying critical conditions to avoid and by clarifying the definitions of depth to fixity.

Findings

Based on the results of the FE analyses performed for laterally loaded single piles, we evaluated the effects of several design factors on the lateral responses of the piles and the *p-y* curves. Soft or weak soil profiles, high load eccentricity, and the presence of axial and lateral loading produced less lateral pile capacity. The impact of load eccentricity and pile diameter on the *p-y* curves is small. According to our findings, we proposed new *p-y* curves for sand and clay that input intrinsic soil variables and state variables (such as relative density, effective stress, and undrained shear strength) to realistically reflect the 3D soil-pile interaction process. When the proposed *p-y* curves were compared with the API *p-y* curves, which are often used in *p-y* analysis, in general, the API *p-y* curves for sand produced stiffer soil responses while the API *p-y* curves for clay produced softer soil responses than the proposed *p-y* curves.

Based on the results of the FE analyses performed for laterally loaded pile groups, the effects of several design factors on the lateral responses of the individual piles in pile groups were evaluated. Piles in the trailing rows provided less lateral capacity than the ones in the leading row, and piles close to the center of the group in the same row provided less lateral capacity than the piles at the edges of the group. Softer, thicker soil layers; large load eccentricities; and small pile spacings lead to comparatively less lateral capacity. In terms of group configurations, the 3×5 pile group provided less lateral capacity per pile than the 1×5 pile group. By analyzing all FE simulation results, we proposed new values of *p*-multipliers that consider the different positions of the individual piles within the group in loose and dense sand, load eccentricities ranging from 1 m (3.28 ft) to 10 m (32.81 ft), and free-standing and soil-supported pile caps. We also developed equations for pile efficiency that consider load eccentricity, position of the individual piles in the group, and pile spacing.

One of our main findings from the FEA results is that the lateral load eccentricity (which can be represented by an equivalent moment acting on the head of the piles) has significant impact on the lateral capacities of single piles and pile groups. The greater the load eccentricity is, the weaker the responses of the pile groups are. This was not only true for single-row pile groups but also for pile groups with multiple rows, because the moment applied on the pile group is not fully absorbed by axial loads on the individual piles in the group. From the analyses, we found that part of the moment applied to the cap of a pile group is transferred to the individual piles as moments in the group, and the moment applied to the individual piles in the pile group weakens their response to lateral loading.

By using the proposed *p-y* curves, *p*-multipliers, and pile efficiencies, we proposed two design approaches for lateral capacity estimation of pile groups—p-y analysis using p-multipliers and p-y analysis using pile efficiencies. When a system consisting of the piles and the superstructure are analyzed at the same time to evaluate the stability of the system, the p-multiplier method can be used to estimate the lateral capacity of the piles. However, without an accurate estimation of the loads and moments at the pile heads, the estimated lateral capacities of pile groups obtained from using the p-multiplier method can be unconservative. On the other hand, when only the loads and moments acting on the pile group are known, the lateral capacity of the pile group can be estimated by using the pile efficiency method. Unlike the p-multiplier method, the pile efficiency method does not require information on the loads and moments at the heads of the individual piles in the pile group because it already implicitly considers it.

From the design examples following our proposed design approaches, we found that the current design method (AASHTO, 2020) can overestimate the lateral capacity of pile groups under certain conditions. Based on the FE simulation results for potentially critical scenarios for the piles, which could lead to either or both issues of insufficient lateral capacity and buckling instability, we found that single-row pile groups installed in weak soil profiles with a top layer thickness greater than 5 times the pile diameter and a representative SPT blow count less than 7 can undergo excessive lateral deflections under service loads when the pile groups are loaded in the weak direction with load eccentricity greater than 5 m (16.40 ft) for NC clay and 10 m (32.81 ft) for loose sand.

We reviewed and clarified the two definitions of depth to fixity and showed that the estimated values of depths to fixity are different depending on the definition selected. We also calculated the depth to fixity from the results of the p-y analysis with the proposed p-y curves and found that the depth to fixity calculated using the p-y method was generally greater than that calculated using the AASHTO (2020) method. Accordingly, the critical buckling load calculated using the depth to fixity obtained from the p-y method was also generally less than that calculated using the AASHTO (2020) method. However, the calculated buckling load was generally considerably greater (3 to 135 times greater) than the axial service load expected to be added to the pile head, regardless of the methods used, indicating that buckling is unlikely to be a critical limit state.

Implementation

Based on our findings, we propose implementation of the following items for laterally loaded piles in weak soils.

1. Single-row pile group loaded laterally in weak soil profiles (with a top layer thickness greater than 5 times the pile diameter and a representative SPT blow count less than 7 should be avoided if loaded in the weak direction.
2. With the new p-y curves developed in this project, p-y analysis can be performed by using any commercially available software (e.g., PYGMY or LPile) to obtain accurate estimates of the load-deflection responses of single piles.
3. Two methods for pile group lateral capacity estimation have been developed and can be used—(1) p-y analysis with p-multipliers and (2) p-y analysis with pile efficiencies. When the axial loads and moments at the pile heads are known or when the piles and pile group are analyzed together with the superstructure as a system, the load and moment distribution between piles will be known. The method using p-multipliers can be used with the p-y curves and the p-multipliers proposed in this study. However, in most cases, the axial loads and moments distributed to the individual piles in the group are unknown. In these cases, the second method, which uses pile efficiencies to relate the capacity of piles in the group to the capacity of a single, isolated pile can be used with the proposed p-y curves and the proposed pile efficiency equations.
4. The process for assessing stability against buckling was reviewed. There are two different definitions of depth to fixity. One is the difference in length between the free length of the pile above ground and the length of a fixed-ended beam required to have the same deflection at its top as that at the top of the pile. Another one is the depth to the final zero-deflection point. To prevent confusion, it is desirable that design flow processes at INDOT clarify which of the two definitions should be used when the critical buckling loads of the laterally loaded piles are estimated. The current design guidance given by AASHTO (2020) is to use depth to fixity equations for sand and clay that depend on the soil stiffness but contain only limited information on how to estimate soil stiffness. The equations suggested by AASHTO (2020) for piles in sand and clay were derived by assuming linear p-y relationships. Depending on the estimated soil stiffness and the p-y relationship extracted from simulation results, the calculated depth to fixity, and the critical buckling load can vary significantly. However, this report shows that the buckling loads calculated following either AASHTO (2020) or the procedures proposed in this report are much greater than the axial service loads on the piles. This means that buckling is unlikely to be a critical limit state in most cases.

CONTENTS

LIST OF TABLES

LIST OF FIGURES

1. INTRODUCTION

1.1 Background

INDOT has expressed an interest in investigating the lateral capacity and overall stability of pile supported piers, particularly when supported by single rows of piles, the most critical foundation arrangement for lateral resistance. Excessive lateral deflection occurred in soil profiles in which the piles crossed a top layer of weak, compliant soil that did not provide sufficient lateral support for the piles. Soft clay, organic soil and very loose sand could all potentially lead to such vulnerabilities. In addition to the problem that the piles are vulnerable under these scenarios and may reach a limit state due to excessive lateral deflection under design loads, the piles can be susceptible to buckling instability when subjected to both vertical and lateral bridge loads with very little lateral support provided by the weak, compliant soil in the vicinity of the pile cap (Aldridge et al., 2005; Davisson & Robinson, 1965). Figure 1.1 shows an example of a possible critical scenario for the piles which can lead to either or both issues of insufficient lateral capacity and buckling instability. In the figure, a single-row pile group installed in a weak-over-strong soil is acted upon by both axial and lateral loads.

The design of laterally loaded piles has traditionally been done using the *p-y* method. In the *p-y* method, the pile is modeled as a 1D Bernoulli beam, and the lateral pile-soil interaction is modeled through a series of springs distributed along the pile length. The results of a *p-y* analysis are highly dependent on the *p-y* curves used in the analysis.

The *p-y* curves routinely used in *p-y* analyses have been derived empirically using data obtained either from a limited number of lateral pile load tests (Reese et al., 1974; Rollins et al., 2005) or from *in situ* test data (Dyson & Randolph, 2001; Suryasentana & Lehane, 2014). Because of that, the predictions using the *p-y* method are not always accurate (Anderson et al., 2003; Choi et al., 2014; Han et al., 2015, 2017). In addition, some of the parameters (e.g., the dimensionless empirical constant *J* in the API method for soft clay (API, 2000)) used to define the *p-y* curves need to be determined by users, requiring engineering judgment because not all input parameters are fundamental soil properties. Only in recent studies (Choobbasti & Zahmatkesh, 2016; Haouari & Bouafia, 2020) have *p-y* curves for certain sands been developed based on finite element analyses results. Choobbasti and Zahmatkesh (2016) derived *p-y* curves for Babolsar and Nevada sands based on finite element analyses results using a two-surface plasticity model.

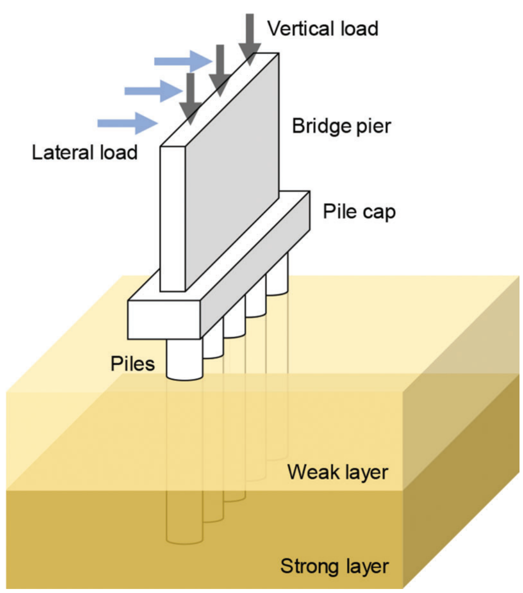

Figure 1.1 A bridge pier supported on a pile group in a layered soil profile that is subjected to axial and lateral loads.

The interactions between piles in a group makes the lateral response of the individual piles in the group different from that of an isolated, single pile of the same size installed in the same soil profile. This group effect can be quantified by using either the concept of p-multiplier (Brown et al., 1988) or the concept of pile efficiency (Prakash & Sharma, 1991). Su and Yan (2019) proposed a relationship between *p*-multipliers and pile efficiencies but they did not consider the effects of load eccentricity and lateral deflection level. Most of the research on *p*-multipliers does not account for the effects of load eccentricity and deflection level (McVay et al., 1998; Rollins et al., 2005). In addition, research considering the use of the pile efficiency concept for laterally loaded pile groups is limited (Su & Yan, 2019).

The critical bucking load of a pile can be calculated using the Euler column formula, in which the bending stiffness and length of the pile appear as variables. Since piles are embedded in soil, a partially embedded pile is modeled as an equivalent fixed-ended Bernoulli beam that reaches the same lateral deflection as the pile under the same loading. The length of the equivalent Bernoulli beam is determined by summing up the free length of the pile above the ground and the *depth to fixity* calculated as the difference between the free length of the pile and the length of the beam. Thus, the correct estimation of the depth to fixity is very important for accurate buckling stability analysis. However, AASHTO (2020) only provides simple equations for calculation of the depth to fixity for sand and clay, which were proposed by Davisson and Robinson (1965) with the assumptions that the pile is only subjected to axial loads, the pile base is fixed, the stiffness of sand increases linearly with depth, and the stiffness of clay is uniform with depth. In addition, AASHTO (2020) also uses the term *depth to fixity* to refer to the distance from the pile head to a zero-deflection point for the laterally loaded pile. These two different definitions for the depth to fixity concept are a source of some confusion when buckling stability analysis for laterally loaded piles are done.

In this study, we performed a series of three-dimensional (3D) finite element (FE) analyses for single piles and piles groups. We considered a wide range of design scenarios, with pile diameters ranging from 0.36 m (14.17 inches) to 1.0 m (39.37 inches), pile lengths ranging from 10 m (32.81 ft) to 20 m (65.62 ft), uniform and multilayered soil profiles containing weak soil layers of loose sand or normally consolidated (NC) clay, lateral load eccentricity ranging from 0 m to 10 m (32.81 ft), combined axial and lateral loads, three different pile group configurations (1×5, 2×5, and 3×5), pile spacings ranging from 3 to 5 times the pile diameter, two different load directions (strong direction and weak direction), and two different pile cap types (free-standing and soil-supported pile caps). From the FE simulation results for single piles, we evaluated the effects of various design factors on the lateral responses of the piles and proposed new sets of *p-y* curves for sand and NC clay. From the FE simulation results for pile groups, we evaluated the effects of various design factors on the lateral responses of individual piles in the group and proposed new sets of *p*-multipliers and pile efficiencies, which can be directly used in our proposed design methods to accurately estimate the lateral capacity of pile groups. Moreover, based on our findings, we proposed general design guidelines for laterally loaded pile groups in soft soils and provided four design examples considering critical scenarios. Based on the FE simulation results, we also identified certain conditions under which single-row pile groups in soft and weak soils should be avoided. We also clarified the definitions of depth to fixity and proposed general guidelines for the buckling stability analysis of piles under lateral loads.

1.2 Current Analysis Methods

1.2.1 p-y Analysis

The design of laterally loaded piles has traditionally been done using the *p-y* method. In a *p-y* analysis, the pile is modeled as a 1D Bernoulli beam, and the lateral pile-soil interaction is modeled through a series of springs distributed along the pile length, as shown in Figure 1.2. In the figure, H is the lateral load applied at the pile head; p_1, p_2, p_3, and p_4 are lateral soil resistances at different depths along the pile; and y_1, y_2, y_3, and y_4 are lateral deflections at depths p_1, p_2, p_3, and p_4, respectively. The relationship between the soil resistance p and the lateral deflection y is referred to as a *p-y* curve; it represents the stiffness of the pile-soil system along the pile.

The lateral deflection of a laterally loaded pile depends on both the stiffnesses of the spring and of the pile. Including the effect of the axial load on the bending response, the governing differential equation for the *p-y* analysis can be expressed by

$$EI\frac{d^4y}{dx^4}+F\frac{d^2y}{dx^2}-p=0 \qquad \text{(Eq. 1.1)}$$

where E is the Young's modulus of the pile, I is the second moment of area of the pile, EI is the bending stiffness of the pile, y is the lateral deflection of the pile, x is the distance along the pile from the pile head, F is the axial load applied on the pile head, and p is the soil resistance.

By solving the governing differential equation, the deflection of the pile at different depths can be calculated for the given boundary conditions, and the global response of the laterally loaded pile problem can be obtained by plotting the lateral load versus the lateral deflection at the pile head (e.g., the load-deflection curve). The finite element method or the finite difference method can be used to solve the governing differential equation of the laterally loaded pile problem.

A number of formulations have been proposed for the *p-y* curves to represent the stiffnesses of different types of soils. For sand, Reese et al. (1974) proposed equations for *p-y* curves based on lateral load test results, and Rollins et al. (2005) proposed *p-y* curves for liquefiable sand based on lateral load test results. For clay, Matlock (1970) proposed *p-y* curves for both static and cyclic loading conditions, and *p-y* curves for stiff clay below and above the water table were proposed by Reese et al. (1975) and Welch (1972), respectively.

In recent years, researchers have tried to improve the *p-y* design method. Amar Bouzid (2018) improved the *p-y* method by considering the vertical shear tractions at the soil-pile interface and the resistances at the pile base. In the design method proposed by Amar Bouzid (2018), the pile is assumed to be a Timoshenko beam instead of a Euler-Bernoulli beam as in the original *p-y* method to obtain more accurate results. The design method proposed by Amar Bouzid (2018) uses soil reaction curves which are equivalent to the *p-y* curves in

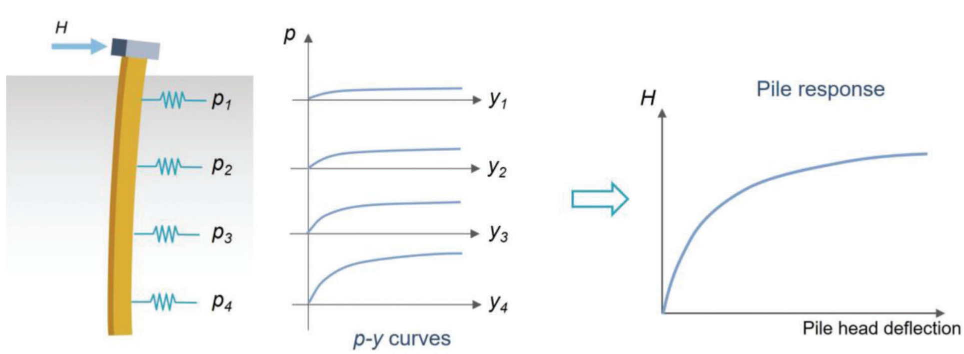

Figure 1.2 The *p-y* method used to calculate the lateral bearing capacity of piles.

the *p-y* method. Burd et al. (2020) proposed soil reaction curves for marine sand, and Byrne et al. (2020) proposed soil reaction curves for glacial clay.

The American Petroleum Institute (API) method *p-y* curves (API, 2000) are commonly used in practice. For sand, the equations for the API *p-y* curves are given by

$$p = Ap_u \tanh\left(\frac{kxy}{Ap_uB}\right) \qquad \text{(Eq. 1.2)}$$

where p is the soil resistance in units of force per length, B is the pile diameter, x is the depth from the ground surface to the point being considered, and y is the lateral deflection. A in the equation is a factor that accounts for static or cyclic loading, and is given by

$A = 0.9$ when the equilibrium has been reached under cyclic loading

$$A = \left(0.3 - 0.8\frac{x}{B}\right) \geq 0.9 \text{ for static loading} \qquad \text{(Eq. 1.3)}$$

where k in the equation is a gradient of the initial modulus of subgrade reaction with depth in units of pressure/length. Figure 1.3 provides the (API, 2000) suggested k values for sand above and below the water table as a function of relative density.

The ultimate bearing pressure p_u appearing in Equation 1.2 at the considered depth x is given by

$$p_u = \min\left[\frac{(C_1x + C_2B)\sigma_v'}{B}, C_3\sigma_v'\right]B \qquad \text{(Eq. 1.4)}$$

where σ'_v is the vertical effective stress at depth x, and C_1, C_2, and C_3 are coefficients given by

$$C_1 = 0.115 \times 10^{0.0405\phi} \qquad \text{(Eq. 1.5)}$$

$$C_2 = 0.571 \times 10^{0.022\phi} \qquad \text{(Eq. 1.6)}$$

$$C_3 = 0.646 \times 10^{0.0555\phi} \qquad \text{(Eq. 1.7)}$$

where ϕ is the friction angle of the sand. The friction angle ϕ can be estimated for different relative densities from Figure 1.3.

For soft clay, the API method specifies the *p-y* curve using a piece-wise linear curve as given in Table 1.1. The ultimate soil resistance p_u in Table 1.1 is given by

$$p_u = \min\left(3s_u + \sigma_v' + J\frac{s_u x}{B}, 9s_u\right)B \qquad \text{(Eq. 1.8)}$$

and y_c is given by

$$y_c = 2.5\varepsilon_{50}B \qquad \text{(Eq. 1.9)}$$

where s_u is the undrained shear strength of clay, J is a dimensionless empirical constant ranging from 0.25 to 0.5 based on field tests (higher values of J produce

TABLE 1.1
The coordinate points for the piece-wise linear curve for the API clay criterion

p/pu	y/yc
0	0
0.5	1.0
0.72	3.0
1.0	8.0
1.0	∞

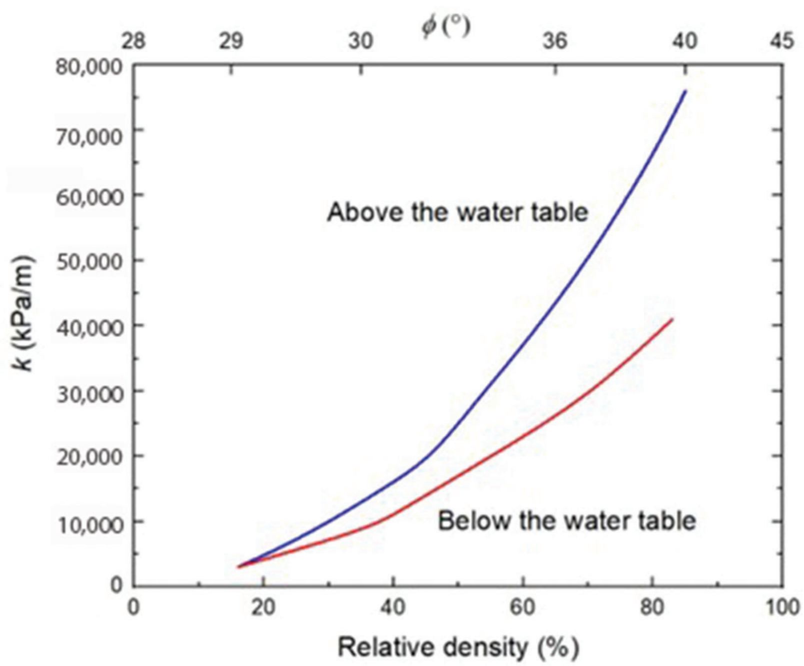

Figure 1.3 The variable k suggested by API (modified from API, 2000).

sharper increases in p_u/B with depth near the surface), and ε_{50} is the strain at 50% of the failure stress in a laboratory undrained compression test. In this study, unless otherwise mentioned, we use $J = 0.25$ and $\varepsilon_{50} = 0.02$ (Peck et al., 1974) when the API curve for soft clay is considered.

1.2.2 p-Multipliers and Pile Efficiencies

When a pile group is subjected to a lateral load, the load-deflection (or load-rotation) response of an individual pile *i* in the pile group is different from that of an isolated, single pile of the same size installed in the same soil profile due to the complex pile-cap-soil interaction. This effect can be quantified by using either the concept of p-multiplier (Brown et al., 1988) or the concept of pile efficiency (Prakash & Sharma, 1991).

The p-multiplier p_m is defined as the ratio of the unit soil resistance p_i of an individual pile *i* in a pile group to the unit soil resistance p_{single} of a single, isolated pile at the same level of lateral deflection y at the same depth (Brown et al., 1988), as represented in Figure 1.4.

$$p_m = \frac{p_i}{p_{\text{single}}} \qquad \text{(Eq. 1.10)}$$

According to Zhou and Tokimatsu (2018), the p-multiplier depends on the position of the individual piles in the group, the load eccentricity h, and the deflection level y. Based on centrifuge test results, McVay et al. (1998) suggested values for *p*-multipliers considering the positions of the individual piles in a group. Rollins et al. (2005) proposed *p*-multipliers that depend on row number, soil properties and group configuration. Based on data collected by Hannigan et al. (2006), AASHTO (2020) suggested values for the *p*-multipliers as a function of pile spacing ($3B$ and $5B$) and row number (1, 2, and 3), as given in Table 1.2; these values were obtained by averaging the *p*-multipliers for different soil types (clay, silt, and sand), test types (field tests, centrifuge tests, and large-scale lab tests), pile spacings (from 3 to 5.65 times the pile diameter), row numbers (1, 2, and 3 or more) and deflection levels (from 25 mm = 1 inch to 89 mm = 3.5 inches).

Pile efficiency η is defined as the ratio of the lateral pile capacity H_i of an individual pile *i* in a pile group to the lateral capacity H_{single} of an isolated, single pile loaded with zero eccentricity h (eccentricity is defined as the vertical distance from the lateral load to the pile head, usually assumed to be at the level of the ground surface), as represented in Figure 1.5.

$$\eta = \frac{H_i}{H_{\text{single}}} \qquad \text{(Eq. 1.11)}$$

As shown in Figure 1.6, a lateral load H applied with an eccentricity h is equivalent to the combination of a lateral load H applied at $h = 0$ and a bending moment $M = H \times h$. Design of laterally loaded pile groups is traditionally done based on the assumption that the bending moment ($M = H \times h$) is balanced by the axial resistance (compression in leading piles and tension in trailing piles) of the piles in the group when there are multiple rows in the group. This means that the lateral load H is applied as if at the pile head, so corresponding to $h = 0$. However, some portion of the bending moment is transferred to the heads of the individual piles in the group as moments. The effect of the moment transferred to the individual piles as moments in the group will be discussed in detail in Section 3.3.1.

When the pile group configuration involves two or more rows in at least one direction and the number of rows in the two plan directions are not the same, the direction in which the number of pile rows is greater is the "strong" loading direction; the one normal to it is the "weak" loading direction, as represented in Figure 1.7. The weak loading direction is particularly critical when there is only one row of piles in the pile group in one direction; in this case, the bending moment applied in the weak direction cannot be carried even partially by axial load increments on the individual piles in the group and, hence, the entire bending moment acting on

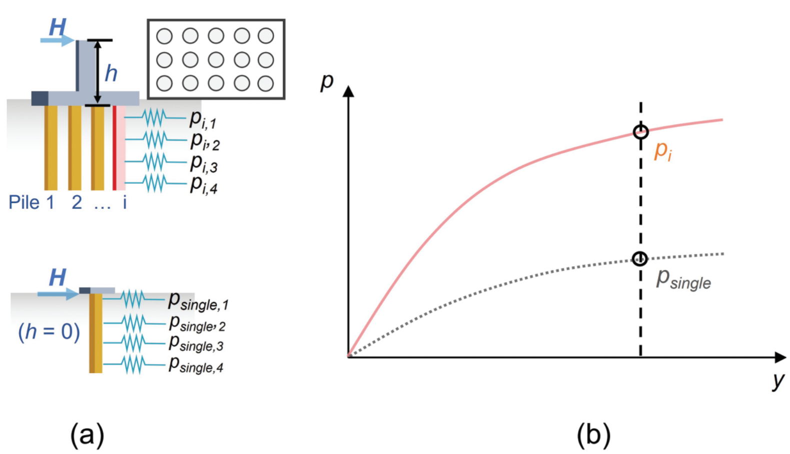

Figure 1.4 Definition of *p*-multiplier: (a) sketch of a pile group and a single pile subjected to lateral loads, and (b) *p-y* curves for an isolated single pile and an individual pile in a pile group at the same depth along the pile.

TABLE 1.2
The *p*-multipliers suggested by AASHTO (2020)

Spacing	*p*-Multiplier for Row 3 or More	*p*-Multiplier for Row 2	*p*-Multiplier for Row 1
3*B*	0.3	0.4	0.8
5*B*	0.7	0.85	1.0

Note: B = pile diameter.

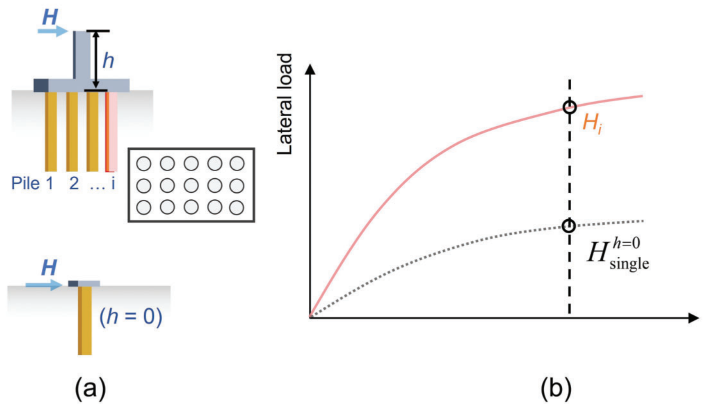

Figure 1.5 Lateral load response of single pile and pile group: (a) sketch of a pile group and a single pile subjected to lateral load, and (b) lateral load vs. pile head deflection response for an isolated single pile and an individual pile in a pile group.

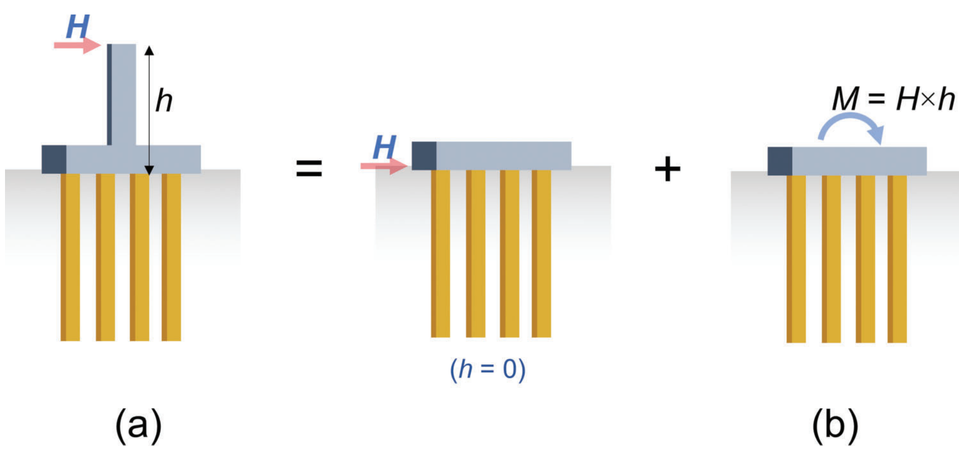

Figure 1.6 Equivalent loading conditions for a laterally loaded pile group: (a) lateral load H applied with a load eccentricity h. This is equivalent to (b) lateral load H applied at the pile head and a bending moment M equal to $H \times h$.

the pile group is transferred to the pile heads and must be considered in the analysis of the individual piles in the group.

1.3 Report Structure

In this report, we present the results of realistic three-dimensional finite element (FE) analyses performed to study the lateral load response of single piles and pile groups installed in soil profiles containing a weak, compliant soil layer in the soil profile. We considered a wide range of design scenarios, with pile diameters ranging from 0.36 m (14.17 inches) to 1.0 m (39.37 inches), pile lengths ranging from 10 m (32.81 ft) to 20 m (65.62 ft), uniform and multilayered soil profiles containing weak soil layers of loose sand or normally consolidated (NC) clay, lateral load eccentricity ranging from 0 m to 10 m (32.81 ft), combined axial and lateral loads, three different pile group configurations (1×5, 2×5, and 3×5), pile spacings ranging from 3 to 5 times the pile diameter, two different load directions (strong direction and weak direction), and two different pile cap types (free-standing and soil-supported pile caps).

In Chapter 2, based on the results of the FE analyses performed for laterally loaded single piles, we evaluated the effects of several design factors on the lateral

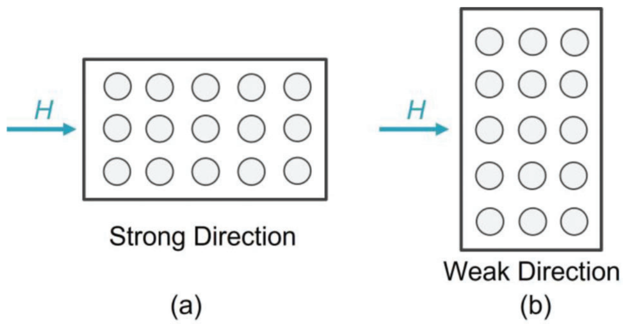

Figure 1.7 Different load directions: (a) strong direction, and (b) weak direction of lateral loading on pile groups.

responses of the piles and the *p-y* curves, and propose new *p-y* curves for sand and clay that have as input intrinsic soil variables and state variables (such as relative density, effective stress, and undrained shear strength) to reflect the 3D soil-pile interaction process. With the new *p-y* curves developed in this project, *p-y* analysis can be performed by using any commercially available software (e.g., PYGMY or LPile) to obtain accurate estimates of the load-deflection responses of single piles.

In Chapter 3, based on the results of the FE analyses performed for laterally loaded pile groups, the effects of several design factors on the lateral responses of the individual piles in pile groups were evaluated, and a new series of *p*-multipliers are proposed considering the different positions of the individual piles in the group in loose and dense sand, load eccentricities ranging from 1 m (3.28 ft) to 10 m (32.81 ft), and free-standing and soil-supported pile caps. We also developed equations for pile efficiency that consider load eccentricity, position of the individual piles in the group and pile spacing. The proposed *p*-multipliers and pile efficiency equations can be directly used in our proposed design frameworks for lateral capacity estimation of pile groups (see Section 4.1.2).

In Chapter 4, by using the proposed *p-y* curves, *p*-multipliers, and pile efficiencies, we propose two design approaches for lateral capacity estimation of pile groups: *p-y* analysis using *p*-multipliers and *p-y* analysis using pile efficiencies. The approaches are illustrated through four solved design examples. The examples show that the current design method (AASHTO, 2020) can overestimate the lateral capacity of pile groups under certain conditions.

Chapter 4 also addresses the problem of pile groups in particularly weak soil profiles loaded laterally in their weak direction. Based on the FE simulation results for these potentially critical scenarios for the piles, which could lead to either or both issues of insufficient lateral capacity and buckling instability, we also identified critical conditions (the thickness and the strength of the top weak soil layer and the loading conditions) to be avoided for laterally loaded pile groups in soft and weak soils. In addition, we clarified the definitions of depth to fixity and proposed some guidelines for the buckling stability analysis of the piles under lateral loads by calculating the depth to fixity from the results of *p-y* analysis using the proposed *p-y* curves and by comparing the results to those calculated using the AASHTO (2020) equations.

2. RESPONSE OF SINGLE PILES TO LATERAL LOADS

2.1 Finite Element Analysis

2.1.1 Simulation Conditions

In the analyses of single piles, pile diameters B ranging from 0.36 m (14.17 inches) to 1.0 m (39.37 inches), which are typically used in Indiana, were considered to quantify the effect of pile stiffness on the response of single piles subjected to lateral loads. In this study, only long piles were considered. Thus, the pile length L is sufficiently long to have a zero deflection at a depth shallower than the pile base when the pile is loaded laterally. The length L of the piles in sand profiles is 10 m (32.81 ft), and the lengths of the piles in uniform normally consolidated (NC) clay and multilayered soil profiles with NC clay are 10 m (32.81 ft) and 20 m (65.62 ft).

To explore the effect of soil profiles on the lateral response of the piles, we considered uniform and multilayered soil profiles containing weak soils that may lead to lateral capacity and stability issues for piles. For the uniform soil profiles, we considered sands with relative densities D_R of 40%, 65%, and 80% and NC clay. The critical-state friction angle ϕ_c is an intrinsic property of a given sand and is therefore independent of initial relative density D_R and confining stress. For Ottawa sand, it is equal to 30°. The peak friction angle ϕ_p, however, increases with relative density and decreases with confining stress. We estimated the peak friction angle using the Bolton (1986) correlation with $Q = 10$ and $R_Q = 1$. The peak friction angle ϕ_p decreases with increasing depth. The range of ϕ_p for sandy soil with different relative densities at depths ranging from 0.5 m to 10 m is summarized in Table 2.1.

For the multilayered soil profiles, we considered two typical problematic soil profiles that may lead to lateral capacity and stability issues for piles in a group. As shown in Figure 2.1, soil profile I is a uniform soil profile, whereas soil profile II consists of a weak layer (loose sand or soft clay) underlain by a dense sand layer. Different values of the thickness t_w of the weak layer was considered: $t_w = 3B$, $5B$, $6B$, and $10B$, where

TABLE 2.1
Range of the peak friction angle for different relative densities at depths ranging from 0.5 m (1.64 ft) to 10 m (32.81 ft)

Relative Density (%)	Peak Friction Angle ϕ_p (°)
40	33–37
65	37–42
80	39–46

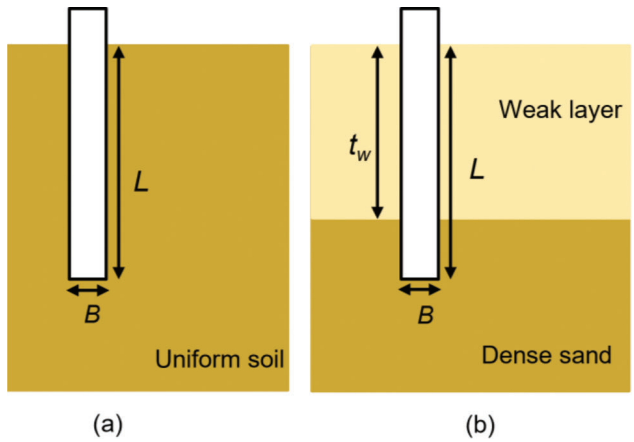

Figure 2.1 Multilayered soil profiles considered in the analyses: (a) soil profile I consists of a uniform soil layer, and (b) soil profile II consists of a weak layer (loose sand or soft clay) underlain by a dense sand layer.

B is the pile diameter. For loose and dense sand layers, D_R of 40% and D_R of 80% were selected, respectively, and NC clay is considered for the soft clay layers.

Different lateral load eccentricities h were considered in the analyses to evaluate the effect of h on the lateral capacity of the single piles: h = 0, 1, 6, and 10 m (0, 3, 20, and 32.81 ft). To evaluate the effect of the existence of an axial load on the lateral load response of single piles, analyses were performed with no axial loads (reference case) and with service loads in addition to the lateral loads. The axial service loads acting on the piles were determined by dividing the nominal axial loads estimated by the Purdue method (Han et al., 2019; Salgado et al., 2011) for closed-ended pipe piles by a factor of safety of 3. Table 2.2 summarizes the simulation conditions considered in the FE analyses for single piles.

2.1.2 Constitutive Models

Since the mechanical responses of sand and clay are highly nonlinear and depend on the soil initial states, loading conditions and intrinsic variables, it is very important to use realistic constitutive models for soils to accurately simulate soil responses under various conditions. In the FE analyses, sand and clay layers are modeled by using the advanced constitutive models developed by Loukidis and Salgado (2009) and Chakraborty et al. (2013), respectively. Both models were developed based on critical-state soil mechanics and by using two-surface plasticity concepts; they are able to capture the mechanical responses of sand and clay realistically. The properties of Ottawa sand and Boston Blue Clay (BBC) were used in the analyses, and Table 2.3 and Table 2.4 provide the input parameters used in the analyses for sand and clay, respectively. In the analyses, both dry and saturated sands and fully saturated clay were considered.

The simulations were performed by using the commercial software ABAQUS/Explicit (SIMULIA, 2021). A user-defined model subroutine VUMAT was coded in FORTRAN to implement the soil models in ABAQUS.

Piles were modeled as an elastic material with a Young's modulus E of 200 GPa (29,008 ksi) and Poisson's ratio v of 0.2. The pile geometry is a cylinder with the same outer diameter as that of the pipe pile considered in the analyses. The Young's modulus of the cylindrical pile is determined such that it has the same bending stiffness as the pipe pile. In the analyses, we consider wall thicknesses of 6 mm (0.24 inches) and 9 mm (0.35 inches) for the outer pile diameter B of 0.36 m (14.17 inches), wall thicknesses of 16 mm (0.63 inches) for B = 0.6 m (23.62 inches), and wall thicknesses of 20 mm (0.79 inches) for B = 1.0 m (39.37 inches). Table 2.5 and Table 2.6 show the calculated Young's modulus of the cylindrical piles having the same bending stiffnesses as the pipe piles considered in the analyses.

According to Hu et al. (2021), when the lateral capacity of a pile obtained from FEA by modeling the pile-soil interface using the Coulomb friction model with an interface friction angle of 21° is compared with the one obtained from FEA by considering perfect contact between the soil and the pile, the difference in the results is less than 2.5%. Thus, we assumed that the effect of an interface model for the soil-pile interface is not significant and considered only perfect contact between the soil and the pile in the analyses performed for this study.

2.1.3 Finite Element Mesh and Boundary Conditions

Figure 2.2 shows the mesh configuration used in the three-dimensional FEA for a single pile with B = 0.36 m

TABLE 2.2
Pile geometries, soil conditions, and lateral load eccentricities considered in the FE analyses for single piles

Pile Diameter B	Pile Length L	Soil Profile	Thickness T_w of Weak Layer of Multilayered Soil Profiles	Lateral Load Eccentricity H	Axial Load
0.36 m (14.17 in.), 0.6 m (23.62 in.), 1.0 m (39.37 in.)	10 m (32.81 ft), 20 m (65.62 ft)	Uniform soil profile (sand with D_R = 40%, 65%, 80% and NC clay), multilayered soil profile (NC clay over dense sand and loose-over-dense sand)	3B, 5B, 6B, 10B	0 m, 1 m (3.28 ft), 6 m (19.69 ft), 10 m (32.81 ft)	0, service load

Note: Relative densities D_R of loose and dense sands are 40% and 80%, respectively.

TABLE 2.3
Model parameters used for Ottawa sand

	Parameter Symbol	Parameter Value
Small-Strain Parameters	ν	0.15
	C_g	611
	n_g	0.437
	γ_1	0.00065
	α_1	0.47
Critical State	Γ_c	0.78
	λ	0.081
	ξ	0.196
	M_{cc}	1.21
Bounding Surface	k_b	1.9
Dilatancy	D_0	1.31
	k_d	2.2
Plastic Modulus	h_1	2.2
	h_2	0.24
	e_{lim}	0.81
	μ	1.2
Stress-Induced Anisotropy	c_1	0.71
	c_2	0.78
	n_s	0.35
Inherent Anisotropy	α	0.31
	k_h	0.39
Yield Surface Radius	m	0.05

TABLE 2.4
Model parameters used for Boston Blue Clay

	Parameter Symbol	Parameter Value
Small-Strain Parameters	ν	0.25
	C_g	250
	ζ	5
	κ	0.036
Normal Consolidation Line	N	1.138
	λ	0.187
Stress Anisotropy	$K_{0,\ NC}$	0.53
Shear Strength	M_{cc}	1.305
	n_s	0.2
	k_b	0.0
	ρ	2.7
Dilatancy Surface	D_0	1
Flow Rule	c_2	0.95
	ξ	0.31
Plastic Modulus	h_0	1.1
Yield Surface Radius	m	0.05

(14.17 inches) and L = 10 m (32.81 ft) installed in a uniform soil profile. As shown in the figure, only half of the problem domain is considered in the analyses because of the symmetry of the problem domain. In the analyses, the width and length of the soil domain is taken as more than 25 times the pile diameter, and the thickness of the soil domain is more than 1.5 times the pile length to avoid any boundary effects. Table 2.7 and Table 2.8 provide the dimensions of the problem domains considered in the analyses for laterally loaded single piles in SI and USCS units.

For the case shown in Figure 2.2, the soil domain, with dimensions of 50 m (164.04 ft) × 25 m (82.02 ft) × 15 m (49 ft), consists of 17,643 linear, 8-noded hexahedral elements with reduced integration. According to Hu et al. (2021), the results of FEA performed for laterally loaded piles in sand are almost the same when the smallest element size ranges from 1 cm (0.4 inch) to 10 cm (4 inches). Thus, the smallest element size used in the FEA for this study is 5 cm (2 inches). The bottom of the problem domain is fixed in the vertical and horizontal directions, and the sides of the problem domain are fixed in their normal directions, as shown in Figure 2.3.

2.1.4 Analysis Steps

The Finite Element analyses consisted of two explicit analysis steps. In the first step, gravity is applied to the problem domain after assigning the initial stress field to the Gauss points of elements representing the soil and pile. The initial stress field is a total vertical stress equal to $\gamma_{sat}z$, where γ_{sat} is the saturated soil unit weight and z is the depth, and a total horizontal stress $\{= [K_0(\gamma_{\text{sat}} - \gamma_d) + \gamma_w]z\}$, where γ_d is the dry soil unit weight, γ_w is the unit weight of water, and K_0 is the coefficient of lateral earth pressure at rest. The first step continues until static equilibrium is reached, which means that the computed stress field matches the predefined stress field. In the second step, the lateral load H is applied at the pile head as a gradually increasing horizontal force.

The applied loading rate ranges from 10 kN/s (2 kips/s) to 25 kN/s (6 kips/s). These loading rates produce a quasi-static response and are high enough to produce an undrained response for clay but are sufficiently low to produce a drained response for sand. When the load eccentricity h is not zero, an equivalent moment M (= $H \times h$) is applied in combination with the lateral load H at the pile head as a gradually increasing moment to represent the eccentricity of the lateral load.

When a non-zero axial load is considered in the analysis, the axial load is applied at the pile head as a gradually increasing axial force at a rate of 268 kN/s (60 kips/s) until the target axial load is reached. The lateral load H and the moment M are applied to the pile head at the loading rate mentioned earlier after the axial load reaches its maximum, from which point it remains constant. In the analyses, the effects of pile installation are not considered.

2.2 Laterally Loaded Single Piles in Uniform Soil

The lateral load response of a single pile in sandy soil is affected by the relative density of the sand.

TABLE 2.5
Young's modulus of the cylindrical piles having the same bending stiffness as the pipe piles considered in the analyses (SI units)

Outer Diameter of the Pile (m)	Wall Thickness (mm)	Young's Modulus of Cylindrical Pile (gpa)
0.36	6	25.4
0.36	9	37.1
0.6	16	39.4
1.0	20	30.1

TABLE 2.6
Young's modulus of the cylindrical piles having the same bending stiffness as the pipe piles considered in the analyses (USCS units)

Outer Diameter of the Pile (inches)	Wall Thickness (inches)	Young's Modulus of Cylindrical Pile (ksi)
14.17	0.236	3,678
14.17	0.354	5,381
23.62	0.629	5,714
39.37	0.787	4,366

TABLE 2.7
Dimensions of the problem domain considered in the analyses for laterally loaded single piles (SI units)

Pile Diameter (m)	Pile Length (m)	Dimension of the Problem Domain (m)
0.36	10	50 × 25 × 15
0.36	20	50 × 25 × 35
0.6	10	50 × 25 × 15
0.6	20	50 × 25 × 35
1.0	10	50 × 25 × 15
1.0	20	50 × 25 × 35

TABLE 2.8
Dimensions of the problem domain considered in the analyses for laterally loaded single piles (USCS units)

Pile Diameter (inches)	Pile Length (ft)	Dimensions of the Problem Domain (ft)
14.17	32.81	164.04 × 82.02 × 49.21
	65.52	164.04 × 82.02 × 114.83
23.62	32.81	164.04 × 82.02 × 49
	65.62	164.04 × 82.02 × 114.83
39.37	32.81	164.04 × 82.02 × 49
	65.62	164.04 × 82.02 × 114.83

Figure 2.4(a) compares the FEA results for a 0.36-m-diameter (14.17 inches) and 10-m-long (32.81 ft) pile laterally loaded in dense sand (D_R = 80%) and in loose sand (D_R = 40%). The lateral load is applied with an eccentricity h of 10 m (32.81 ft) from the ground surface, representing a scenario in which the lateral load is applied at the top of a bridge pier (at a height of 1 m = 3.281 ft) and then transferred to the pile head. As shown in Figure 2.4, the x axis of the graph is the lateral deflection y_{top} at the pile head, while the y axis of the graph is the lateral load H applied at the pile head. The lateral pile deflection at the ground surface in loose sand (= 36 mm = 1.4 inch) is twice as much as that in dense sand (= 18 mm = 0.7 inch) for a small load (= 13 kN = 3 kips).

Figure 2.4(b) shows the lateral load responses obtained from 3D FEA of a 0.36-m-diameter (14.17 inches) and 10-m-long (32.81 ft) single pile with a load eccentricity of 10 m (32.81 ft) in a saturated normally consolidated (NC) clay under drained and undrained conditions. The response of single piles in NC clay is generally softer than that in sandy soil (even if sand is in a loose state). The lateral capacity of the pile under undrained conditions is less than that under drained conditions. Considering that lateral loads are usually transient in nature, leading to undrained response in the

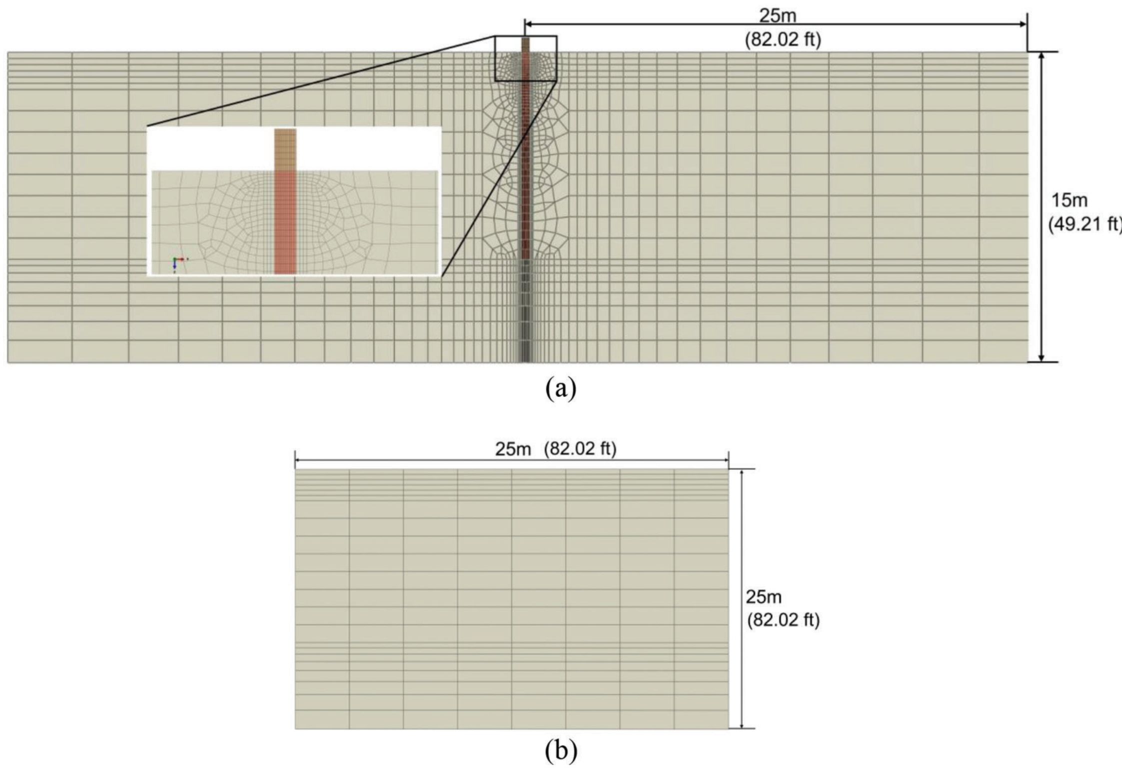

Figure 2.2 Mesh configuration in the three-dimensional FE analysis for a single pile with diameter $B = 0.36$ m (14.17 inches) and length $L = 10$ m (32.81 ft) in a uniform soil profile: (a) front view, and (b) side view. Pile is marked in red.

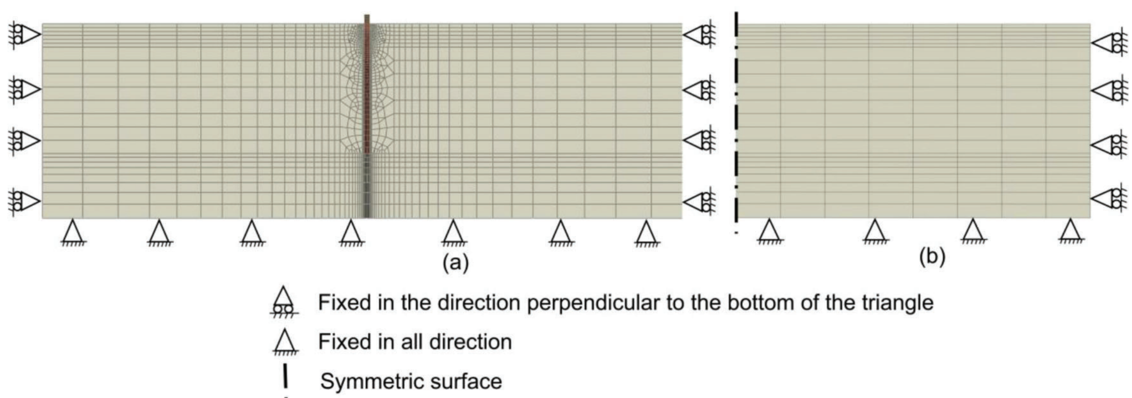

Figure 2.3 Boundary conditions applied in the three-dimensional FE analysis for a single pile with diameter $B = 0.36$ m (14.17 inches) and length $L = 10$ m (32.81 ft) in a uniform soil profile: (a) front view, and (b) side view.

clay next to the pile, undrained conditions should be considered to estimate the lateral capacity of piles in clay to be conservative.

The load eccentricity h has an impact on the lateral capacity of single piles. Figure 2.5 compares the lateral load-deflection responses of a 0.36-m-diameter (14.17 inches) and 10-m-long (32.81 ft) single pile loaded laterally in dense sand ($D_R = 80\%$) with three different eccentricities: $h = 2$ m (6.56 ft), 5 m (16.40 ft) and 10 m (32.81 ft). For the same load magnitude of 44 kN (10 kips), the pile lateral deflection at the ground level is over 76 mm (3 inches) if the load is applied at $h = 10$ m (32.81 ft), whereas the lateral deflection at the ground level is only 18 mm (0.7 inch) if the load is applied at $h = 2$ m (6.56 ft). The lateral load capacity of a single pile decreases significantly with increasing load eccentricity.

2.3 Effect of Axial Load on the Lateral Response of Single Piles

Piles can be subjected to a combination of axial loads, lateral loads, and moments. To study the effect of the presence of an axial load, FEA for single piles in dense sand ($D_R = 80\%$) with a load eccentricity $h = 10$ m (32.81 ft) were performed with and without the

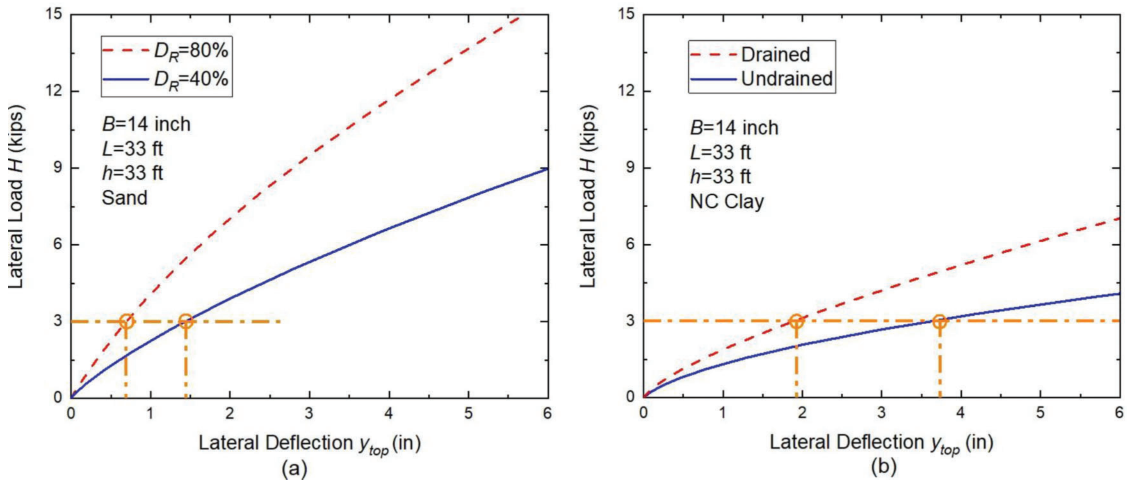

Figure 2.4 Response of a 0.36-m-diameter (14.17 inches) and 10-m-long (32.81 ft) single pile to lateral loads in (a) dense and loose sand, and (b) NC clay under drained and undrained conditions.

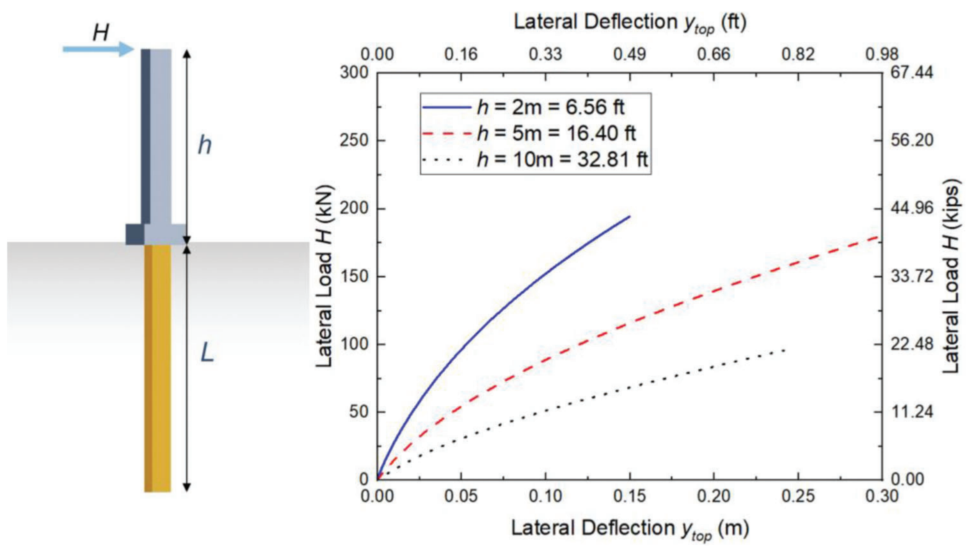

Figure 2.5 Effect of load eccentricity h on the lateral load response of single piles: FE analysis results for a 0.36-m-diameter (14.17 inches) and 10-m-long (32.81 ft) single pile loaded laterally with three different load eccentricities h in dense sand (D_R = 80%).

application of an axial load of 536 kN (120 kips) at the pile head. The service axial load of 536 kN (120 kips) was determined by dividing the nominal load estimated by using the Purdue method (Han et al., 2019; Salgado et al., 2011) for closed-ended pipe piles by a factor of safety of 3. Figure 2.6 shows the load-deflection curves for the piles with B = 0.36 m (14.17 inches) and L = 10 m (32.81 ft) installed in a uniform dense sand; the piles were subjected to a lateral load with an eccentricity of 10 m (32.81 ft) and axial service loads of 0 and 536 kN (120 kips). As shown in the figure, when the axial load is applied to the pile head, the lateral capacity at a lateral deflection of 50 mm (2 inches) is about 6% less than the one without the application of the axial load. The difference between the lateral capacities of the pile with and without the axial load increases as the lateral deflection at the pile head increases.

2.4 *p-y* Relationship for Sand

From the 3D FEA results, it is possible to extract *p-y* curves at different depths along the pile length. Figure 2.7 shows the *p-y* curves derived from the FE analyses at different depths for a single pile with B = 0.36 m (14.17 inches) and L = 10 m (32.81 ft) in sand for two different relative densities. For the same normalized pile deflection y/B, the normalized unit soil resistance p/B increases as the depth increases because of the increasing confining stress with increasing depth. The *p-y* curve is stiffer for dense sand (D_R = 80%) than for loose sand (D_R = 40%) at the same depth, leading to a stiffer global load-deflection response for a single pile in dense sand, as shown in Figure 2.4(a).

Figure 2.8 shows *p-y* curves obtained from the FEA at different depths for single piles (B = 0.36 m (14.17 inches) and L = 10 m (32.81 ft)) in uniform loose and

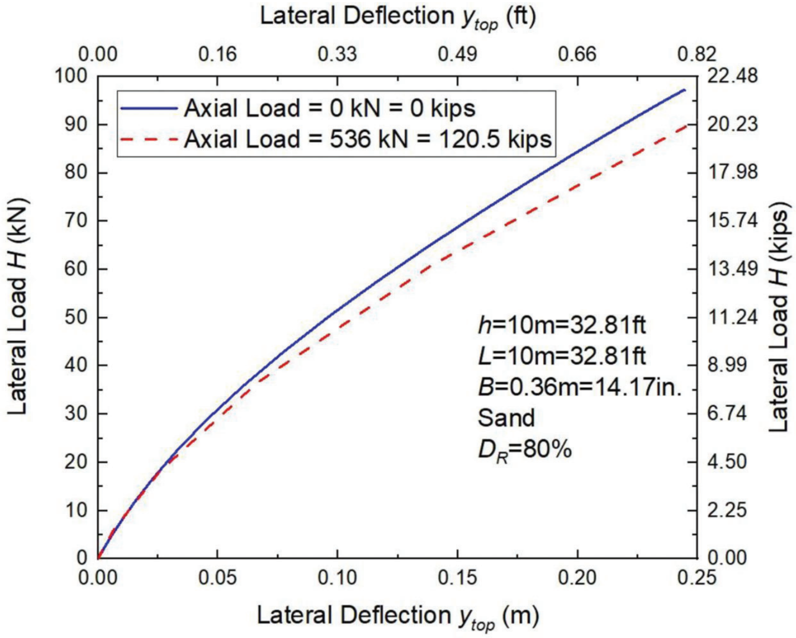

Figure 2.6 Load deflection curve for single pile (B = 0.36 m = 14.17 inches, and L = 10 m = 32.81 ft) in dense sand (D_R = 80%) with a load eccentricity h = 10 m (32.81 ft).

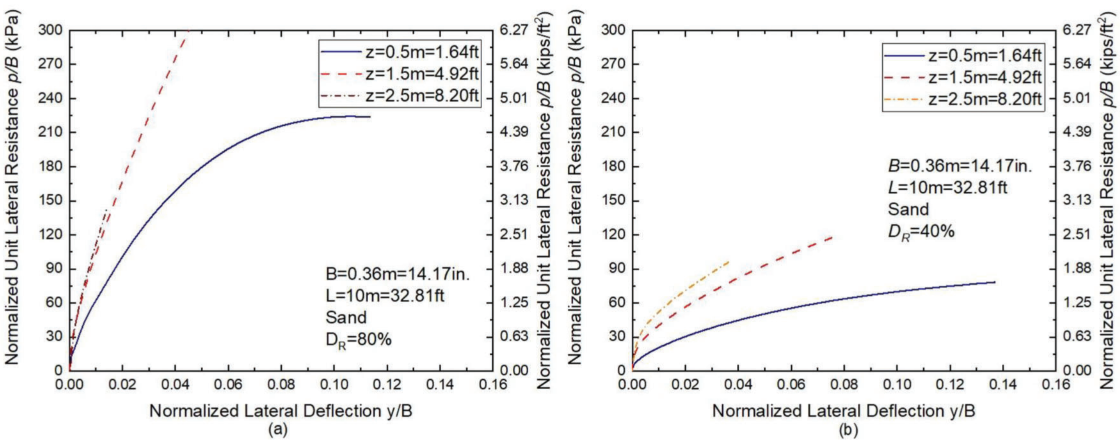

Figure 2.7 The p-y curves obtained from the FE analyses at different depths: (a) in dense (D_R = 80%) sand, and (b) in loose (D_R = 40%) sand.

dense sand when the lateral load is applied with load eccentricities h of 0 m (0 ft) and 10 m (32.81 ft). Unlike what is observed for the global lateral load capacity of a single pile, which decreases significantly with increasing load eccentricity, as shown in Figure 2.5, the p-y curves at different depths for a single pile in sand are almost the same for different load eccentricities. This is an important result, confirming that the same p-y curves can be used regardless of the load eccentricity.

The effect of the groundwater level on the p-y curves for single piles in sand was also evaluated. Two different levels of the groundwater table were considered on the FEA: one with the groundwater level at a depth greater than the height of the soil domain (= 20 m = 65.62 ft) with the entire soil domain under fully dry conditions; and the other one with the groundwater level at the ground surface, with the entire soil domain fully saturated. Figure 2.9 shows the p-y curves obtained from the FEA for a single pile (B = 0.36 m = 14.17 inches, and L = 10 m = 32.81 ft) in loose sand with the groundwater table at different depths. When the p-y curves at the same depths are compared for the cases with different groundwater levels, the case with the groundwater table at the ground surface provides a lower unit soil resistance p at the same pile deflection y, as shown in Figure 2.9(a). This is because saturated sand has a smaller vertical effective stress than dry sand at the same depth. When the p-y curves at the same level of initial vertical effective stress σ'_{v0} are compared for the cases with different groundwater levels, it is seen

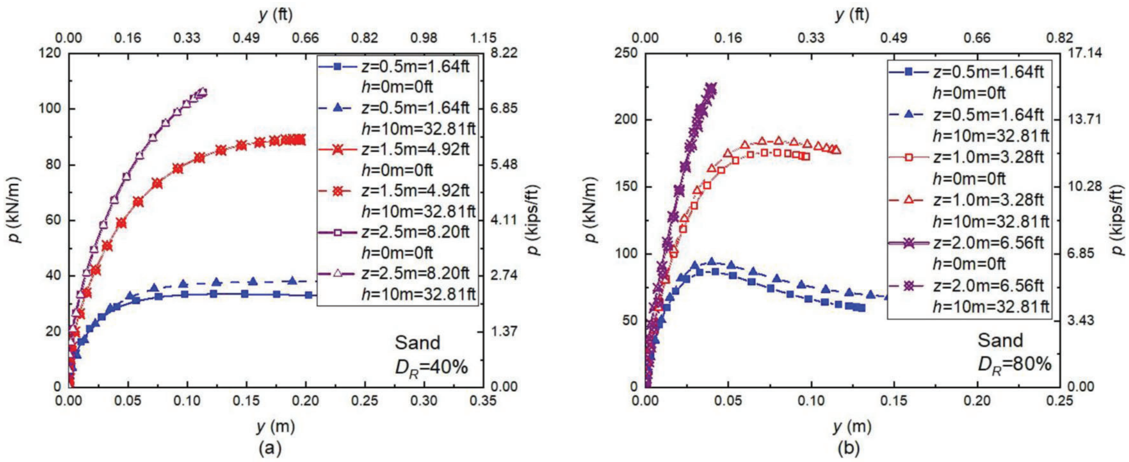

Figure 2.8 The *p-y* curves obtained from the FEA at different depths for single piles with values of load eccentricity $h = 0$ m (0 ft) and 10 m (32.81 ft): (a) in loose ($D_R = 40\%$) sand, and (b) in dense ($D_R = 80\%$) sand.

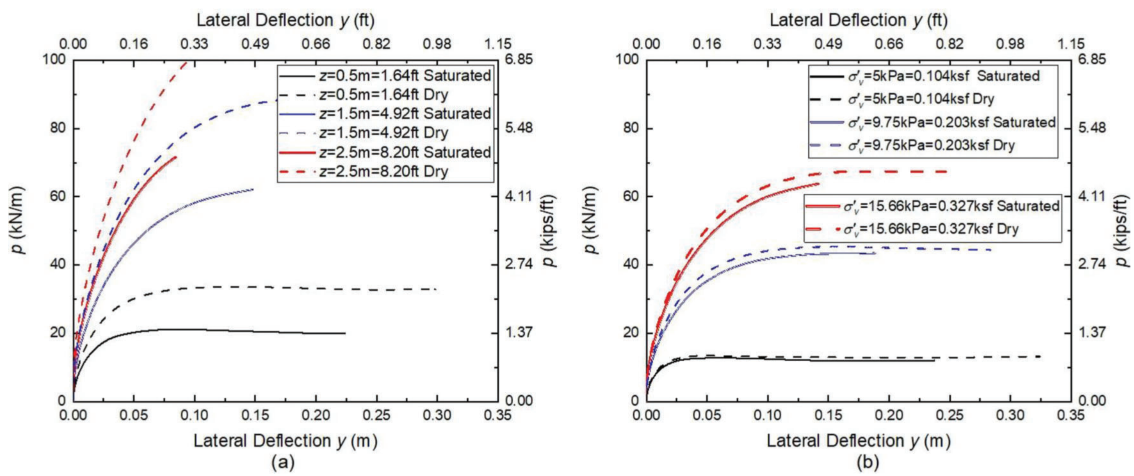

Figure 2.9 The *p-y* curves obtained from the FEA for a single pile in loose ($D_R = 40\%$) sand with the groundwater table at the ground surface (fully saturated case) and at a depth greater than 20 m (65.62 ft) (fully dry case): (a) *p-y* curves at different depths, and (b) *p-y* curves at different values of initial vertical effective stress σ'_{v0}.

that they are almost the same, as shown in Figure 2.9(b). This confirms that we can use effective stresses to normalize *p-y* curves.

Figure 2.10 shows the effect of pile diameter on the *p-y* curves for single piles in uniform dense and loose sands. In Figure 2.10, the normalized unit soil resistance p/B is plotted versus normalized pile deflection y/B for different depths for 10-m-long (32.81 ft) single piles with two different diameters: $B = 0.36$ m (14.17 inches) and 0.6 m (23.62 inches). As shown in Figure 2.10, for both dense and loose sands, a slightly lower p/B results for a given value of normalized pile deflection y/B for the pile with the larger diameter at shallow depths—less than 1 m (3.28 ft)—but the opposite result is obtained for depths greater than 1 m (3.28 ft).

2.5 Proposed *p-y* Curves for Sand

Based on the results of the FEA performed for laterally loaded single piles, new *p-y* curves are proposed for sand. The relationship between the unit soil resistance p (with units of force per length) and the pile deflection y (with units of length) is given by

$$p = p_u \tanh\left[\left(b\frac{y}{L_R}\right)^c\right] \qquad \text{(Eq. 2.1)}$$

where the limit unit soil resistance p_u (with units of force per length) is given by

$$p_u = \left(\frac{D_R}{100\%}\right)^{1.4} \min\left(46.6, 13.8 + 7.00\left(\frac{p_A}{\sigma'_{v0}}\right)\right)\sigma'_{v0}B \qquad \text{(Eq. 2.2)}$$

with

$$b = \frac{32.2}{\left(\frac{p_u}{p_A B}\right)^{0.860}} \exp\left[4.10\left(\frac{D_R}{100\%}\right)^5\right] \qquad \text{(Eq. 2.3)}$$

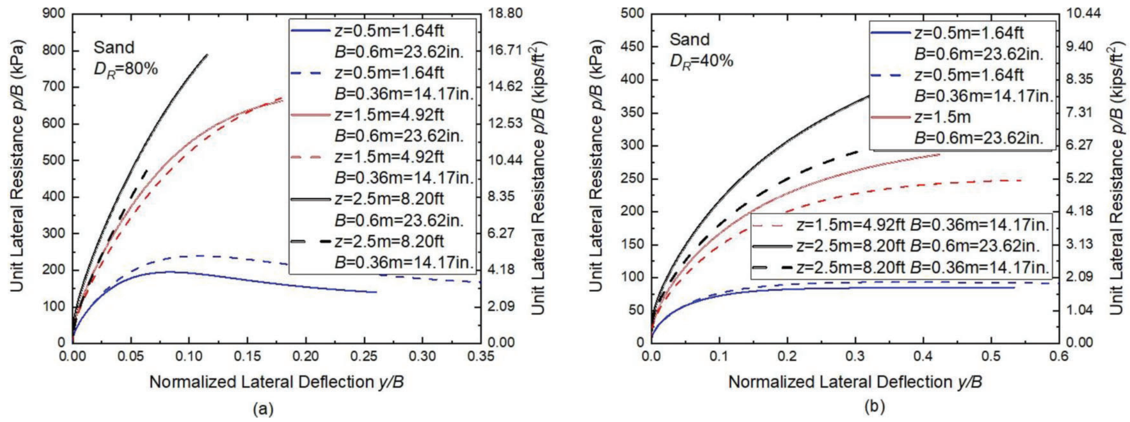

Figure 2.10 The *p-y* curves obtained from the FEA at different depths for single piles with a diameter B of 0.36 m (14.17 inches) and 0.6 m (23.62 inches): (a) in dense (D_R = 80%) sand, and (b) in loose (D_R = 40%) sand.

$$c = \exp\left[11.6\left(\frac{D_R}{100\%}\right) - 11.0\right] + 0.598 \qquad \text{(Eq. 2.4)}$$

and D_R = relative density of the sand in % ($0\% \leq D_R \leq 100\%$), σ'_{v0} = initial vertical effective stress, B = pile diameter, p_A (= 100 kPa ≈ 1 tsf) = the reference stress, and L_R (= 1 m ≈ 3.281 ft or equivalent in other units) = the reference length. The equation is fitted to the data extracted from FEA results using the least squares method.

Figure 2.11 shows a comparison between the *p-y* curves obtained using Equations 2.1 to 2.4 and the *p-y* curves obtained from the API method for the single pile (B = 0.36 m = 14.17 inches) in dense sand. As shown in the figure, the *p-y* curves proposed in this study provide softer responses than those obtained from the API method. As discussed in the previous section, *p-y* curves are independent of pile length L and load eccentricity h.

Figure 2.12 shows the pile lateral load-deflection responses obtained by performing *p-y* analyses on a 0.36-m-diameter (14.17 inches) and 10-m-long (32.81 ft) pile using the *p-y* curves proposed in this study. The commercial *p-y* analysis software PYGMY (Stewart, 2000) was used to perform the *p-y* analyses for single piles in uniform loose and dense sands. As shown in Figure 2.12, the *p-y* curves obtained using Equations 2.1 through 2.4 generate lateral load-deflection pile responses that are in good agreement with the ones from the 3D FE analyses.

The proposed *p-y* curves for sand also work well for layered sand profiles. Figure 2.13 shows the results of *p-y* analyses for a single pile (B = 0.36 m = 14.17 inches, and L = 10 m = 32.81 ft) performed using PYGMY (Stewart, 2000) with the proposed *p-y* curves for two different layered sand profiles: dense-over-loose (D_R = 80% over D_R = 40%) sand profile with the upper layer with a thickness of 3B, and loose-over-dense (D_R = 40% over D_R = 80%) sand profile with the upper layer with a thickness of 3B. As shown in the figure, the pile lateral load-deflection responses obtained from the *p-y* analyses are in close agreement with those obtained from the 3D FE analyses. This suggests that the *p-y* curves may be generally applied.

2.6 *p-y* Relationship for Clay

As done for sand, *p-y* curves for clay can be derived from the results of the 3D FE analyses. Figure 2.14(a) shows the *p-y* curves obtained at different depths for a single pile (B = 0.36 m = 14.17 inches, and L = 10 m = 32.81 ft) in normally consolidated (NC) clay loaded under undrained conditions. The normalized unit soil resistance p/B increases with increasing depth. Referring to the *p-y* curves for the same pile in loose sand (D_R = 40%), shown in Figure 2.14(b), the *p-y* curves at a fixed depth are softer for the NC clay than for the loose sand, leading to a softer global load-deflection response in NC clay (see Figure 2.4).

Figure 2.15 shows the *p-y* curves obtained from the FE analyses at different depths for a single pile (B = 0.36 m = 14.17 inches, and L = 20 m = 65.62 ft) in uniform NC clay under undrained conditions when the lateral load is applied with load eccentricity h = 0 m (0 ft) and 10 m (32.81 ft). Similar to the results for sand shown in Figure 2.8, the *p-y* curves at different depths for a single pile in NC clay are almost the same for different load eccentricities.

Figure 2.16 shows the effect of the pile diameter on the *p-y* curves for a single pile in NC clay under undrained conditions. Three diameters are considered, 0.36 m (14.17 inches), 0.6 m (23.62 inches) and 1.0 m (39.37 inches) for 20-m-long (65.62 ft) piles. As shown in Figure 2.16, a single pile with a larger pile diameter in NC clay provides slightly lower p/B for the same pile deflection y at the same depth, but the difference in *p-y* curves for different pile diameters becomes negligible as the depth increases.

2.7 Proposed *p-y* Curves for Clay

Based on the results of the FE analyses performed for laterally loaded single piles, new *p-y* curves are proposed for NC clay. The relationship between the

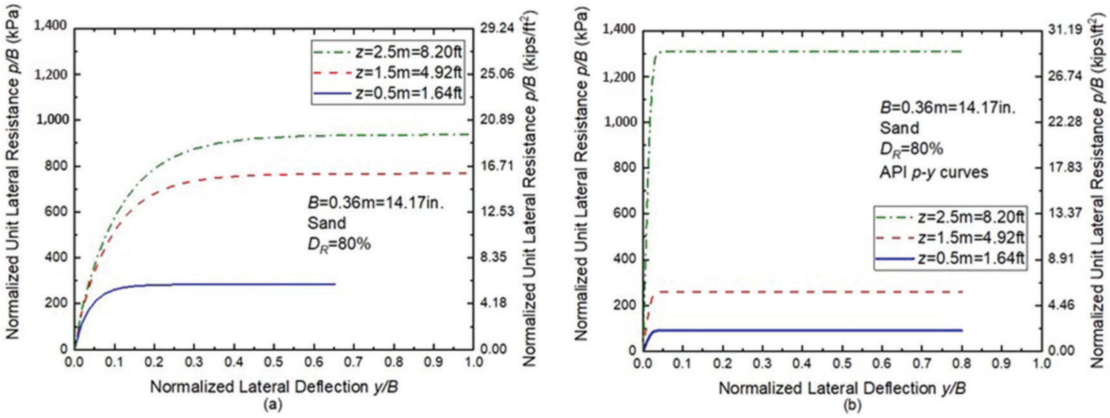

Figure 2.11 Comparison between (a) *p-y* curves proposed in this study, and (b) *p-y* curves obtained from the API method for the single pile with $B = 0.36$ m (14.17 inches) in dense sand.

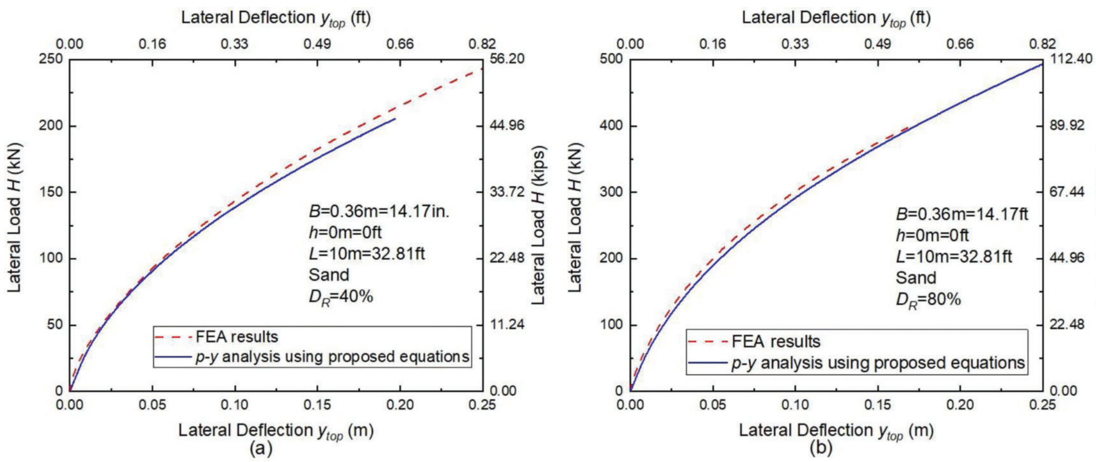

Figure 2.12 Results of *p-y* analyses using the *p-y* curves proposed in this study for (a) uniform loose ($D_R = 40\%$) sand, and (b) uniform dense ($D_R = 80\%$) sand.

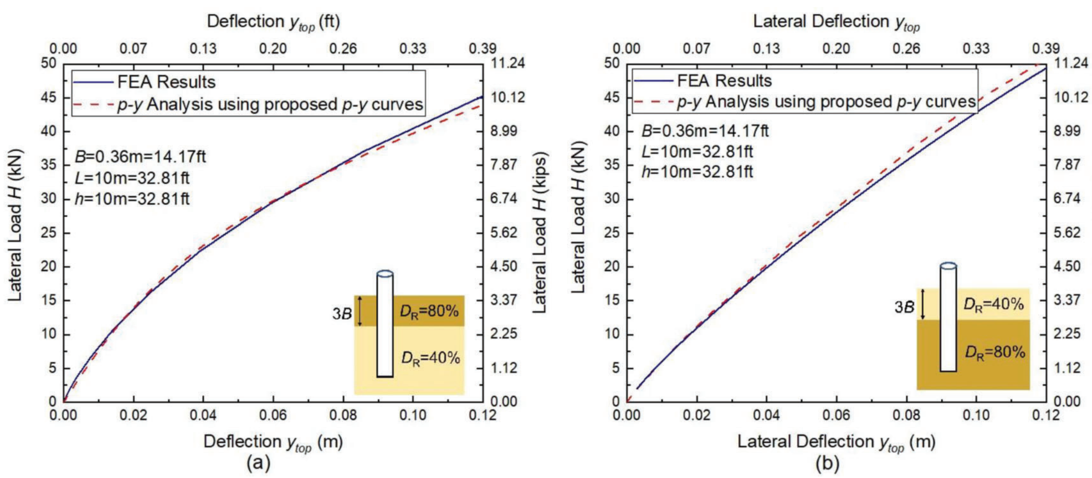

Figure 2.13 Results of *p-y* analysis using the *p-y* curves proposed in this study for single piles ($B = 0.36$ m = 14.17 inches, $L = 10$ m = 32.81 ft, and $h = 10$ m = 32.81 ft) in two layered sand profiles: (a) dense-over-loose ($D_R = 80\%$ over $D_R = 40\%$) sand profile, and (b) loose-over-dense ($D_R = 40\%$ over $D_R = 80\%$) sand profile.

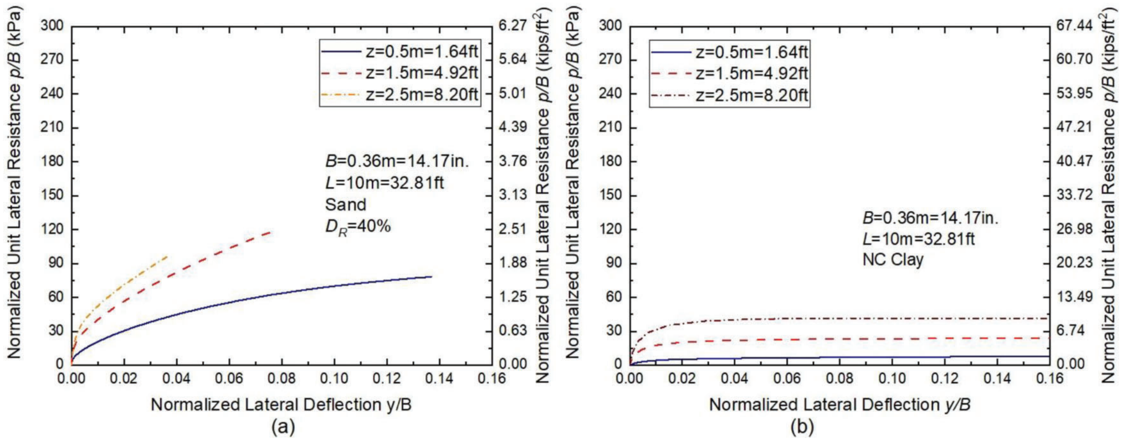

Figure 2.14 The *p-y* curves obtained at different depths from the FE analyses of single piles in (B = 0.36 m = 14.17 inches, and L = 10 m = 32.81 ft): (a) NC clay under undrained conditions, and (b) loose sand (D_R = 40%).

unit soil resistance p (with units of force per length) and the pile deflection y (with units of length) is given by

$$p = p_u \left[\frac{\frac{y}{y_c}}{a\left(\frac{y}{y_c}\right) + 1 - a} \right] \quad \text{when } y < y_c \qquad \text{(Eq. 2.5)}$$

$$p = p_u \quad \text{when } y \geq y_c$$

where the limit unit soil resistance p_u (with units of force per length) is given by

$$p_u = \min\left[64.0\left(\frac{s_u}{p_A}\right) + \left(1.75\frac{L_R}{B} + 5.05\right), 11.67\right] s_u B \qquad \text{(Eq. 2.6)}$$

with

$$y_c = \left(-0.0196\left(\frac{B}{L_R}\right)^{-1} + 0.0775\right) L_R + \left(-0.0192\left(\frac{B}{L_R}\right)^{-2.5} + 0.368\right) \exp\left[\left(-23.0\frac{B}{L_R} - 80.0\right)\frac{s_u}{P_A}\right] L_R \qquad \text{(Eq. 2.7)}$$

$$a = 0.96 \qquad \text{(Eq. 2.8)}$$

and s_u = undrained shear strength of the clay, B = pile diameter, p_A (= 100 kPa ≈ 1 tsf) is the reference stress, and L_R (= 1 m ≈ 3.281 ft or equivalent in other units) is the reference length. The equation is fitted to the data extracted from FEA results using the least squares method.

Figure 2.17 shows a comparison between *p-y* curves obtained by using Equations 2.5 to 2.8 and *p-y* curves obtained from the API method for the 0.36-m-diameter (14.17 inches) single pile in NC clay. As shown in the figure, the *p-y* curves proposed in this study provide stiffer responses than those from the API method.

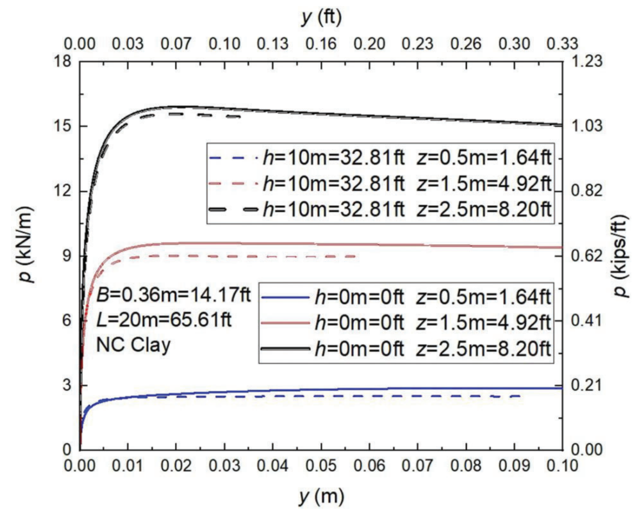

Figure 2.15 The *p-y* curves obtained at different depths from the FE analyses of single piles (B = 0.36 m = 14.17 inches, and L = 20 m = 65.62 ft) with load eccentricities h = 0 m (0 ft) and 10 m (32.81 ft) in NC clay under undrained conditions.

Using the *p-y* curves proposed in this study for clay, we performed *p-y* analyses using PYGMY (Stewart, 2000). As shown in Figure 2.18, the load-deflection response obtained from the *p-y* analysis using the proposed *p-y* curves is in close agreement with that obtained from the 3D FE analysis. In the *p-y* analysis, 0.36-m-dimater (14.17 inches) and 10-m-long (32.81 ft) piles in uniform NC clay are considered; the top 6 m (19.69 ft) of the soil profile was discretized into 19 layers, each with a thickness equal to approximately 0.32 m (1 ft). The *p-y* curves given by Equations 2.5 to 2.8 are used to represent the mechanical response of each layer. Below the top 6 m (19.69 ft), the API *p-y* curves are specified in PYGMY (Stewart, 2000); however, the lateral deflections are approximately zero there. The load-deflection response obtained from the *p-y* analyses using the API *p-y* curves for clay is conservative when compared with that obtained from

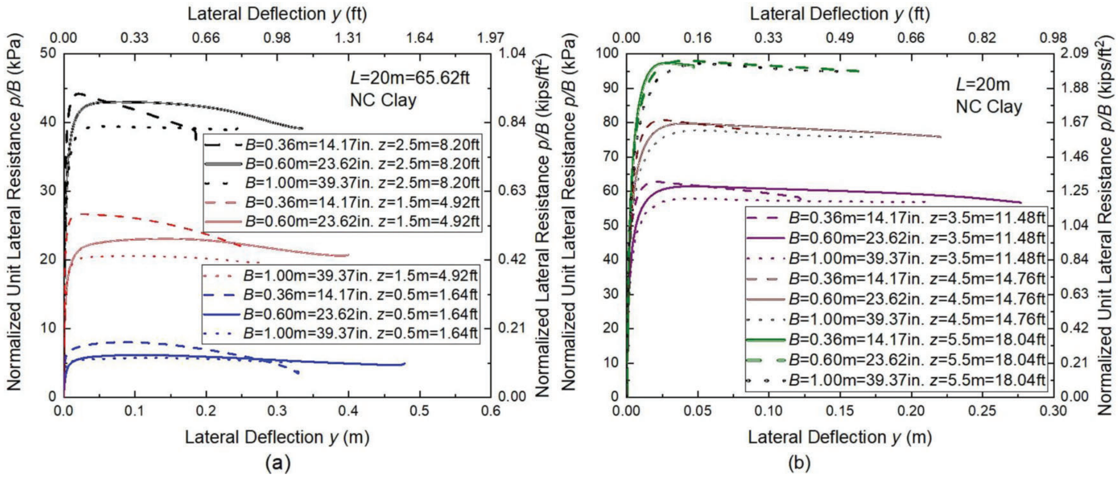

Figure 2.16 The p-y curves obtained from the FE analyses for single piles with a diameter B of 0.36 m (14.17 inches), 0.6 m (23.62 inches), and 1.0 m (39.37 inches) in NC clay under undrained condition: (a) at shallow depths less than 3 m (10 ft), and (b) at depths greater than 3 m (10 ft).

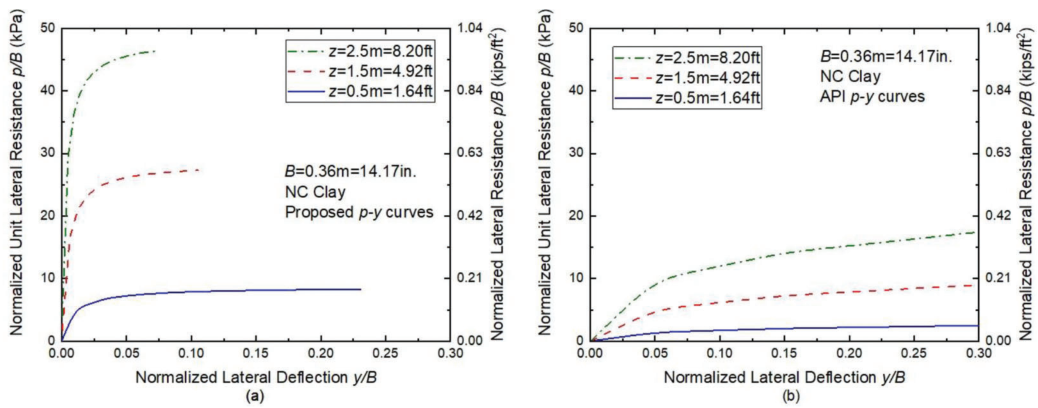

Figure 2.17 Comparison between (a) p-y curves proposed in this study, and (b) p-y curves obtained from the API method for the single pile with $B = 0.36$ m (14.17 inches) in NC clay.

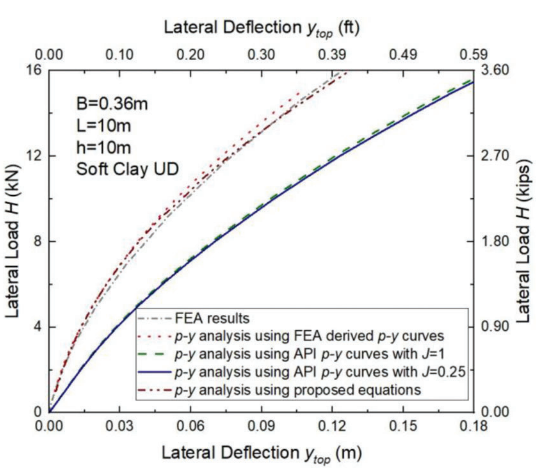

Figure 2.18 Results of p-y analysis using the p-y curves proposed in this study for NC clay under undrained conditions. The load-deflection responses obtained using the API p-y curves with the empirical parameter $J = 0.25$ and $J = 1$ are also plotted for comparison.

the 3D FE analysis, regardless of the value of the empirical parameter J used in the analysis.

3. RESPONSE OF GROUP PILES TO LATERAL LOADS

3.1 Finite Element Analysis

3.1.1 Simulation Conditions

For the pile group analyses, three pile group layouts (with one, two and three rows) with pile spacings s_c ranging from 3B to 5B were considered to study the effect of pile group layout on the lateral resistance mobilization of a pile group, as shown in Figure 3.1. The distance s_{edg} from the center of the edge pile to the edge of the pile cap is 2B.

The same geometry of the piles and soil profiles considered in the single pile analyses were considered in the pile group analyses. For a given pile group configuration, two different lateral load directions were

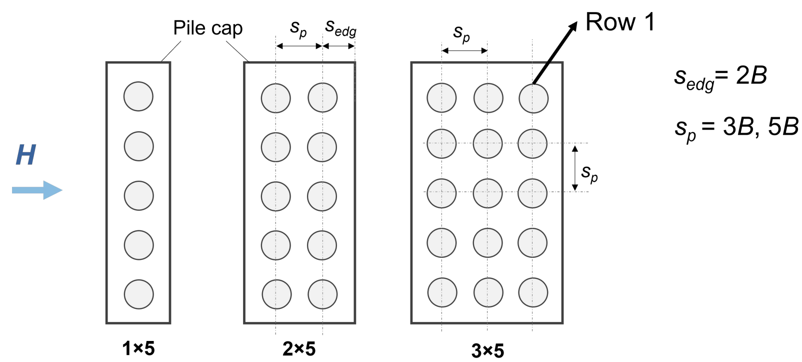

Figure 3.1 Pile group layouts considered in the analyses: one row, two rows, and three rows of piles with various pile spacings s_c.

TABLE 3.1
Pile group configurations, pile spacings, lateral load direction and eccentricity, and the pile cap type considered in the FE analyses for pile groups (SI units)

Group Configuration	Pile Spacing s_c	Lateral Load Direction	Lateral Load Eccentricity h (m)	Pile Cap Type
1×5, 2×5, 3×5	$3B$, $5B$	Strong direction, weak direction	1, 2, 5, 6, 10	Free-standing, soil-supported

TABLE 3.2
Pile group configurations, pile spacings, lateral load direction and eccentricity, and the pile cap type considered in the FE analyses for pile groups (USCS units)

Group Configuration	Pile Spacing s_c	Lateral Load Direction	Lateral Load Eccentricity h (ft)	Pile Cap Type
1×5, 2×5, 3×5	$3B$, $5B$	Strong direction, weak direction	3.28, 6.56, 16.40, 19.69, 32.81	Free-standing, soil-supported

considered (weak and strong directions) to study the effect of load direction on the lateral responses of the individual piles in the group. Lateral load eccentricities h ranging from 1 m (3.28 ft) to 10 m (32.81 ft) were considered to evaluate the effect of load eccentricity on the lateral responses of the individual piles in the group. In addition, two different types of pile cap were considered (free-standing and soil-supported) to study the effect of pile cap-soil interaction on the lateral responses of the pile groups. Table 3.1 and Table 3.2 summarize the simulation conditions considered in the pile group analyses.

3.1.2 Finite Element Modeling

Similar to the FE analyses for single piles, sand and clay layers were modeled using the advanced constitutive models developed by Loukidis and Salgado (2009) and Chakraborty et al. (2013), respectively. The properties of Ottawa sand and Boston Blue Clay (BBC) were used to represent sand and clay in the analyses with the input parameters of the constitutive model provided in Table 2.3 and Table 2.4. Piles are modeled as an elastic material with a Young's modulus E of 200 GPa (29,008 ksi) and Poisson's ratio v of 0.2. The Young's modulus of a cylindrical pile with the same diameter as the pipe pile considered in the analyses is determined such that the cylindrical pile has the same bending stiffness as the pipe pile, as shown in Table 3.3. Perfect contact between the soil and the pile was assumed.

Figure 3.2 shows the mesh configuration used in the three-dimensional FEA for a 1×5 pile group installed in a uniform soil profile. The piles in the group have $B = 0.36$ m (= 14.17 inches) and $L = 10$ m (= 32.81 ft), and the spacing $s_c = 3B$. Similarly, to the FEA performed for single piles, half of the problem domain was considered in the analyses based on the symmetry of the problem domain. The width and length of the soil domain is taken as more than 25 times the pile diameter, and the thickness of the soil domain is more than 1.5 times the pile length to avoid any boundary effects. Table 3.3 summarizes the dimensions of the problem domains considered in the analyses for laterally loaded pile groups.

For the case shown in Figure 3.2, the dimensions of the soil domain are 50 m (164.04 ft) $\times$ 25 m (82.02 ft) $\times$ 20 m (65.62 ft). In the FEA, 131,369 linear, 8-noded hexahedral elements with reduced integration were used. The smallest element size in the figure is 5 cm (2 inches). Figure 3.3 shows the applied boundary conditions for the pile group analyses.

Similar to the FE analyses for single piles, two explicit steps were used in the analyses. In the first step,

TABLE 3.3
Dimension of the problem domain considered in the analyses for laterally loaded pile groups

Group Configuration	Pile Diameter	Pile Length	Pile Spacing	Dimension of the Problem Domain
1 × 5	0.36 m (14.17 in.)	10 m (32.81 ft)	3B	50 m × 25 m × 20 m (164.04 ft × 82.02 ft × 65.62 ft)
1 × 5	0.36 m (14.17 in.)	10 m (32.81 ft)	5B	50 m × 25 m × 20 m (164.04 ft × 82.02 ft × 65.62 ft)
1 × 5	0.36 m (14.17 in.)	20 m (65.62 ft)	3B	50 m × 25 m × 35 m (164.04 ft × 82.02 ft × 114.83 ft)
2 × 5	0.36 m (14.17 in.)	10 m (32.81 ft)	3B	50 m × 25 m × 35 m (164.04 ft × 82.02 ft × 114.83 ft)
3 × 5	0.36 m (14.17 in.)	10 m (32.81 ft)	3B	50 m × 25 m × 35 m (164.04 ft × 82.02 ft × 114.83 ft)

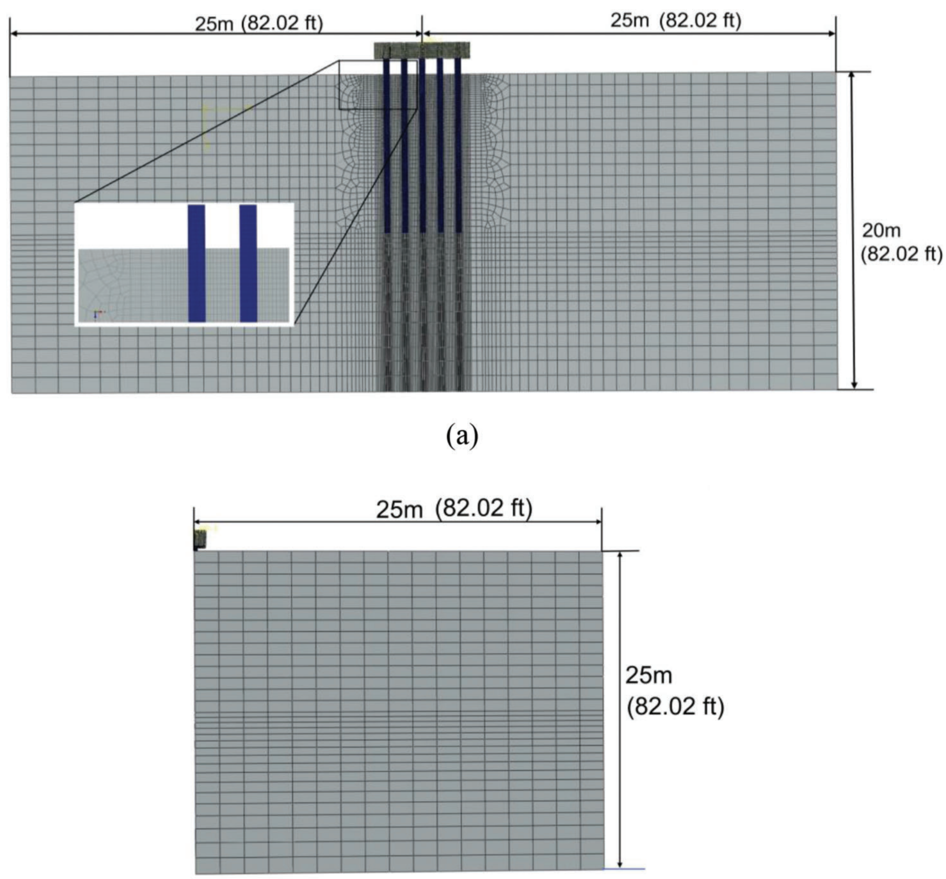

Figure 3.2 Mesh configuration in the three-dimensional FE analysis for a 1 × 5 pile group with a pile diameter B = 0.36 m (= 14.17 inches), pile length L = 10 m (= 32.81 ft), and pile spacing s_c = 3B in a uniform soil profile: (a) front view, and (b) side view. Piles are marked in blue.

gravity is applied to the problem domain after assigning to Gauss points in the soil and pile domains a predefined initial stress field. The first step continues until static equilibrium is reached, which means the vertical stress of the soil match the one that we input in the predefined field. In the second step, the lateral load H is applied at the top of the pile cap as a gradually increasing horizontal force. The applied loading rate ranges from 10 kN/s (2 kips/s) to 25 kN/s (6 kips/s) per pile. When the load eccentricity h is not zero, an equivalent moment M (= $H \times (h - h_{cap})$), where h_{cap} is the height from the ground surface to the top of the pile cap, is applied in combination with the lateral load H at the top of the pile cap as a gradually increasing

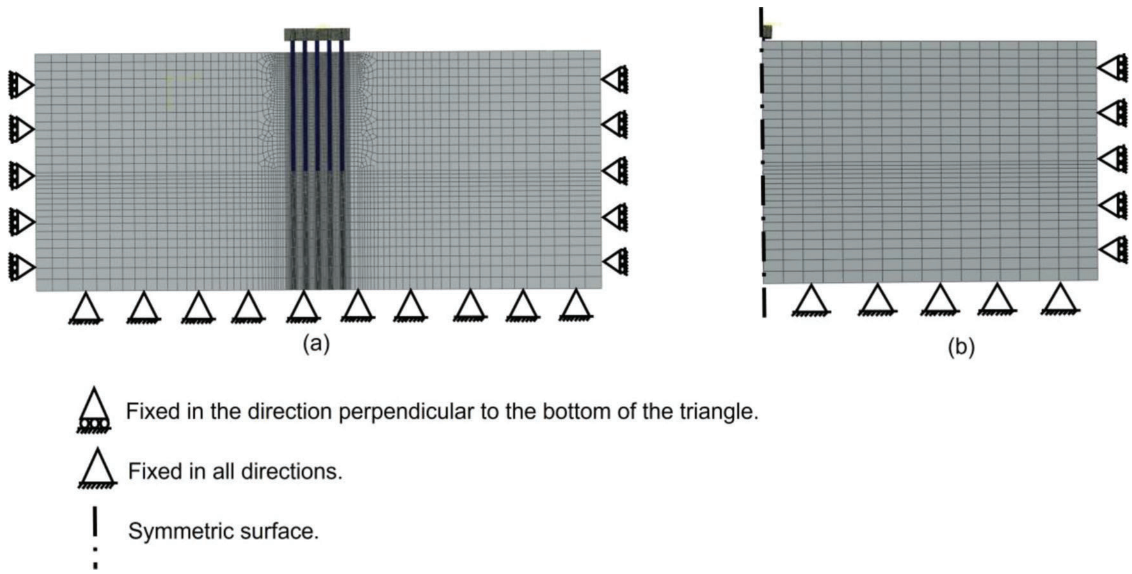

Figure 3.3 Boundary conditions applied in the three-dimensional FE analysis for a 1×5 pile group with diameter $B = 0.36$ m (= 14.17 inches), pile length $L = 10$ m (= 32.81 ft), and pile spacing $s_c = 3B$ in a uniform soil profile: (a) front view, and (b) side view.

moment. For a non-zero axial load, the axial load is applied at the top of the pile cap as a gradually increasing axial force at a rate of 268 kN/s (60 kips/s) until the maximum axial load that we set up is reached. The lateral load H and the moment M are applied to the pile group at a load rate mentioned before after the axial load reaches its maximum and starts to keep constant. In the analyses, the effect of pile installation is not considered.

3.2 Laterally Loaded Group Piles in Uniform Soil

3.2.1 Tolerable Lateral Deflection

Bozozuk (1978) summarized case histories with acceptable and unacceptable movements of bridges in Canada and the United States and proposed a value of 50 mm (2 inches) for the maximum tolerable lateral deflection (horizontal displacement), as shown in Figure 3.4. In this study, we defined the lateral capacity of the piles as the load corresponding to a lateral deflection of 50 mm (2 inches), unless otherwise specified.

3.3 Responses of Individual Piles in a Group

Table 3.4 and Table 3.5 show the lateral capacities of five piles in four 1×5 pile groups in sand loaded in the strong direction. The definition of row numbers is given in Figure 3.5. The piles are 0.36 m (=14.17 inches) in diameter and 10 m (32.81 ft) in length. The spacing between the piles is 3B. As shown in the table, the piles in the leading row (Row 1) have the largest capacities when compared to the piles in the trailing rows (Rows 2–5). The lateral capacities of the piles tend to decrease as the row number increases from 1 to 3. The piles in Rows 3–5 have similar capacities.

Within the same row, the lateral capacities of the piles are also different depending on the position of the pile. Table 3.6 and Table 3.7 show the capacities of individual piles in a 3×5 pile group in dense sand ($D_R = 80\%$) loaded in the weak direction with a load eccentricity $h = 10$ m (32.81 ft). The piles are 0.36 m (=14.17 inches) in diameter and 10 m (32.81 ft) in length. The spacing between the piles is $3B$. The definition of the pile numbers is given in Figure 3.6. Out of the fifteen piles in the group, only 9 piles were considered because of the symmetry of the problem. As shown in the table, the edge piles (pile numbers 1, 4, and 7) of each row have the greatest capacities when compared to the other two piles in the same row. Two inner piles (pile numbers 2 and 3 in Rows 1 and 5, and 6 in Row 2; and 8 and 9 in Row 3) of each row have similar capacities.

3.3.1 Moment Distribution and Effect of Load Eccentricity

Pile efficiency depends on the load eccentricity. In general, pile efficiency decreases as the load eccentricity increases, just like the lateral load capacity of a single pile decreases with increasing load eccentricity (see Figure 2.5). For example, the average pile efficiency of the 3×5 pile group in uniform dense sand loaded in the pile group's strong direction decreases from 0.57 to 0.33 when the load eccentricity increases from 2 m (6.56 ft) to 10 m (32.81 ft). When the 3×5 pile group in uniform dense sand is loaded in the weak direction instead, the pile efficiency decreases from 0.92 to 0.46 as the load eccentricity increases from 1 m (3.28 ft) to 10 m (32.81 ft). Table 3.8 and Table 3.9 provide the lateral capacities of the 3×5 pile groups in loose sand ($D_R = 40\%$) loaded in the weak direction with load eccentricities $h = 6$ m (19.69 ft) and 10 m (32.81 ft). As shown in the

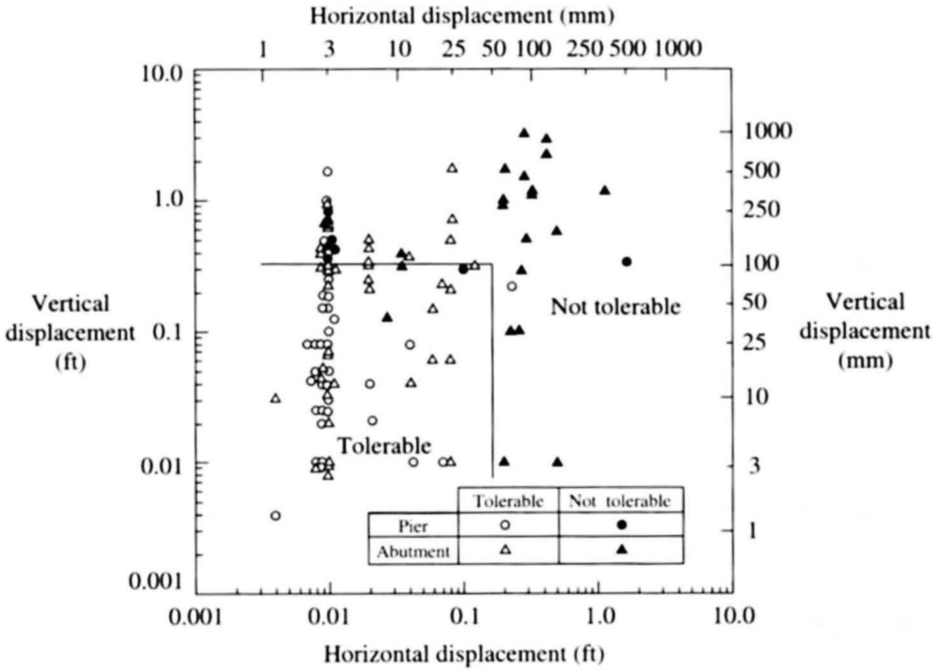

Figure 3.4 Tolerable movements for bridge foundations (Bozozuk, 1978).

TABLE 3.4
Capacity of individual piles (B = 0.36 m = 14.17 inches, and L = 10 m = 32.81 ft) in 1×5 pile groups loaded in the strong direction (SI units)

		Lateral Capacity (kN)				
Load Eccentricity h (m)	**Relative Density D_R (%)**	**Row 5**	**Row 4**	**Row 3**	**Row 2**	**Row 1**
10	40	36.46	35.59	46.87	57.29	75.52
	80	108.65	120.09	139.15	148.68	184.90
2	40	78.12	79.86	80.72	82.46	100.69
	80	186.81	184.90	183.00	186.81	226.84

TABLE 3.5
Capacity of individual piles (B = 0.36 m = 14.17 inches, and L = 10 m = 32.81 ft) in 1×5 pile groups loaded in the strong direction (USCS units)

		Lateral Capacity (kips)				
Load Eccentricity h (ft)	**Relative Density D_R (%)**	**Row 5**	**Row 4**	**Row 3**	**Row 2**	**Row 1**
32.81	40	8.20	8.00	10.54	12.87	16.98
	80	24.43	27.00	31.28	33.42	41.57
6.56	40	17.56	17.95	6.91	18.54	22.64
	80	42.00	41.57	41.14	42.00	51.00

table, when the load eccentricity increases from 6 m (19.69 ft) to 10 m (32.81 ft), the lateral capacity of the pile group decreases from 652 kN (147 kips) to 462 kN (104 kips). In these analyses, B = 0.36 m (14.17 inches), L = 10 m (32.81 ft) and $s_c = 3B$.

The lateral capacity of a pile group is affected by the load eccentricity because the bending moment applied on the cap is partly transferred to the individual piles in the group as moments. In Figure 3.7, we represented a pile group with a soil-supported pile cap and with multiple rows of piles in the direction of the lateral loading The figure shows the three components of the reaction moments resulting from the application of an external moment on a laterally loaded pile group—(1) the moment M_a that is absorbed by axial deformation of the piles at the pile heads (2) the moment M_t that is

TABLE 3.6
The lateral capacity of individual piles (B = 0.36 = 14.17 inches, L = 10 m = 32.81 ft) in a 3 × 5 pile group loaded in the weak direction in dense sand (D_R = 80%) with a load eccentricity h = 10 m (32.81 ft) (SI units)

Row 3		Row 2		Row 1	
Pile Number	**Capacity (kN)**	**Pile Number**	**Capacity (kN)**	**Pile Number**	**Capacity (kN)**
7	50.29	4	80.23	1	128.00
8	41.44	5	57.26	2	117.12
9	45.29	6	62.71	3	123.75

TABLE 3.7
The lateral capacity of individual piles (B = 0.36 m = 14.17 inches, L = 10 m = 32.81 ft) in a 3 × 5 pile group loaded in the weak direction in dense sand (D_R = 80%) with a load eccentricity h = 10 m (32.81 ft) (USCS units)

Row 3		Row 2		Row 1	
Pile Number	**Capacity (kips)**	**Pile Number**	**Capacity (kips)**	**Pile Number**	**Capacity (kips)**
7	11.31	4	18.03	1	28.77
8	9.32	5	12.87	2	26.32
9	10.18	6	14.10	3	27.82

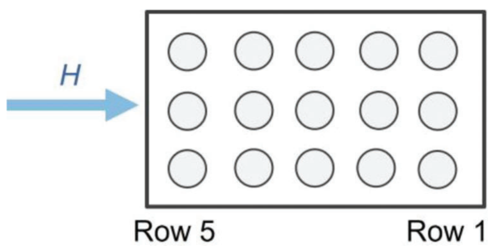

Figure 3.5 Row number definition.

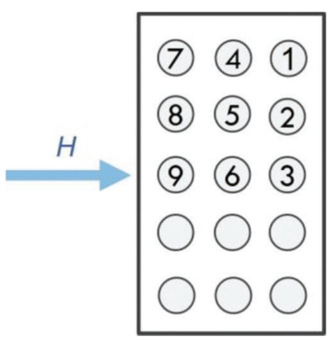

Figure 3.6 Numbers of individual piles in the 3 × 5 pile group.

transferred to the individual piles in the group as moments, and (3) the moment M_s absorbed by the resistance of the soil in contact with the pile cap. Traditionally, it has been assumed that the bending moment acting on a pile group with multiple pile rows is fully balanced by the moment M_a resulting from the increments of axial resistances of the piles in the group. However, FE simulation results show that nonnegligible moments are transferred to each of the individual piles as moments in the group, thus affecting their response to loading.

TABLE 3.8
Lateral capacities of 3 × 5 pile groups (B = 0.36 m = 14.17 inches, L = 10 m = 32.81 ft, s_c = 3B) in loose sand (D_R = 40%) loaded in the weak direction with load eccentricities h = 6 m (19.69 ft) and 10 m (32.81 ft) (SI units)

Load Eccentricity h (m)	Lateral Capacity (kN)
6	652
10	462

TABLE 3.9
Lateral capacities of 3 × 5 pile groups (B = 0.36 m = 14.17 inches, L = 10 m = 32.81 ft, s_c = 3B) in loose sand (D_R = 40%) loaded in the weak direction with load eccentricities h = 6 m (19.69 ft) and 10 m (32.81 ft) (USCS units)

Load Eccentricity h (ft)	Lateral Capacity (kips)
19.69	146
32.81	103

Figure 3.8 shows the acting (external) moment and the reaction moment components of a 3 × 5 pile group in uniform dense sand when the pile group is loaded laterally in the weak direction with a load eccentricity h = 10 m (32.81 ft). The piles in the group have a diameter B = 0.36 m (14.17 inches) and length L = 10 m (32.81 ft), and the pile spacing s_c = 3B. As shown in the figure, as the lateral deflection y_{top} of the pile head increases from 0 to 50 mm (2 inches), the reaction moment M_t transferred to the individual piles as moments in the group increases from 0% to 10% of the acting external moment. This is the main reason why the global lateral load capacity of the pile group (and the pile efficiency) decreases as the load eccentricity of the pile group increases.

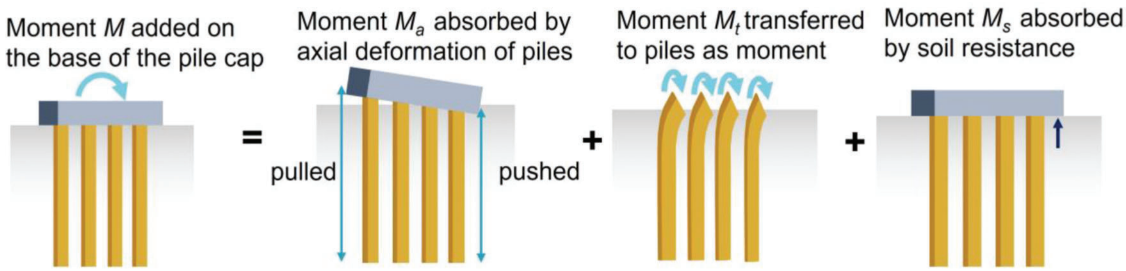

Figure 3.7 The components of reaction moments to an external moment acting on a laterally loaded pile group.

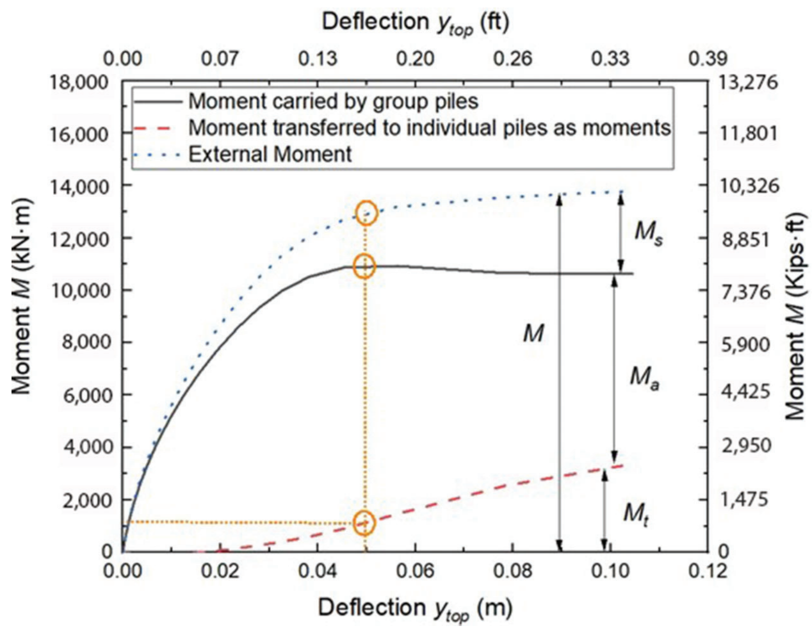

Figure 3.8 Acting (external) moment and reaction moment components of a 3 × 5 pile group in uniform dense sand laterally loaded in the weak direction.

3.3.2 Effect of Soil Properties

Table 3.10 shows the pile efficiencies and the lateral capacities of 1 × 5 pile groups in sand with relative densities D_R = 40%, 65%, and 80% loaded in the strong direction with a load eccentricity h = 2, 5, and 10 m (= 6.56 ft, 16.40 ft, and 32.81 ft). In these analyses, B = 0.36 m (14.17 inches), L = 10 m (32.81 ft) and s_c = 3B. As shown in the last column of the table, for the same load eccentricity, the lateral capacity of the pile group increases as the relative density of the sand increases.

The effect of the relative density of the sand on pile efficiency is different depending on the row number and load eccentricity. For example, when the load eccentricity is 2 m (6.56 ft), the difference in pile efficiencies for different relative densities is about 3%–10%, while when the load eccentricity is 10 m (32.81 ft), the difference is about 10%–35%. The piles in rows 4 and 5 have decreasing pile efficiencies as the relative density of the sand decreases, but the piles in the other rows do not show clear trends in pile efficiencies for different relative densities. For example, for the load eccentricity h = 5 m (16.40 ft), the average efficiency of the piles in the leading row (Row 1) decreases from 1.13 to 1.09 when the relative density decreases from 80% to 65%, but it increases from 1.09 to 1.16 when the relative density decreases from 65% to 40%.

3.3.3 Effect of Pile Group Configuration

The effects of pile group layout, pile spacing and pile cap type on the pile efficiencies and lateral capacities of the pile groups were also evaluated in this study.

Table 3.11 shows the pile efficiencies and total lateral capacities of the 1 × 5 and 3 × 5 pile groups with free-standing pile caps in dense sand (D_R = 80%) loaded in the strong direction with a load eccentricity h = 10 m (32.81 ft). In these analyses, B = 0.36 m (14.17 inches), L = 10 m (32.81 ft) and s_c = 3B. As shown in the table, a larger pile group (the 3 × 5 pile group) has a larger capacity, a slightly greater pile efficiency in the leading row (Row 1) and smaller pile efficiencies in the trailing rows (Rows 2–5). Table 3.12 provides the pile efficiencies and total lateral capacities of 1 × 5 pile groups with a free-standing pile cap and a pile spacing of 3B and 5B (B = 0.36 m = 14.17 inches and L = 10 m = 32.81 ft) in dense sand (DR = 80%) loaded in the

TABLE 3.10
Pile efficiencies and total lateral capacities of 1 × 5 pile groups (B = 0.36 m, L = 10 m, s_c = 3B) in sand with relative density D_R = 40%, 65%, and 80% loaded in the strong direction with load eccentricity h = 2, 5, and 10 m (7, 16, and 32.81 ft)

Load Eccentricity h	Soil Profile	Average Efficiency Row 5	Average Efficiency Row 4	Average Efficiency Row 3	Average Efficiency Row 2	Average Efficiency Row 1	Total Capacity
2 m (6.56 ft)	Sand (D_R = 80%)	0.98	0.97	0.96	0.98	1.19	972.16 kN (218.55 kips)
	Sand (D_R = 65%)	0.9	0.92	0.93	0.95	1.16	736.39 kN (165.55 kips)
	Sand (D_R = 40%)	0.87	0.9	0.95	1	1.3	436.12 kN (98.04 kips)
5 m (16.40 ft)	Sand (D_R = 80%)	0.84	0.87	0.9	0.93	1.13	886.38 kN (199.27 kips)
	Sand (D_R = 65%)	0.7	0.8	0.85	0.87	1.09	652.88 kN (146.67 kips)
	Sand (D_R = 40%)	0.66	0.69	0.82	0.88	1.16	362.71 kN (81.54 kips)
10 m (32.81 ft)	Sand (D_R = 80%)	0.57	0.63	0.73	0.78	0.97	705.29 kN (158.56 kips)
	Sand (D_R = 65%)	0.49	0.5	0.62	0.69	0.89	485.86 kN (109.23 kips)
	Sand (D_R = 40%)	0.42	0.41	0.54	0.66	0.87	250.44 kN (56.30 kips)

TABLE 3.11
Pile efficiencies and total lateral capacities of the 1 × 5 and 3 × 5 pile groups (B = 0.36 m = 14.17 inches, L = 10 m = 32.81 ft, s_c = 3B) with free-standing pile caps in dense sand (D_R = 80%) loaded in the strong direction with a load eccentricity h = 10 m (32.81 ft)

Layout and Load Direction	Average Efficiency Row 5	Average Efficiency Row 4	Average Efficiency Row 3	Average Efficiency Row 2	Average Efficiency Row 1	Total Capacity
1 × 5-Strong	0.57	0.63	0.73	0.78	0.97	705.29 kN (158.56 kips)
3 × 5-Strong	0.31	0.32	0.43	0.64	1.05	1,572.62 kN (353.54 kips)

TABLE 3.12
Pile efficiencies and total lateral capacities of 1 × 5 pile groups with a free-standing pile cap and a pile spacing of 3B and 5B (B = 0.36 m = 14.17 inches, L = 10 m = 32.81 ft) in dense sand (D_R = 80%) loaded in the strong direction with load eccentricity h = 2, 5, and 10 m (7, 16, and 32.81 ft)

Load Eccentricity h	Pile Spacing	Average Efficiency Row 5	Average Efficiency Row 4	Average Efficiency Row 3	Average Efficiency Row 2	Average Efficiency Row 1	Total Capacity
2 m (6.56 ft)	3B	0.98	0.97	0.96	0.98	1.19	972.16 kN (218.55 kips)
	5B	1.47	1.47	1.46	1.48	1.72	1,448.71 kN (325.68 kips)
5 m (16.40 ft)	3B	0.84	0.87	0.9	0.93	1.13	886.38 kN (199.27 kips)
	5B	1.34	1.4	1.42	1.45	1.71	1,391.53 kN (312.83 kips)
10 m (32.81 ft)	3B	0.57	0.63	0.73	0.78	0.97	705.29 kN (158.56 kips)
	5B	0.96	1.08	1.25	1.34	1.59	1,181.84 kN (265.69 kips)

Note: B = pile diameter.

strong direction with load eccentricity h = 2, 5 and 10 m (7, 16 and 32.81 ft). In these analyses, B = 0.36 m (14.17 inches), L = 10 m (32.81 ft). As shown in the table, a pile group with greater pile spacing has greater capacity and significantly higher pile efficiencies.

3.4 Laterally Loaded Group Piles in Multilayered Soil

In multilayered soil profiles, the properties of the top layers are more important than the deeper layers. We illustrate this through calculations performed for cases differing only in the thickness or stiffness of the top layer. Table 3.13 shows the lateral capacities of 1×5 pile groups in different soil profiles loaded in the weak direction with load eccentricity h = 2 m and 10 m (7 and 32.81 ft). The bottom layers of the layered soil profiles are dense sand with D_R = 80%. For all the cases, the pile diameter B is 0.36 m (14.17 inches). The considered pile lengths are shown in Table 3.13.

As shown in the table, the lateral capacity of the pile group decreases as the top weak layer increases in thickness. When the top weak layer is thicker than $10B$, the lateral capacity of the pile group becomes almost the same as the capacity of the same pile group in uniform weak soil with the same properties. In practical terms, the soil properties within the top $10B$ of the top layer of the soil profile determines the lateral capacity of the pile group.

3.5 *p*-multipliers of Individual Piles in a Group

A p-multiplier p_m is defined as the ratio of the unit soil resistance p_i of an individual pile i in the group to the unit soil resistance p_{single} of a single pile at the same level of lateral deflection y and at the same depth, as discussed earlier (see Equation 1.10).

AASHTO (2020) provides only six values for p-multipliers (these are given in Table 1.2). They depend only on pile spacing and on which row the pile is in. Estimation of pile capacities using the p-multipliers proposed by AASHTO (2020) can be exceedingly unconservative in some cases. This can be because the p-multipliers proposed by AASHTO (2020) do not consider the effects of load eccentricity (or moment), location of individual piles in a group, soil properties, and pile cap type.

Based on the FE simulation results, we suggest a new set of p-multipliers that can be used in p-y analyses of pile group. The proposed p-multipliers were developed based on analyses of the 3×5 pile groups (B = 0.36 m = 14.17 inches, L = 10 m = 32.81 ft, and s_c = $3B$) with different pile cap types (free-standing and soil-supported pile caps) in loose and dense sands (D_R = 40% and 80%) loaded in the weak direction with load eccentricity h ranging from 1 m (3.28 ft) to 10 m (32.81 ft), and are summarized in Table 3.14. The position of the pile is defined by whether the pile is located on the edge of the pile group. If the pile is located on the edge

TABLE 3.13
Lateral capacities of 1×5 pile groups (B = 0.36 m = 14.17 inches, s_c = $3B$) in different soil profiles loaded in the weak direction with a load eccentricity h = 2 and 10 m (7 and 32.81 ft)

Soil in Top Layer	Pile Length L	Load Eccentricity H	Thickness of Top Layer	Load Capacity
NC clay	20 m (65.62 ft)	10 m (32.81 ft)	$5B$	91 kN (20 kips)
			$6B$	72 kN (16 kips)
			Uniform NC clay	50 kN (11 kips)
		2 m (6.56 ft)	$10B$	137 kN (31 kips)
			Uniform NC clay	136 kN (31 kips)
Loose sand (D_R = 40%)	10 m (32.81 ft)	10 m (32.81 ft)	0 (Uniform dense sand)	172 kN (39 kips)
			$5B$	107 kN (24 kips)
			$6B$	93 kN (21 kips)
			Uniform loose sand	77 kN (17 kips)

Note: D_R = relative density, and B = pile diameter.

TABLE 3.14
Proposed *p*-multipliers

Relative Density D_r of Sand	Load Eccentricity h	Pile Cap Type	Position	Row 1	Row 2	Row 3
40%	6 m	Free-standing	Edge	0.76	0.33	0.22
	(19.69 ft)		Middle	0.56	0.22	0.16
	10 m	Soil-supported	Edge	0.95	0.25	0.2
	(32.81 ft)		Middle	0.95	0.14	0.14
80%	1 m	Free-standing	Edge	0.62	0.39	0.33
	(3.28 ft)		Middle	0.56	0.32	0.29
	10 m	Soil-supported	Edge	0.86	0.17	0.14
	(32.81 ft)		Middle	0.86	0.1	0.1

TABLE 3.15
The *p-y* analysis results using proposed *p*-multipliers

Relative Density D_R of Sand	Load Eccentricity h	Row #	*p-y* Analysis Results: Position	*p-y* Analysis Results: *p*-multiplier p_m	*p-y* Analysis Results: Capacity	*p-y* Analysis Results: Total Capacity of Each Row	*p-y* Analysis Results: Total Capacity of Pile Group	FEA Results: Total Capacity of Each Row	FEA Results: Total Capacity of Pile Group
40%	6 m	1	Edge	0.76	70 kN (16 kips)	344 kN	652 kN	330 kN	616 kN
	(19.69 ft)		Middle	0.56	68 kN (15 kips)	(77 kips)	(147 kips)	(74 kips)	(138 kips)
		2	Edge	0.33	40 kN (9 kips)	176 kN		178 kN	
			Middle	0.22	32 kN (7 kips)	(40 kips)		(40 kips)	
		3	Edge	0.22	30 kN (7 kips)	132 kN		108 kN	
			Middle	0.16	24 kN (5 kips)	(30 kips)		(24 kips)	
40%	10 m	1	Edge	0.95	65 kN (15 kips)	325 kN	440 kN	347 kN	456 kN
	(32.81 ft)		Middle	0.95	65 kN (15 kips)	(73 kips)	(99 kips)	(78 kips)	(12 kips)
		2	Edge	0.25	15 kN (3 kips)	66 kN		66 kN	
			Middle	0.14	12 kN (3 kips)	(15 kips)		(15 kips)	
		3	Edge	0.2	11 kN (2 kips)	49 kN		43 kN	
			Middle	0.14	9 kN (2 kips)	(11 kips)		(10 kips)	
80%	1 m	1	Edge	0.62	165 kN (37 kips)	786 kN	2,002 kN	836 kN	2,053 kN
	(3.28 ft)		Middle	0.56	152 kN (34 kips)	(177 kips)	(450 kips)	(188 kips)	(462 kips)
		2	Edge	0.39	152 kN (34 kips)	637 kN		638 kN	
			Middle	0.32	111 kN (25 kips)	(143 kips)		(143 kips)	
		3	Edge	0.33	123 kN (28 kips)	579 kN		579 kN	
			Middle	0.29	111 kN (25 kips)	(130 kips)		(130 kips)	
80%	10 m	1	Edge	0.86	128 kN (29 kips)	640 kN	899.5 kN	709 kN	953 kN
	(32.81 ft)		Middle	0.86	128 kN (29 kips)	(144 kips)	(202 kips)	(159 kips)	(214 kips)
		2	Edge	0.17	30 kN (7 kips)	127.5 kN		126 kN	
			Middle	0.1	22.5 kN (5 kips)	(29 kips)		(28 kips)	
		3	Edge	0.14	28.5 kN (6 kips)	132 kN		118 kN	
			Middle	0.1	25 kN (6 kips)	(30 kips)		(27 kips)	

of the pile group, the position of the pile is labeled as *Edge*, otherwise it is labeled as *Middle*. As shown in the table, the *p*-multipliers proposed in this study consider the effects of soil properties, load eccentricity, pile cap type, and position of the individual piles in the group.

Table 3.15 shows the results of *p-y* analyses using the proposed *p*-multipliers. The *p-y* analyses are performed for the pile groups in sand with relative densities D_R = 40% and 80% loaded in the weak direction with load eccentricities h = 1, 6, and 10 m (3, 20, and 32.81 ft). The moments and axial loads acting on individual piles in the group are extracted from the corresponding FEA results and considered in the *p-y* analyses. The *p-y* analyses results are also compared with FE simulation results in Table 3.15. As shown in the table, the estimated lateral capacities of pile groups from the *p-y* analyses match reasonably well the FEA results.

It is not well recognized that the moments acting on individual pile heads must be considered to perform *p-y* analysis accurately for non-zero load eccentricity cases. Table 3.16 shows an example calculation using *p-y* analysis with and without consideration of the moments at the individual pile heads. In the example calculation, the 3×5 pile group in dense sand (D_R = 80%) loaded in the weak direction with a load eccentricity h = 10 m (32.81 ft) is considered. When the actual moments at individual pile heads are not considered in the *p-y* analysis, the estimated total lateral capacity is 1,294 kN (291 kips), which is 341 kN (77 kips) greater than that obtained from the FEA results.

3.6 Estimation of Pile Efficiency for Group Piles

Pile efficiency is defined as the ratio of the lateral capacity H_i of an individual pile i in the group to the lateral capacity H_{single} of a single pile in the same soil profile loaded with an eccentricity h = 0, as we discussed earlier (see Equation 1.11).

Table 3.17 and Table 3.18 summarize the pile efficiencies obtained from the realistic 3D FE simulation results for the commonly used pile groups. Table 3.17 shows the results for pile groups with a free-standing pile cap, and Table 3.18 shows the results for pile groups with a soil-supported pile cap. The tables show average pile efficiencies of each row in the pile group, as well as the average pile efficiency for all rows in the group. With the proposed values of pile efficiency η, we can calculate the lateral capacity H_i of the i^{th} pile in the group using $H_i = \eta_i H_{single}$, where η_i is the pile efficiency of the i^{th} pile in the group.

When estimating the pile efficiency of individual piles in a group, both position and row number of the pile should be considered. Based on the FE simulation

TABLE 3.16
The *p-y* analysis for a 3 × 5 pile group loaded in weak direction in 80% sand with h = 10 m (32.81 ft) both considering and not considering the moments at the pile heads

Consideration of Moment	Row #	Position	p-multiplier p_m	Capacity	Total Capacity of Each Row	Total Capacity of Pile Group	Total Capacity of Each Row	Total Capacity of Pile Group
		p-y Analysis Results					FEA Results	
Yes	1	Edge	0.86	128 kN (30 kips)	640 kN	899.5 kN	709 kN	953 kN
		Middle	0.86	128 kN (30 kips)	(144 kips)	(202 kips)	(159 kips)	(214 kips)
	2	Edge	0.17	30 kN(7 kips)	127.5 kN		126 kN	
		Middle	0.1	22.5 kN (5 kips)	(29 kips)		(28 kips)	
	3	Edge	0.14	28.5 kN (6 kips)	132 kN		118 kN	
		Middle	0.1	25 kN (6 kips)	(30 kips)		(27 kips)	
No	1	Edge	0.86	164 kN (37 kips)	820 kN	1,294 kN	709 kN	953 kN
		Middle	0.86	164 kN (37 kips)	(184 kips)	(291 kips)	(159 kips)	(214 kips)
	2	Edge	0.17	57 kN (13 kips)	243 kN		126 kN	
		Middle	0.1	43 kN (10 kips)	(55 kips)		(28 kips)	
	3	Edge	0.14	51 kN (11 kips)	231 kN		118 kN	
		Middle	0.1	43 kN (10 kips)	(52 kips)		(26 kips)	

TABLE 3.17
Row-averaged pile efficiencies obtained from the FE analyses for individual piles in commonly used pile group layouts with a free-standing pile cap

Spacing, Layout, and Load Direction	Soil Profile	Load Eccentricity h	Row 5	Row 4	Row 3	Row 2	Row 1	Average
3B-1 × 5-strong	Sand	2 m (6.56 ft)	0.98	0.97	0.96	0.98	1.19	1.02
	(D_R = 80%)	5 m (16.40 ft)	0.84	0.87	0.90	0.93	1.13	0.93
		10 m (32.81 ft)	0.57	0.63	0.73	0.78	0.97	0.74
	Sand	2 m (6.56 ft)	0.90	0.92	0.93	0.95	1.16	0.97
	(D_R = 65%)	5 m (16.40 ft)	0.70	0.80	0.85	0.87	1.09	0.86
		10 m (32.81 ft)	0.49	0.50	0.62	0.69	0.89	0.64
	Sand	2 m (6.56 ft)	0.87	0.90	0.95	1.00	1.30	1.01
	(D_R = 40%)	5 m (16.40 ft)	0.66	0.69	0.82	0.88	1.16	0.84
		10 m (32.81 ft)	0.42	0.41	0.54	0.66	0.87	0.58
3B-2 × 5-strong	Sand	1 m (3.28 ft)	0.96	0.96	0.97	1.07	1.43	1.08
	(D_R = 80%)	5 m (16.40 ft)	0.63	0.69	0.77	0.92	1.32	0.87
		10 m (32.81 ft)	0.38	0.41	0.53	0.74	1.14	0.64
3B-3 × 5-strong	Sand	1 m (3.28 ft)	0.83	0.82	0.86	0.96	1.28	0.95
	(D_R = 80%)	5 m (16.40 ft)	0.54	0.57	0.66	0.82	1.19	0.75
		10 m (32.81 ft)	0.31	0.32	0.43	0.64	1.05	0.55
3B-3 × 5-weak	Sand	1 m (3.28 ft)	–	–	0.78	0.87	1.12	0.92
	(D_R = 80%)	6 m (19.69 ft)	–	–	0.36	0.54	0.92	0.61
		10 m (32.81 ft)	–	–	0.25	0.42	0.72	0.46
	Sand	1 m (3.28 ft)	–	–	0.65	0.78	1.12	0.85
	(D_R = 40%)	6 m (19.69 ft)	–	–	0.30	0.42	0.77	0.50
		10 m (32.81 ft)	–	–	0.18	0.28	0.60	0.35
3B-1 × 5-weak	Sand	2 m (6.56 ft)	–	–	–	–	0.55	0.55
	(D_R = 80%)	5 m (16.40 ft)	–	–	–	–	0.31	0.31
		10 m (32.81 ft)	–	–	–	–	0.18	0.18
	Sand	2 m (6.56 ft)	–	–	–	–	0.59	0.59
	(D_R = 40%)	5 (16.40 ft)	–	–	–	–	0.36	0.36
		10 (32.81 ft)	–	–	–	–	0.20	0.20
5B-1 × 5-strong	Sand	2 (6.56 ft)	1.47	1.47	1.46	1.48	1.72	1.52
	(D_R = 80%)	5 (16.40 ft)	1.34	1.40	1.42	1.45	1.71	1.46
		10 (32.81 ft)	0.96	1.08	1.25	1.34	1.59	1.24

Note: D_R = relative density; B = pile diameter.

TABLE 3.18
Row-averaged pile efficiencies obtained from the FE analyses for individual piles in commonly used pile group layouts with a soil-supported pile cap

Spacing, Layout, and Load Direction	Soil Profile	Eccentricity *h*	Row 5	Row 4	Row 3	Row 2	Row 1	Average
$3B$-1 × 5-weak	Sand (D_R = 40%)	10 m (32.81 ft)	–	–	–	–	0.18	0.18
	Sand (D_R = 80%)	10 m (32.81 ft)	–	–	–	–	0.18	0.18
$3B$-1 × 5-strong	Sand (D_R = 80%)	10 m (32.81 ft)	0.36	0.23	0.35	0.89	1.40	0.64
	Sand (D_R = 40%)	10 m (32.81 ft)	0.31	0.28	0.28	0.68	1.20	0.55
$3B$-2 × 5-strong	Sand (D_R = 80%)	10 m (32.81 ft)	0.27	0.21	0.31	0.66	1.28	0.54
$3B$-3 × 5-weak	Sand (D_R = 40%)	10 m (32.81 ft)	–	–	0.10	0.15	0.80	0.35
	Sand (D_R = 80%)	10 m (32.81 ft)	–	–	0.12	0.13	0.74	0.33
$3B$-1 × 5-weak	NC clay over sand (D_R = 80%) (t_w = $5B$)	10 (32.81 ft)					0.23	0.23
$3B$-1 × 5-weak	NC Clay	10 (32.81 ft)					0.23	0.23
$3B$-1 × 5-weak	Sand (D_R = 40%) over sand (D_R = 80%) (t_w = $5B$)	10 (32.81 ft)			0.44	0.54	0.85	0.6

Note: D_R = relative density; B = pile diameter; t_w = thickness of weak soil layer.

TABLE 3.19
Factors considered in the pile efficiency equation

Factors	Units	Meaning
h	Length	Load eccentricity
x	Length	Distance from the pile center to the center of the nearest pile on the leading edge of the group, as shown in Figure 3.9
y	Length	Distance of the pile center to the center of the nearest pile on an edge of the pile group that is parallel to the load direction, as shown in Figure 3.9
B^*	Length	Distance between the midline of the leading row and the midline of the very last trailing row, as shown in Figure 3.9
L^*	Length	Distance from an edge of the pile group parallel to the load direction to the line passing through the center of all rows, as shown in Figure 3.9

results, we propose an equation for the pile efficiencies of individual piles in a group. The factors considered in the equation are listed in Table 3.19.

The equation for pile efficiency η for pile groups with free-standing pile cap is given by

$$\eta = -0.020h\left(\frac{x}{B^*}\right)^2 + 0.00053h^2L^{*2} + 0.0062hB^* + 0.63\left(\frac{x}{B^*}\right)^2 - 0.92\frac{x}{B^*} - 0.074\frac{y}{L^*} + 0.16B^* - 0.067h + 0.66 \quad \text{(Eq. 3.1)}$$

where L_R is the reference length, which is either 1 m for SI units or 3.281 ft for U.S. customary units.

The equation was derived based on FE simulation results. The fitting results are shown in Figure 3.10. As shown in the figure, data lie evenly on two sides of the identity line. Note that soil properties and pile group configurations are not considered in Equation 3.1. Equation 3.1 is applicable for soil profiles and pile group configurations falling within the range broadly defined by the soil profiles and pile group configurations considered in this study.

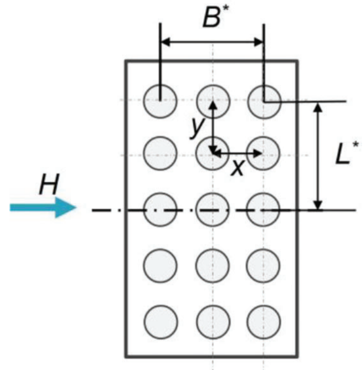

Figure 3.9 Factors considered in the pile efficiency equations.

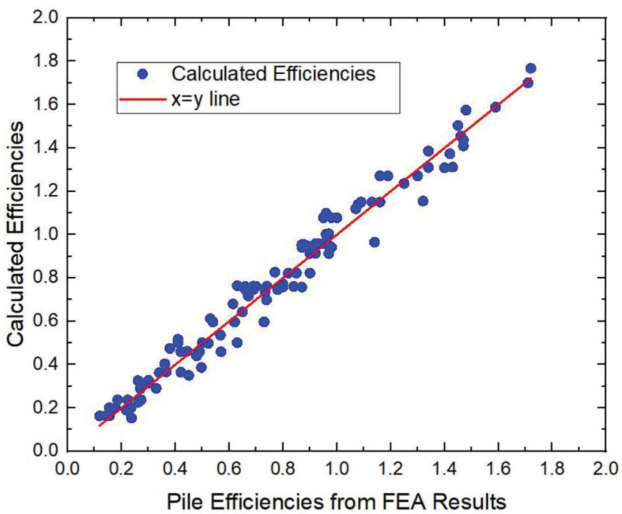

Figure 3.10 Fitting results for pile efficiency equation.

Because the data set used to derive Equation 3.1 contains more results for 1×5 pile groups in sand than for other group configurations or piles in clay, the equation should be improved by performing additional simulations covering a wider range of soil profiles and pile group configurations.

4. PROPOSED DESIGN GUIDELINES AND EXAMPLES

4.1 Design Guidelines for Piles in Weak Soils

4.1.1 Critical Scenarios

Single-row pile group may be very vulnerable to lateral loads, especially under large load eccentricity. The lateral capacities of all the single row pile groups considered in the research are summarized in Table 4.1. We assumed that a pile group is designed to carry 8.9 kN (2 kips) of lateral load per pile, and we chose a factor of safety equal to 3 to apply to this load. We selected two deflection levels of 25 mm (1 inch) and 50 mm (2 inches) to define two possible ultimate limit states. Table 4.1 also indicates whether the pile group passed the safety check for these two deflection levels.

We can see from Table 4.1 that acceptable designs for 1-inch lateral deflection are not achievable. For 50-mm (2 inches) lateral deflection, single-row pile groups should be avoided when they are loaded in the weak direction and the following conditions exist.

- The load eccentricity is large (5 m (16.40 ft) for NC clay and 10 m (32.81 ft) for loose sand).
- The thickness of the top weak soil layer is greater than 5*B*, where *B* is pile diameter.
- The soil at the top is loose sand ($D_R < 40\%$) or NC clay. The corresponding limiting representative corrected SPT blow count for these weaker layers can be taken as 7. The representative blow count can be taken as the average N_{60} over the top 5*B* of pile length.

In addition to the lateral deflection, rotation at the pile head may also be considered during design. The rotation at the pile head for the single-row pile groups are summarized in Table 4.2. The piles used in sand are 10 m (32.81 ft) in length and 0.36 m (14.17 inches) in diameter, and the piles used in clay are 20 m (65.62 ft) in length and 0.36 m (14.17 inches) in diameter. The spacing between piles is 3*B,* where *B* is pile diameter.

4.1.2 Lateral Capacity Estimation

4.1.2.1 Method 1: *p-y* analysis using *p*-multipliers. When the entire structural system, composed of the piles and the superstructure, are analyzed at the same time to evaluate the stability of the system, the concept of the *p*-multiplier could be easier to use than the concept of pile efficiency, because an engineer just needs to consider soil resistances (*p-y* curves) around the piles, and does not need to concern himself with the actual loads and/or moments acting on the pile group. The estimation of pile lateral capacity using a *p-y* analysis together with *p*-multipliers is represented in flowchart form in Figure 4.1.

As discussed in Section 3.5, the *p*-multiplier method requires knowledge of the actual loads and moments acting at the individual pile heads in the pile group to produce accurate results using *p-y* analysis. However, in most cases, the actual loads and moments at individual pile heads are unknown for pile groups when there are multiple rows aligned with the loading direction. Without an accurate estimation of loads and moments at the pile heads, the estimated lateral capacities of pile groups using *p-y* analysis and *p*-multipliers could be very unconservative.

4.1.2.2 Method 2: *p-y* analysis using pile efficiencies. For the given loads and moments acting on the pile group, the lateral capacity of the pile group can be estimated using *p-y* analysis and pile efficiencies. Unlike the p-multiplier method, this method does not require an information of loads and moments at individual pile heads in the pile group.

TABLE 4.1
Lateral capacity of single-row pile groups

Soil Profile	Representative SPT Blow Count N_{60} Over the Depth of $5B$	Pile Cap Type	Load Eccentricity H	Lateral Capacity Per Pile for Y_{top} = 1 in.	Passed Safety Check? (FS = 3)	Lateral Capacity Per Pile for Y_{top} = 2 in.	Passed Safety Check? (FS = 3)
Sand $D_R = 65\%$	19	Soil-supported	10 m (32.81 ft)	10.39 kN (2.3 kips)	No	32.02 kN (7.2 kips)	Yes
Sand $D_R = 80\%$	28	Soil-supported	10 m (32.81 ft)	–	–	34.31 kN (7.7 kips)	Yes
Sand $D_R = 40\%$	7	Soil-supported	10 m (32.81 ft)	6.78 kN (1.5 kips)	No	15.32 kN (3.4 kips)	No
NC clay	3	Soil-supported	2 m (6.56 ft)	18.74 kN (4.2 kips)	No	27.12 kN (6.1 kips)	Yes
	3	Free-standing	5 m (16.40 ft)	12.01 kN (2.7 kips)	No	19.47 kN (4.4 kips)	No
	3	Soil-supported	10 m (32.81 ft)	6 kN (1.3 kips)	No	10 kN (2.2 kips)	No
NC clay over sand $D_R = 80\%$ ($t_w = 5B$)	3	Soil-supported	10 m (32.81 ft)	9.64 kN (2.2 kips)	No	18.2 kN (4.1 kips)	No
NC clay over sand $D_R = 80\%$ ($t_w = 6B$)	3	Soil-supported	10 m (32.81 ft)	7.99 kN (1.8 kips)	No	14.34 kN (4.2 kips)	No
NC clay over sand $D_R = 80\%$ ($t_w = 10B$)	3	Soil-supported	2 m (6.56 ft)	17.82 kN (4.0 kips)	No	27.44 kN (6.2 kips)	Yes
Sand $D_R = 40\%$ over sand $D_R = 80\%$ ($t_w = 5B$)	7	Soil-supported	10 m (32.81 ft)	9.42 kN (2.1 kips)	No	21.4 kN (4.8 kips)	No
Sand $D_R = 40\%$ over sand $D_R = 80\%$ ($t_w = 6B$)	7	Soil-supported	10 m (32.81 ft)	8.63 kN (1.9 kips)	No	18.52 kN (4.2 kips)	No

Note: D_R = relative density of sand; t_w = thickness of top weak soil layer; B = pile diameter; y_{top} = lateral deflection at the pile head; and FS = factor of safety.

With the new proposed *p-y* curves and the pile efficiencies discussed earlier, we can estimate the lateral capacity of a pile group in three steps.

Step 1. Perform a p-y analysis to obtain the lateral load capacity H_{single} of a single pile. This can be done using any reliable *p-y* analysis program. The *p-y* analysis should be done using the *p-y* curves developed in this project. Use Equation 2.1 for sandy soil and Equation 2.5 for NC clay for the *p-y* curves at different depths. A load eccentricity $h = 0$ should be used in the analysis to determine H_{single}.

Step 2. Obtain the pile efficiency for each individual pile in the pile group. Obtain the pile efficiency for each individual pile in the pile group by referring to Equation 3.1

Step 3. Calculate the lateral capacity H_{group} for the pile group. The lateral capacity H_{group} of the pile group with a number n_{p} of piles can be calculated from:

$$H_{group} = \sum_{i=1}^{n_p} \eta_i H_{\text{single}} \qquad \text{(Eq. 4.1)}$$

where η_i is the pile efficiency of i^{th} pile in the group, and n_p is the total number of piles in the pile group.

Figure 4.2 summarizes the design process for laterally loaded piles using *p-y* analysis and pile efficiencies.

4.1.3 Lateral Stability Evaluation

Engineers sometimes analogize a pile partially embedded in soil to a fixed-end Bernoulli beam using a "depth to fixity" for doing the buckling check. The calculated depth to fixity has direct impact on the calculated buckling load. We calculated the depth to fixity from the results of *p-y* analysis using the proposed *p-y* curves and compared the results to those calculated using the AASHTO (2020) equations.

The idea behind the depth to fixity is that the partially embedded pile is modeled as an equivalent fixed-ended Bernoulli beam that reaches the same lateral deflection as the pile when acted upon by the loading. The required length of the equivalent Bernoulli beam L_e will exceed the length of the free length L_u (the length above ground) of the pile. The difference between the two lengths is called the depth to fixity d_f. The concept is illustrated in Figure 4.3.

The critical buckling load P_{cr} would then be calculated using Euler buckling theory.

TABLE 4.2
Rotation at pile head in single-row pile group

Soil Profile	Cap Type	Eccentricity *h*	Rotation θ_2 for y_{top} = 50 mm (2 in.)	Lateral Displacement at Load Point $\theta_2 h$	Rotation θ_1 for y_{top} = 25 mm (1 in.)	Lateral Displacement at Load Point $\Theta_1 h$
Sand D_R = 65%	Soil-supported	10 m (32.81 ft)	2.31°	0.40 m (15.7 in.)	1.26°	0.22 m (8.7 in)
Sand D_R = 80%	Soil-supported	10 m (32.81 ft)	2.57°	0.45 m (17.7 in)	1.39°	0.24 m (9.4 in)
Sand D_R = 40%	Soil-supported	10 m (32.81 ft)	1.84°	0.32 m (12.6 in)	1.00°	0.17 m (6.7 in)
NC clay	Soil-supported	2 m (6.56 ft)	0.98°	0.03 m (1.2 in)	0.56°	0.02 m (0.8 in)
	Free-standing	5 m (16.40 ft)	1.16°	0.10 m (3.9 in)	0.64°	0.06 m (2.4 in)
	Soil-supported	10 m (32.81 ft)	1.20°	0.21 m (8.3 in)	0.69°	0.12 m (4.7 in)
NC clay over sand D_R = 80% (t_w = 5*B*)	Soil-supported	10 m (32.81 ft)	1.42°	0.25 m (9.8 in)	1.42°	0.25 m (9.8 in)
NC clay over sand D_R = 80% (t_w = 6*B*)	Soil-supported	10 m (32.81 ft)	1.35°	0.23 m (9.1 in)	0.72°	0.13 m (5.1 in)
NC clay over sand D_R = 80% (t_w = 10*B*)	Soil-supported	2 m (6.56 ft)	1.00°	0.03 m (1.2 in)	0.55°	0.02 m (0.8 in)
Sand D_R = 40% over sand D_R = 80% (t_w = 5*B*)	Soil-supported	10 m (32.81 ft)	2.12°	0.37 m (14.6 in)	1.08°	0.19 m (7.5 in)
Sand D_R = 40% over sand D_R = 80% (t_w = 6*B*)	Soil-supported	10 m (32.81 ft)	1.94°	0.34 m (13.4 in)	1.06°	0.19 m (7.5 in)

Note: D_R = relative density of sand; t_w = thickness of top weak soil layer; *B* = pile diameter; and y_{top} = lateral deflection at the pile head.

$$P_{cr} = \frac{\pi^2 EI}{\left(L_u + d_f\right)^2} \qquad \text{(Eq. 4.2)}$$

where *EI* is the bending stiffness of the pile.

AASHTO (2020) has provided equations for the depth to fixity that can also be used with Equation 4.2. In the AASHTO (2020) equations, depth to fixity is a function of the bending stiffness *EI* of the pile and the Young's modulus E_s of the soil. For clay:

$$d_f = 1.4\sqrt[4]{\frac{EI}{E_s}} \qquad \text{(Eq. 4.3)}$$

where E_s is equal to $0.465 s_u$, and s_u is the undrained shear strength of clay. AASHTO (2020) also provides suggested values for E_s, as shown in Table 4.3.

For sand, the depth to fixity according to AASHTO (2020) is given by:

$$d_f = 1.8\sqrt[5]{\frac{EI}{n_h}} \qquad \text{(Eq. 4.4)}$$

where n_h is the rate of increase of soil modulus with increasing depth for sand, which is given in Table 4.4.

To calculate the depth to fixity, we first perform *p-y* analyses with the free length L_u of the pile above the ground, the embedded length *L* of the pile, the cross section of the pile, the soil profile and the axial load acting on the pile as variables. For any given combination of values for these variables, we obtain, from the *p-y* analyses, the load-deflection curve. From the load-deflection curve, we obtain the axial load, lateral load and the moment acting on the pile at a targeted lateral deflection level. After that, we solve a partial differential equation (PDE) for the fixed-ended Bernoulli beam with the same pile geometry under the same axial and lateral loads and moment acting on the pile at the targeted lateral deflection. By trying different lengths for the beam, we can find the depth to fixity d_f, which is the length of the beam providing the targeted lateral deflection under the axial load, lateral load and moment acting on the pile at the targeted lateral deflection.

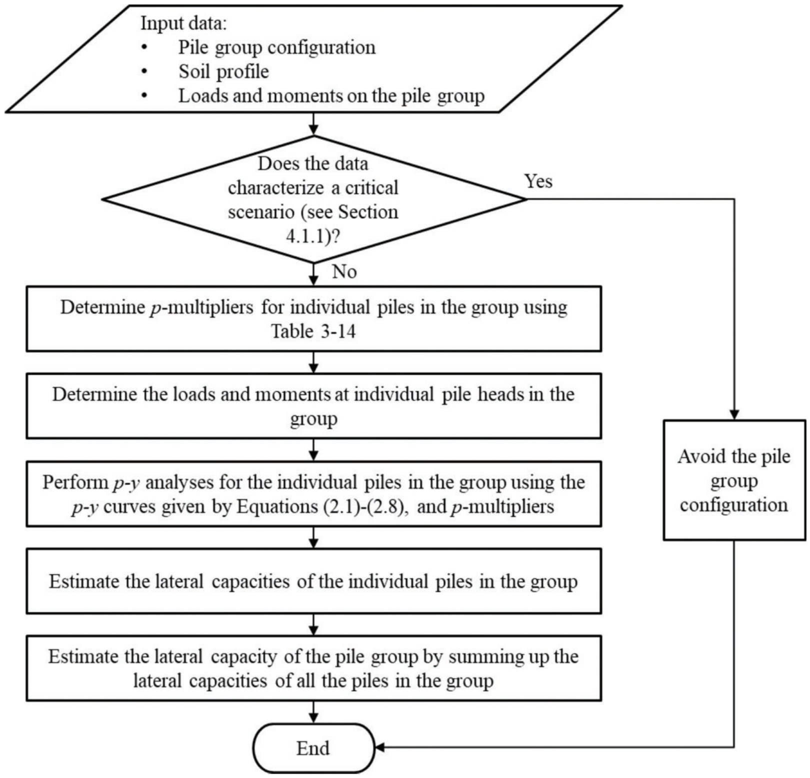

Figure 4.1 Flowchart for p-multiplier method.

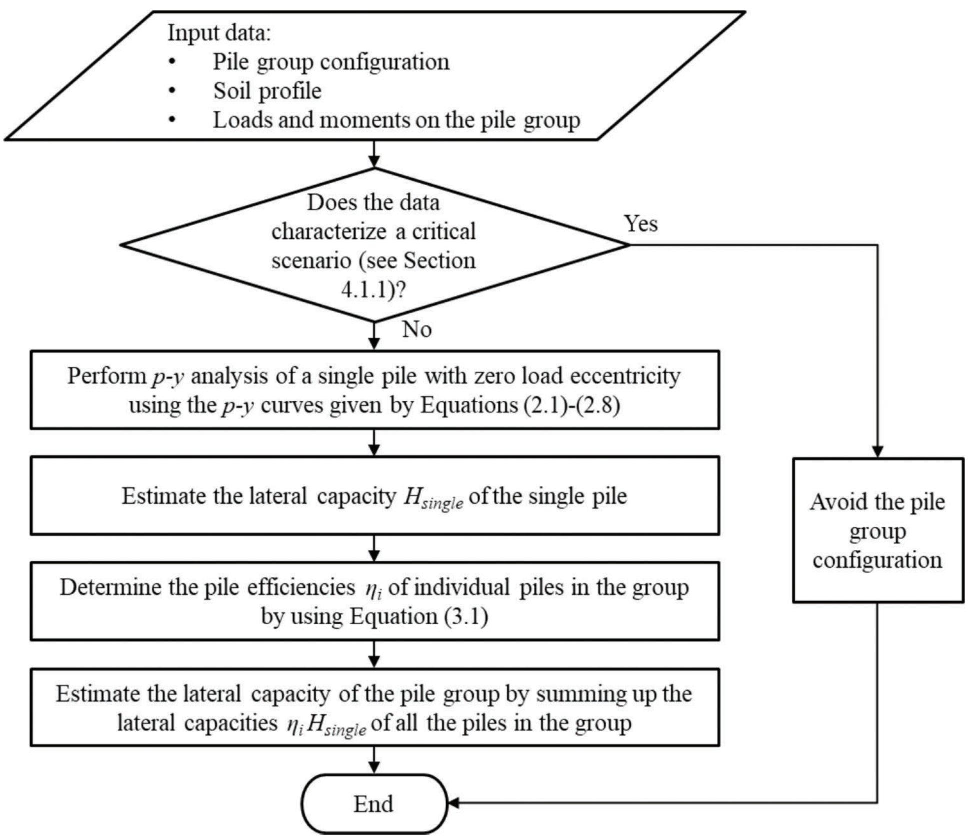

Figure 4.2 Flowchart for pile efficiency method.

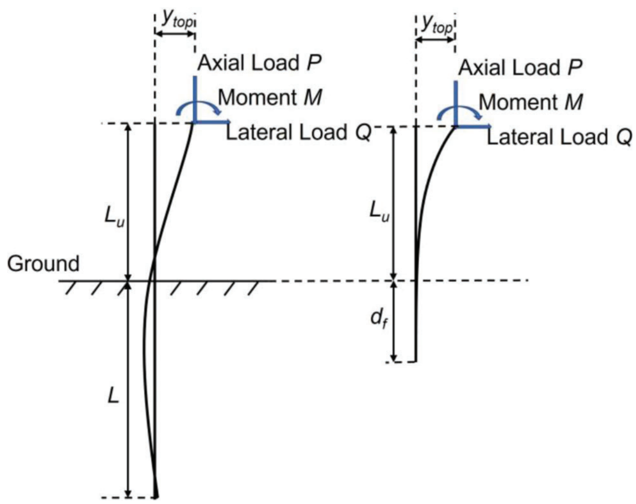

Figure 4.3 The depth to fixity d_f is the difference in length between the free length of the pile above ground and the length of a fixed-ended beam required to have the same deflection at its top as that at the top of the pile (modified from Davisson & Robinson, 1965).

TABLE 4.3
Young's modulus E_s for clay suggested by AASHTO (2020)

Clay Type	E_s (ksi)
Soft Sensitive	0.347–2.08
Medium Stiff to Stiff	2.08–6.94
Very Stiff	6.94–13.89

TABLE 4.4
The n_h for sand suggested by AASHTO (2020)

Consistency	Dry or Moist (ksi/ft)	Submerged (ksi/ft)
Loose	0.417	0.208
Medium	1.11	0.556
Dense	2.78	1.39

The governing differential equation of the fixed-end Bernoulli beam is

$$EI\left(\frac{d^4y}{dx^4}\right)+P\left(\frac{d^2y}{dx^2}\right)=0 \qquad \text{(Eq. 4.5)}$$

where P is the axial load in the beam. The directions of the x and y coordinates are shown in Figure 4.3.

For some cases, we performed p-y analysis and calculated the depth to fixity as well as the critical buckling load and compared the results with those calculated using the AASHTO (2020) method. The axial load added to the pile while performing p-y analysis was considered to be the service load, which was taken as the ultimate load estimated using the Purdue Pile Design Method (Salgado, 2022) divided by a factor of safety of 3. The cases considered in the p-y analyses are summarized in Table 4.5. In cases 3 and 4, the Young's modulus E_s of NC clay is determined in different ways. In case 3, E_s is determined from Table 4.3 as 2,392 kPa (0.347 ksi), and in case 4, E_s is determined by the relationship $E_s = 0.465s_u$, where s_u is the undrained shear strength of clay. The undrained shear strength s_u of NC Boston Blue Clay, for example, increases linearly with increasing vertical effective stress σ'_v according to: $s_u = 0.2\sigma'_v$. To find the representative s_u within the depth to fixity d_f, we iterated calculations until we found the value of s_u at the depth of $0.5d_f$ and determined E_s to be 8 kPa (0.0012 ksi).

It is important to stress that partially embedded piles cannot be equivalent to a fixed-end Bernoulli beam for all deflections. We selected three values of lateral deflections and calculated the corresponding values of depth to fixity for each. The results are summarized in Table 4.6.

We can see from Table 4.6 that the depth to fixity calculated using the p-y analysis is generally greater than that calculated using the AASHTO (2020) method. Accordingly, the critical buckling load calculated by using the depth to fixity obtained from p-y analysis is also generally less than that calculated using the AASHTO (2020) method. However, the calculated buckling load is generally much greater than the service load added to the pile head, regardless of the method used. This means that buckling is unlikely to be a critical limit state.

There is another definition of depth to fixity mentioned in the AASHTO (2020) manual. This independent definition of depth to fixity is used to check the pile resistance against external forces. The piles are assumed to be fixed for depths greater than the depth to fixity. This means that, for those cross sections, only axial resistance is checked. Above the depth to fixity, combined axial load and flexure would be considered. No equations are provided by AASHTO (2020) for this definition of depth to fixity, but AASHTO (2020) seems to suggest that this second "depth to fixity" should be obtained from p-y analysis results. If that is the case, this seems unnecessary, because the shear force and bending moment along the pile are directly obtained from p-y analysis results.

From the p-y analysis results, we can extract two zero-deflection points, as shown in Figure 4.4. The depths to those two zero-deflection points are referred to as depths to fixity 1 and 2. In finite element analysis results, only one depth to fixity could be seen. We performed p-y analysis for single piles with combined axial and lateral load as well as with only lateral load. The p-y analysis results and the finite element results for the depth to fixity are summarized in Table 4.7.

If structural engineers wished to do a safety check using the second definition of the depth to fixity, they should select the largest possible depth to fixity (depth

TABLE 4.5
Cases considered in *p-y* analyses to determine the depths of fixity and critical buckling loads

Case #	Soil Profile	Pile Geometry: Diameter B	Length L	Bending Stiffness EI	Axial Load at Pile Head
1	Sand DR = 40%	0.36 m (14.17 in.)	10 m (32.81 ft)	20,911 kN·m^2 (436 kips·ft^2)	256 kN (28 kips)
2	Sand DR = 80%	0.36 m (14.17 in.)	10 m (32.81 ft)	20,911 kN·m^2 (436 kips·ft^2)	536 kN (120 kips)
3	NC clay (Es = 2,392 kPa = 0.347 ksi)	0.36 m (14.17 in.)	20 m (65.62 ft)	30,587 kN·m^2 (637 kips·ft^2)	193 kN (43 kips)
4	NC clay (Es = 8 kPa = 0.0012 ksi)	0.36 m (14.17 in.)	20 m (65.62 ft)	30,587 kN·m^2 (637 kips·ft^2)	193 kN (43 kips)

Note: D_R = relative density of sand, and E_s = Young's modulus of clay.

TABLE 4.6
Depth to fixity calculated from *p-y* analysis and from AASHTO (2020) method

Case #	L_u	Depth to Fixity d_f: *p-y* Analysis for y_{top} = 2 in.	*p-y* Analysis for y_{top} = 0.8 in.	*p-y* Analysis for y_{top} = 0.2 in.	AASHTO (2020)	Critical Buckling Load: *p-y* Analysis for y_{top} = 2 in.	AASHTO (2020)
1	1 m (3.28 ft)	2.27 m (7.45 ft)	2.09 m (6.86 ft)	2.02 m (6.63 ft)	1.44 m (4.72 ft)	19,291 kN (4,336 kips)	34,647 kN (7,788 kips)
	2 m (6.56 ft)	2.15 m (7.05 ft)	2.04 m (6.69 ft)	2.04 m (6.69 ft)	1.44 m (4.72 ft)	11,977 kN (2,692 kips)	1,7431 kN (3,918 kips)
	5 m (16.40 ft)	1.86 m (6.10 ft)	1.86 m (6.10 ft)	1.86 m (6.10 ft)	1.44 m (4.72 ft)	4,383 kN (985 kips)	4,974 kN (1,118 kips)
2	1 m (3.28 ft)	2.99 m (9.81 ft)	2.75 m (9.02 ft)	2.63 m (8.63 ft)	2.11 m (6.92 ft)	12,957 kN (2,912 kips)	21,327 kN (4,794 kips)
	2 m (6.56 ft)	2.81 m (9.22 ft)	2.62 m (8.60 ft)	2.61 m (8.56 ft)	2.11 m (6.92 ft)	8,916 kN (2,004 kips)	12,211 kN (2,745 kips)
	5 m (16.40 ft)	2.46 m (8.06 ft)	2.45 m (8.04 ft)	2.45 m (8.03 ft)	2.11 m (6.92 ft)	3,707 kN (833 kips)	4,080 kN (917 kips)
	8 m (26.24 ft)	2.51 m (8.23 ft)	2.51 m (8.23 ft)	2.51 m (8.23 ft)	2.11 m (6.92 ft)	1,867 kN (419 kips)	2,018 kN (454 kips)
3	1 m (3.28 ft)	3.69 m (12.11 ft)	3.14 m (10.30 ft)	2.71 m (8.89 ft)	2.65 m (8.69 ft)	13,726 kN (3,085 kips)	22,662 kN (5,095 kips)
	2 m (6.56 ft)	3.28 m (10.76 ft)	2.79 m (9.15 ft)	2.48 m (8.14 ft)	2.65 m (8.69 ft)	10,830 kN (2,434 kips)	13,963 kN (3,139 kips)
	5 m (16.40 ft)	2.55 m (8.36 ft)	2.32 m (7.61 ft)	2.18 m (7.15 ft)	2.65 m (8.69 ft)	5296 kN (1,190 kips)	5,159 kN (1,160 kips)
	8 m (26.24 ft)	1.72 m (5.64 ft)	1.64 m (5.38 ft)	1.47 m (4.82 ft)	2.65 m (8.69 ft)	3,196 kN (718 kips)	2,662 kN (598 kips)
	10 m (32.81 ft)	1.26 m (4.13 ft)	1.22 m (4.00 ft)	1.02 m (3.35 ft)	2.65 m (8.69 ft)	2,381 kN (535 kips)	1,887 kN (424 kips)
4	1 m (3.28 ft)	3.69 m (12.11 ft)	3.14 m (10.30 ft)	2.71 m (8.89 ft)	10.97 m (35.99 ft)	13,726 kN (3,085 kips)	2,107 kN (474 kips)
	2 m (6.56 ft)	3.28 m (10.76 ft)	2.79 m (9.15 ft)	2.48 m (8.14 ft)	10.97 m (35.99 ft)	10,830 kN (2,434 kips)	1,795 kN (403 kips)
	5 m (16 ft)	2.55 m (8.36 ft)	2.32 m (7.61 ft)	2.18 m (7.15 ft)	10.97 m (35.99 ft)	5,296 kN (1,190 kips)	1,184 kN (266 kips)
	8 m (26.24 ft)	1.72 m (5.64 ft)	1.64 m (5.38 ft)	1.47 m (4.82 ft)	10.97 m (35.99 ft)	3,196 kN (718 kips)	839 kN (189 kips)
	10 m (32.81 ft)	1.26 m (4.13 ft)	1.22 m (4.32 ft)	1.02 m (3.35 ft)	10.97 m (10.99 ft)	2,381 kN (535 kips)	687 kN (154 kips)

Note: L_u = free length of the pile above the ground and y_{top} = lateral deflection at the pile head.

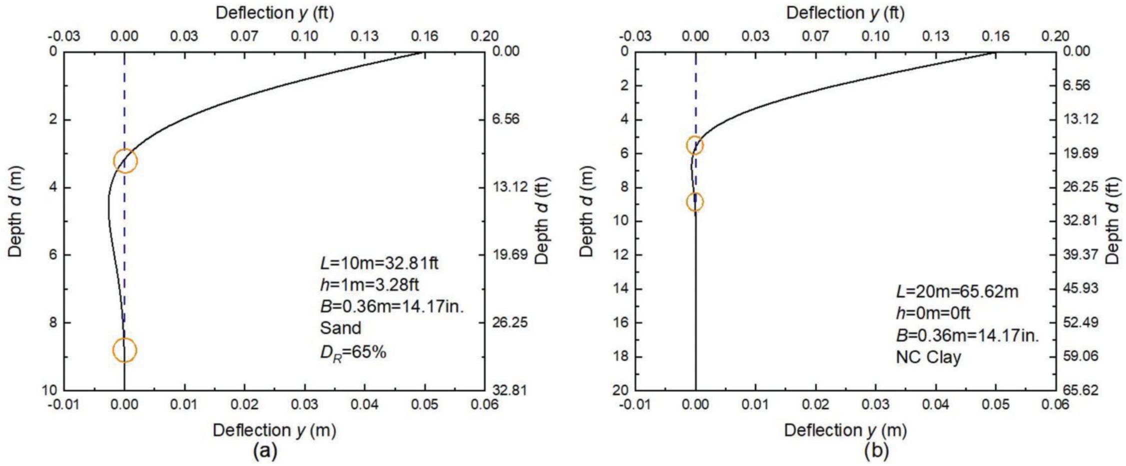

Figure 4.4 Typical deformed configurations for lateral loaded piles at the ultimate limit state in (a) sand, and (b) NC clay.

to fixity 2), which corresponds to the second, deeper zero deflection point calculated by the *p-y* analysis.

We stress again that there are two different definitions of depth to fixity in AASHTO (2020). One should not use the equations provided in the AASHTO (2020) manual—Equations 4.3 and 4.4 in this report—to calculate the depth to fixity for the purpose of performing cross-section resistance checks or use the depth to fixity corresponding to the zero-deflection point obtained from a *p-y* analysis to do buckling checks.

4.2 Design Examples for Lateral Capacity Estimation

In this chapter, four design examples are prepared to show how the proposed design method are used in actual design work. In the examples, we use the pile efficiency method (Method 2 described in Section 4.1.2.2) to estimate lateral capacities of pile groups. As mentioned before, the equation for pile efficiency was developed deliberately to be conservative. Thus, the calculated pile capacity would be smaller than that from FEA more frequently than not.

4.2.1 3 × 5 Pile Group in Layered Sand

A 3×5 pile group with a center-to-center spacing $s_c = 3B$ in a two-layer sand profile (as shown in Figure 4.5) is loaded laterally in its weak direction. The piles are 0.36 m (14.17 inches) in diameter and 10 m (32.81 ft) in length. The load is applied at a height of 10 m (32.81 ft) from the ground surface. To estimate the lateral load capacity of the pile group, we follow the three steps specified in Section 4.1.2.2.

Step 1. Perform p-y analysis to obtain the lateral load capacity H_{single} of a single pile. Using the *p-y* curves developed in this project, we performed a *p-y* analysis for a single pile with the same dimensions as those of the individual piles in the group using *p-y* analysis software PYGMY (Stewart, 2000). We considered a load eccentricity h = 0 in the analysis. Figure 4.6 shows the lateral load-deflection response obtained from the *p-y* analysis. The detailed *p-y* curve data used in the *p-y* analysis are shown in Figure 4.7. In the *p-y* analysis, we discretized soil into 18 layers, each with a thickness equal to approximately 0.18 m (0.59 ft). The *p-y* curves shown in Figure 4.7 were used to represent the mechanical response of each layer. Below the top 4 m (13.28 ft), the API *p-y* curves were used; however, the lateral deflections were approximately zero there. The lateral capacity of the single pile corresponding to a lateral deflection y = 50 mm (2 inches) is obtained from the load-deflection curve: H_{single} = 103 kN (23.16 kips).

Step 2. Obtain the pile efficiencies for the individual piles in the pile group. Using Equation 3.1, the pile efficiency η for all the individual piles in the pile group can be calculated. Because of symmetry, only nine piles must be considered. The results are summarized in Table 4.8. The pile indexes are shown in Figure 4.8.

Step 3. Calculate the lateral capacity H_{group} for the pile group. The lateral capacity of the individual piles in the pile group can now be calculated. The results are summarized in Table 4.8.

The total lateral capacity H_{group} of the pile group is 628 kN (141 kips), which is smaller than that (= 955 kN = 215 kips) obtained from the 3D FE analysis, as shown in Table 4.9. In comparison, the lateral capacity of the pile group is estimated to be 1,735 kN (390 kips) by using the design method prescribed by AASHTO (2020), which is exceedingly unconservative for this example. The *p-y* curved used by the AASHTO (2020) method are the API curves shown in Figure 4.9.

4.2.2 1 × 5 Pile Group in Layered Sand

A 1×5 pile group with a center-to-center spacing $s_c = 3B$ in a two-layer sand profile (as shown in Figure 4.10) is loaded laterally in its weak direction. The piles are 0.36 m (14.17 inches) in diameter and 10 m (32.81 ft) in length. The load is applied at a height of 10 m (32.81 ft) from the ground surface. To estimate the lateral load capacity of the pile group, we follow the three steps specified in Section 4.1.2.2.

TABLE 4.7
Depth to fixity read from *p-y* analysis results and finite element analysis results

Soil Profile	Axial Load	Load Eccentricity	Lateral Capacity	Depth to Fixity 1	Depth to Fixity 2	Depth to Fixity from FE Result (if available)
Dry Sand D_R = 40%	0	0	87 kN (20 kips)	4 m (13.1 ft)	9.1 m (29.9 ft)	4.24 m (13.91 ft)
Dry Sand D_R = 40%	800 kN (180 kips)	0	75 kN (17 kips)	3.8 m (12.5 ft)	9 m (29.5 ft)	
Dry Sand D_R = 40%	1,600 kN (360 kips)	0	63 kN (14 kips)	3.7 m (12.1 ft)	9 m (29.5 ft)	
Dry Sand D_R = 40%	800 kN (180 kips)	5 m (16.40 ft)	27 kN (6 kips)	3 m (9.8 ft)	8.5 m (27.9 ft)	
Dry Sand D_R = 65%	0	0	130 kN (29 kips)	3.5 m (11.5 ft)	9.4 m (30.8 ft)	
Dry Sand D_R = 65%	0	1 m (3.28 ft)	93 kN (21 kips)	3.2 m (10.5 ft)	9.2 m (30.2 ft)	3.56 m (11.6 ft)
Dry Sand D_R = 65%	800 kN (180 kips)	0	117 kN (26 kips)	3.4 m (11.2 ft)	9.3 m (30.5 ft)	
Dry Sand D_R = 65%	1,600 kN (360 kips)	0	104 kN (23 kips)	3.3 m (10.8 ft)	9.3 m (30.5 ft)	
Dry Sand D_R = 65%	800 kN (180 kips)	5 m (16.40 ft)	38 kN (9 kips)	2.9 m (9.5 ft)	8.4 m (27.6 ft)	
Dry Sand D_R = 80%	0	0	182 kN (41 kips)	3.1 m (10.2 ft)	8.2 m (26.9 ft)	3.56 m (11.6 ft)
Dry Sand D_R = 80%	800 kN (180 kips)	0	167 kN (38 kips)	3.1 m (10.2 ft)	8.1 m (26.6 ft)	
Dry Sand D_R = 80%	1,600 kN (360 kips)	0	152 kN (34 kips)	2.9 m (9.5 ft)	8.1 m (26.6 ft)	
Dry Sand D_R = 80%	800 kN (160 kips)	5 m (16.40 ft)	50 kN (11 kips)	2.3 m (7.5 ft)	7.5 m (25.6 ft)	
Fully Saturated Sand D_R = 40%	0	0	72 kN (16 kips)	4.2 m (13.8 ft)	9.3 m (30.5 ft)	
Fully Saturated Sand D_R = 40%	800 kN (180 kips)	0	61 kN (14 kips)	4 m (13.1 ft)	9.1 m (29.9 ft)	
Fully Saturated Sand D_R = 40%	1,600 kN (380 kips)	0	50 kN (11 kips)	3.8 m (12.5 ft)	8.9 m (29.2 ft)	
Fully Saturated Sand D_R = 40%	800 kN (180 kips)	5 m (16.40 ft)	22.5 kN (5 kips)	3.2 m (10.5 ft)	8.7 m (28.5 ft)	
Fully Saturated Sand D_R = 80%	0	0	151 kN (34 kips)	3.3 m (10.8 ft)	8.4 m (27.6 ft)	
Fully Saturated Sand D_R = 80%	800 kN (180 kips)	0	137 kN (31 kips)	3.2 m (10.5 ft)	8.3 m (27.2 ft)	
Fully Saturated Sand D_R = 80%	1,600 kN (360 kips)	0	123 kN (28 kips)	3.1 m (10.2 ft)	8.2 m (26.9 ft)	
Fully Saturated Sand D_R = 80%	800 kN (180 kips)	5 m (16.40 ft)	21.5 kN (5 kips)	2.5 m (8.2 ft)	7.7 m (25.3 ft)	
NC Clay	0	0	42.5 kN (10 kips)	5.6 m (18.4 ft)	10 m (32.8 ft)	7.75 m (25.4 ft)
NC Clay	800 kN (180 kips)	0	34.5 kN (8 kips)	5.4 m (17.6 ft)	9.9 m (32.5 ft)	
NC Clay	1,600 kN (360 kips)	0	25.8 kN (6 kips)	5.2 m (17.1 ft)	9.7 m (31.8 ft)	
NC Clay	800 kN (180 kips)	5 m (16.40 ft)	15 kN (3 kips)	4.8 m (15.6 ft)	9.4 m (30.8 ft)	

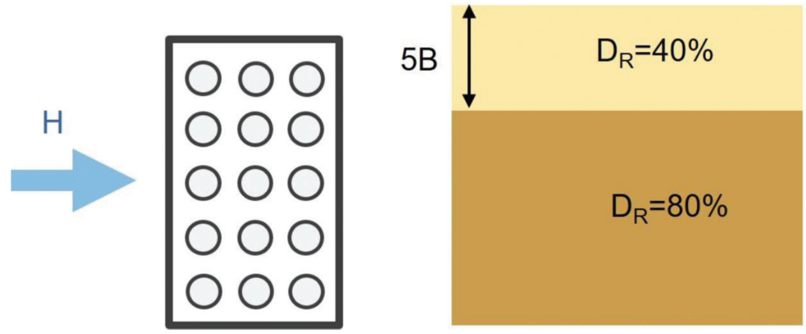

Figure 4.5 Design example: a 3×5 pile group laterally loaded in a two-layer (loose-over-dense) sand. The load is applied in the weak direction of the pile group.

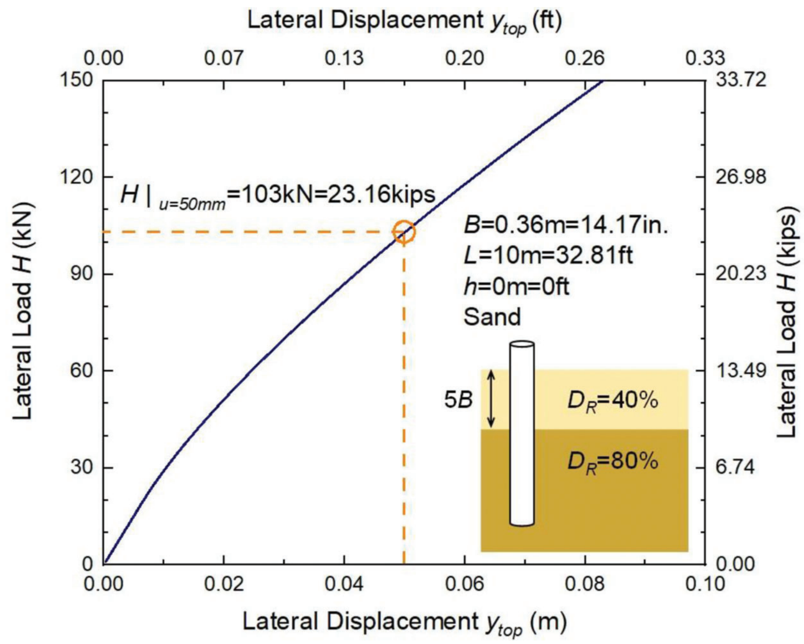

Figure 4.6 Lateral load-deflection response of a single pile with the same geometry as the pile group in the two-layer (loose-over-dense) sand.

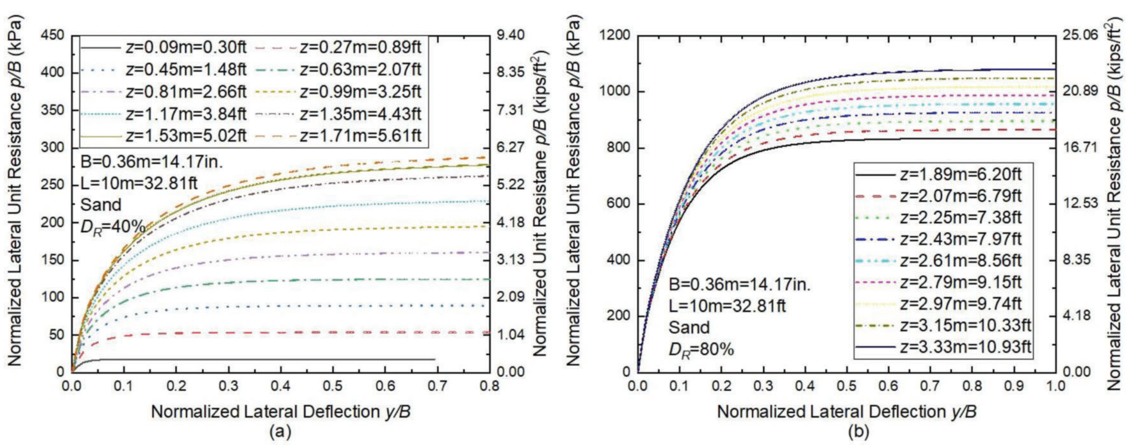

Figure 4.7 The *p-y* curves for 10-m-long (32.81 ft) pile in loose-over-dense sand with $B = 0.36$ m (14.17 inches): (a) *p-y* curves for loose sand layer, and (b) *p-y* curves for dense sand layer.

Step 1. Perform p-y analysis to obtain the lateral load capacity H_{single} for a single pile. Recognizing the pile geometry and soil profile are the same as the previous example (the 3×5 pile group), we obtain the same lateral capacity for the single pile: $H_{\text{single}} = 103$ kN (23 kips).

Step 2. Obtain the pile efficiencies for the individual piles in the pile group. Using Equation 3.1, the pile efficiency η for all the individual piles in the pile group can be calculated. Because of symmetry, only three piles must be considered. The results are summarized in Table 4.10. The pile indexes are shown in Figure 4.11.

Step 3. Calculate the lateral capacity H_{group} for the pile group. The lateral capacity of the individual piles in the pile group can now be calculated. The results are summarized in Table 4.10. The total lateral capacity H_{group} of the pile group is 103 kN (23 kips), which is in great agreement with that (= 107 kN = 24 kips) obtained from the 3D FE analysis, as shown in Table 4.9. In comparison, the lateral capacity of the pile group is estimated to be 130 kN (29 kips) by using the design method prescribed by AASHTO (2020), which is also slightly unconservative for this example. The *p-y* curved used by the AASHTO (2020) method are the API curves used in last example.

4.2.3 1×5 Pile Group in Clay Over Sand

A 1×5 pile group with a center-to-center spacing $s_c = 3B$ in a two-layer soil profile (as shown in Figure 4.12) is loaded laterally in its weak direction. The piles

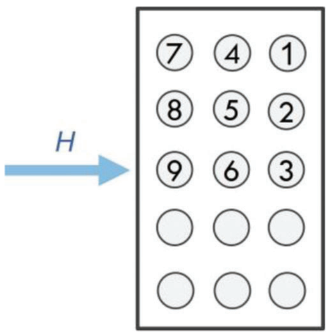

Figure 4.8 Pile numbers for individual piles in 3×5 pile group loaded in the weak direction.

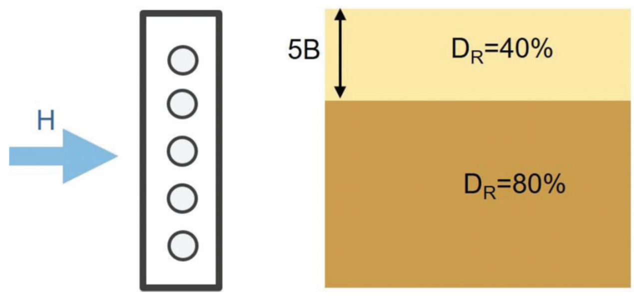

Figure 4.10 Design example: a 1×5 pile group laterally loaded in a two-layer (loose-over-dense) sand. The load is applied in the weak direction of the pile group.

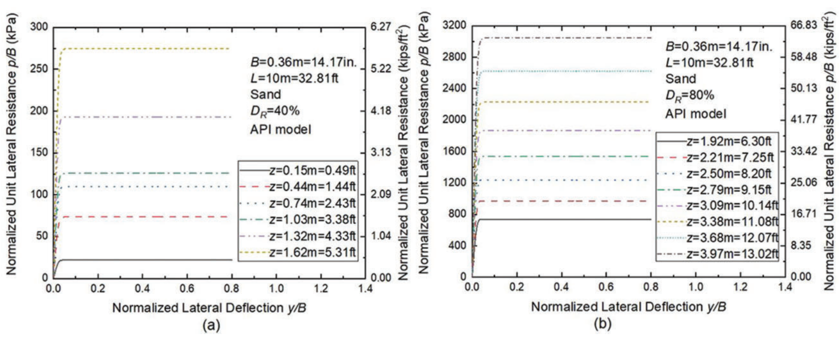

Figure 4.9 API *p-y* curves for 10-m-long (32.81 ft) pile in loose-over-dense sand with $B = 0.36$ m (14.17 inches): (a) *p-y* curves for loose sand layer, and (b) *p-y* curves for dense sand layer.

TABLE 4.8
Calculated lateral capacity of the 3×5 pile group loaded in the weak direction in layered sand

Row #	Pile #	Pile Efficiency	Lateral Capacity of Each Pile	Lateral Capacity of Each Row	Lateral Capacity of Pile Group
1	1	0.72	73.8 kN (16.6 kips)	353.9 kN (79.6 kips)	627.8 kN (141.1 kips)
	2	0.68	70.0 kN (15.7 kips)		
	3	0.64	66.2 kN (14.8 kips)		
2	4	0.36	37.8 kN (8.50 kips)	172.4 kN (38.8 kips)	
	5	0.33	33.7 kN (7.58 kips)		
	6	0.29	29.9 kN (6.72 kips)		
3	7	0.23	23.4 kN (5.26 kips)	101.5 kN (22.8 kips)	
	8	0.19	19.5 kN (4.38 kips)		
	9	0.15	15.7 kN (3.53 kips)		

are 0.36 m (14.17 inches) in diameter and 20 m (65.62 ft) in length. The load is applied at a height of 10 m (32.81 ft) from the ground surface. To estimate the lateral load capacity of the pile group, we follow the three steps specified in Section 4.1.2.2.

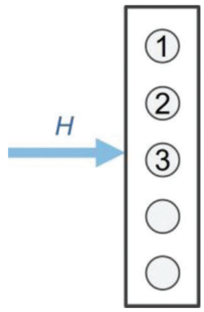

Figure 4.11 Pile numbers for 1×5 pile group loaded in the weak direction.

Step 1. Perform p-y analysis to obtain the lateral load capacity H_{single} of a single pile. Using the *p-y* curves developed in this project, we performed a *p-y* analysis for a single pile with the same dimensions as those of the individual piles in the group using *p-y* analysis software PYGMY (Stewart, 2000). We considered a load eccentricity $h = 0$ in the analysis. Figure 4.13 shows the lateral load-deflection response obtained from the *p-y* analysis. The detailed *p-y* curve data used in the *p-y* analysis are shown in Figure 4.14. In the *p-y* analysis, we discretized soil into 18 layers, each with a thickness equal to approximately 0.36 m (1 ft). The *p-y* curves shown in Figure 4.14 were used to represent the mechanical response of each layer. Below the top 6 m (19.69 ft), the API *p-y* curves were used; however, the lateral deflections were approximately zero there. The lateral capacity of the single pile corresponding to a lateral deflection $y = 50$ mm (2 inches) is obtained from the load-deflection curve: $H_{\text{single}} = 77$ kN (17 kips).

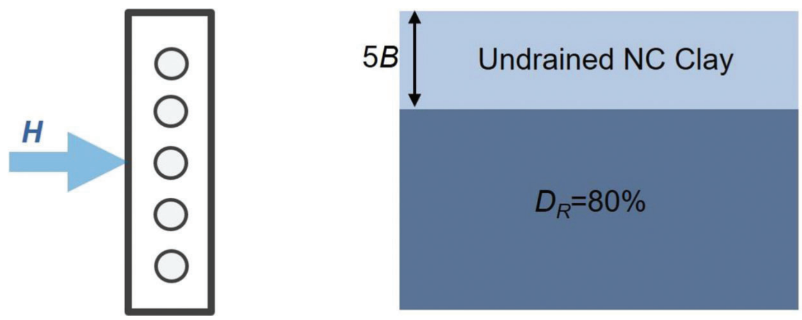

Figure 4.12 Design example: a 1×5 pile group laterally loaded in a two-layer (clay-over-dense sand) soil. The load is applied in the weak direction of the pile group.

TABLE 4.9
Lateral capacities obtained from the 3D FE analyses, the proposed method and the AASHTO (2020) design method for example problems

Case	Soil Profile	3D FEA	Proposed Method	AASHTO (2020)
3×5 pile group (weak direction)	2-layer sand (loose-over-dense sand)	955 kN (215 kips)	628 kN (141 kips)	1,735 kN (390 kips)
1×5 pile group (weak direction)	2-layer sand (loose-over-dense sand)	107 kN (24 kips)	103 kN (23 kips)	130 kN (29 kips)
1×5 pile group (weak direction)	2-layer soil (NC clay over dense sand)	91 kN (20 kips)	77 kN (17 kips)	109 kN (25 kips)
1×5 pile group (weak direction)	Uniform NC clay	50 kN (11 kips)	41 kN (9 kips)	31 kN (7 kips)

TABLE 4.10
Pile efficiencies and pile capacities for individual piles in 1×5 pile group loaded in the weak direction in layered sand

Pile Number	Pile Efficiency	Lateral Capacity of Each Pile	Lateral Capacity of Pile Group
1	0.24	24.44 kN (5.5 kips)	103.14 kN (23 kips)
2	0.20	20.63 kN (4.6 kips)	
3	0.16	16.82 kN (3.8 kips)	

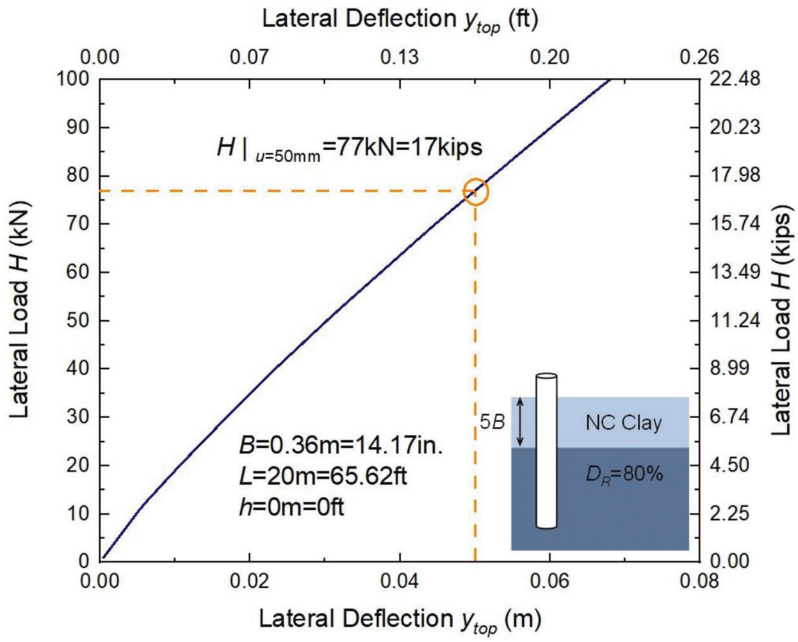

Figure 4.13 Lateral load-deflection response of a single pile with the same geometry as those in the pile group in clay over dense sand.

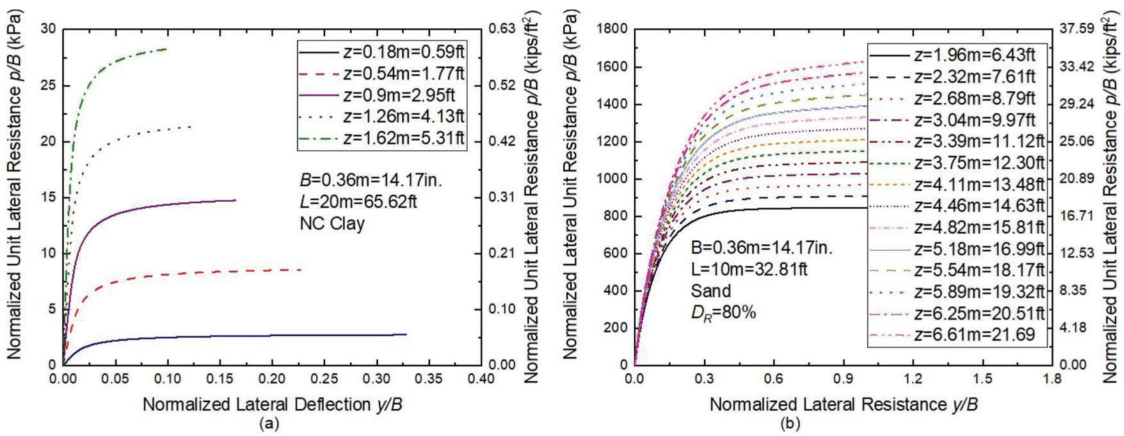

Figure 4.14 The *p-y* curves used in *p-y* analysis for pile groups in clay over dense sand: (a) *p-y* curves for clay layer, and (b) *p-y* curves for sand layer.

TABLE 4.11
Pile efficiencies and pile capacities for individual piles in 1 × 5 pile group loaded in the weak direction in layered soil

Pile Number	Pile Efficiency	Lateral Capacity of Each Pile	Lateral Capacity of Pile Group
1	0.24	18.3 kN (5.5 kips)	77.1 kN
2	0.20	15.4 kN (4.6 kips)	(17.3 kips)
3	0.16	12.6 kN (3.8 kips)	

Step 2. Obtain the pile efficiencies for the individual piles in the pile group. Using Equation 3.1, the pile efficiency η for all the individual piles in the pile group can be calculated. Because of symmetry, only three piles must be considered. The results are summarized in Table 4.11. The pile indexes are shown in Figure 4.11.

Step 3. Calculate the lateral capacity H_{group} for the pile group. The lateral capacity of the individual piles in the pile group can now be calculated. The results are summarized in Table 4.11.

The total lateral capacity H_{group} of the pile group is 77 kN (17 kips), which in slightly smaller than that (= 103 kN = 23 kips) obtained from the 3D FE analysis, as shown in Table 4.9. In comparison, the lateral capacity of the pile group is estimated to be 109 kN (25 kips) by using the design method prescribed by

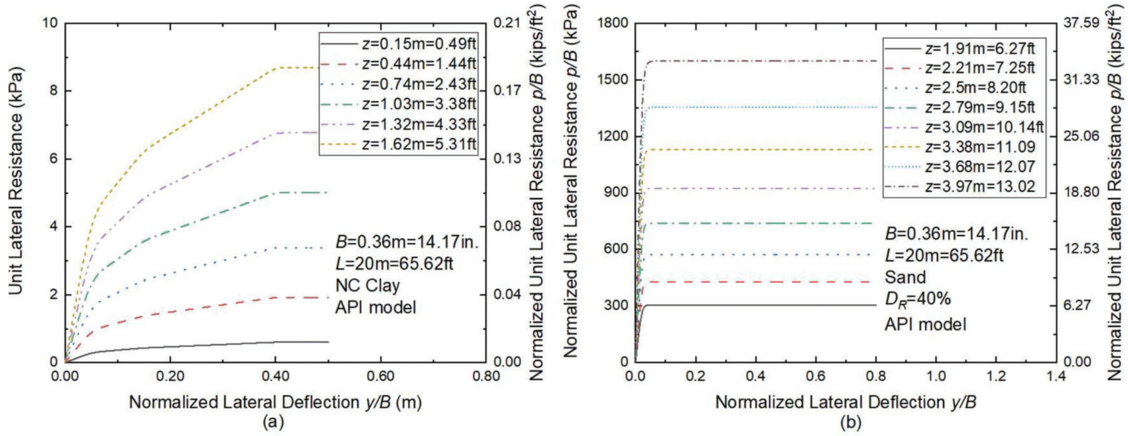

Figure 4.15 API *p-y* curves for 20-m-long (65.62 ft) pile in NC clay over dense sand with $B = 0.36$ m (14.17 inches): (a) *p-y* curves for clay layer, and (b) *p-y* curves for sand layer.

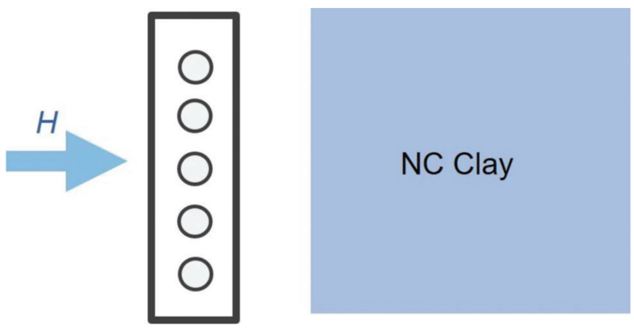

Figure 4.16 Design example: a 1×5 pile group laterally loaded in uniform NC clay. The load is applied in the weak direction of the pile group.

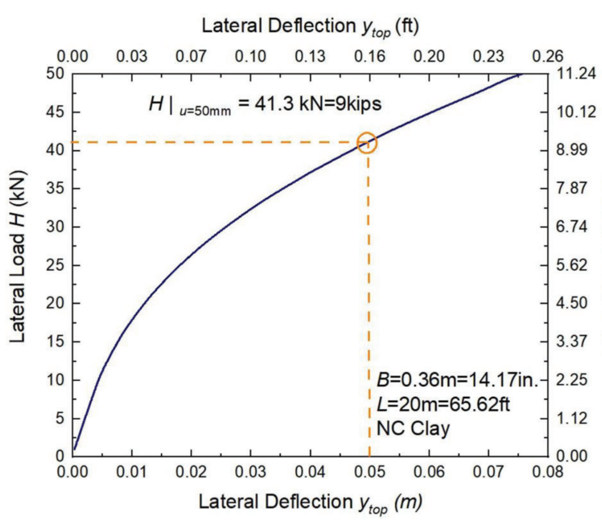

Figure 4.17 Lateral load-deflection response of a single pile with the same geometry as the pile group in NC clay.

AASHTO (2020), which is also slightly unconservative for this example. The *p-y* curved used by the AASHTO (2020) method are the API curves shown in Figure 4.15.

4.2.4 1×5 Pile Group in Normally Consolidated (NC) Clay

A 1×5 pile group with a center-to-center spacing $s_c = 3B$ in normally consolidated clay (shown in Figure 4.16), is loaded laterally in its weak direction. The piles are 0.36 m (14.17 inches) in diameter and 20 m (65.62 ft) in length. The load is applied at a height of 10 m (32.81 ft) measured from the ground surface. We repeat the three steps specified in Section 4.1.2.2.

Step 1. Perform p-y analysis to obtain the lateral load capacity H_{single} of a single pile. Using the *p-y* curves developed in this project, we performed a *p-y* analysis for a single pile with the same dimensions as those of the individual piles in the group using *p-y* analysis software PYGMY (Stewart, 2000). We considered a load eccentricity $h = 0$ in the analysis. Figure 4.17 shows the lateral load-deflection response obtained from the *p-y* analysis. The detailed *p-y* curve data used in the *p-y* analysis are shown in Figure 4.18. In the *p-y* analysis, we discretized soil into 18 layers, each with a thickness equal to approximately 0.36 m (1 ft). The *p-y* curves shown in Figure 4.18 were used to represent the mechanical response of each layer. Below the top 6 m (19.69 ft), the API *p-y* curves were used; however, the lateral deflections were approximately zero there. The lateral capacity of the single pile corresponding to a lateral deflection $y = 50$ mm (2 inches) is obtained from the load-deflection curve: $H_{\mathrm{single}} = 41.3$ kN (9 kips).

Step 2. Obtain the pile efficiencies for the individual piles in the pile group. Using Equation 3.1, the pile efficiency η for all the individual piles in the pile group can be calculated. Because of symmetry, only three piles must be considered. The results are summarized in Table 4.12. The pile indexes are shown in Figure 4.11.

Step 3. Calculate the lateral capacity H_{group} for the pile group. The lateral capacity of the individual piles in the pile group can now be calculated. The results are summarized in Table 4.12. The total lateral capacity H_{group} of the pile group is 41 kN (9 kips), which is

TABLE 4.12
Pile efficiencies and pile capacities for individual piles in 1 × 5 pile group loaded in the weak direction in NC clay

Pile Number	Pile Efficiency	Lateral Capacity of Each Pile	Lateral Capacity of Pile Group
1	0.24	9.79 kN (2.2 kips)	41.36 kN
2	0.20	8.27 kN (1.9 kips)	(9.30 kips)
3	0.16	6.74 kN (1.5 kips)	

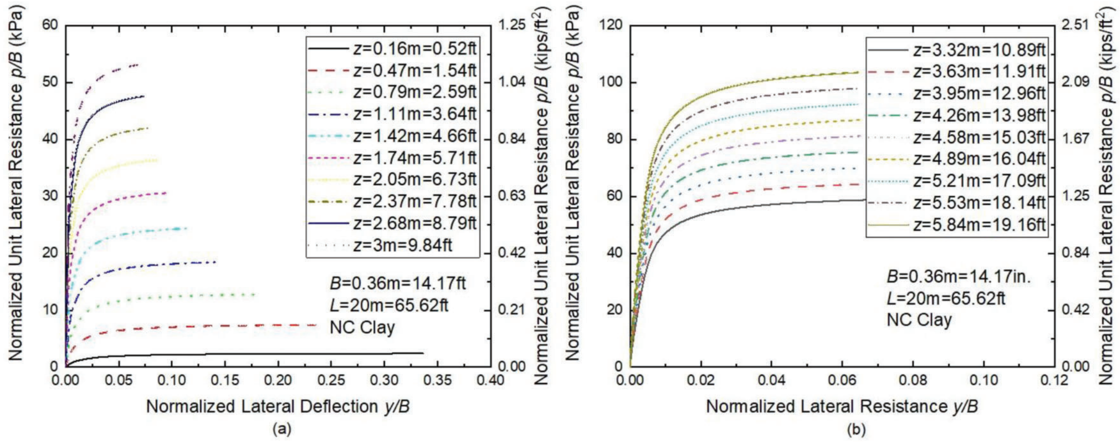

Figure 4.18 The *p-y* curves used in *p-y* analysis for pile group in NC clay: (a) *p-y* curves at shallower depth, and (b) *p-y* curves at deeper depth.

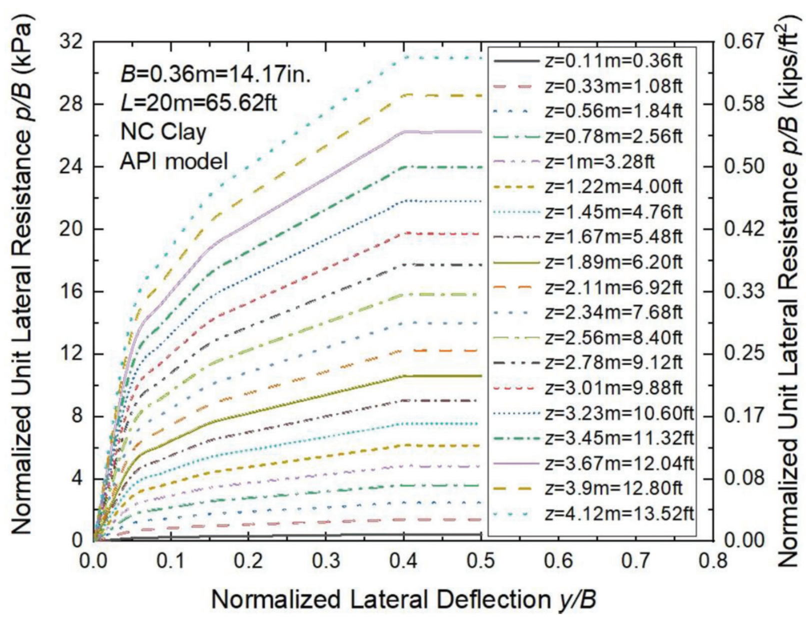

Figure 4.19 API *p-y* curves of 20-m-long (65.62 ft) pile in NC clay with $B = 0.36$ m (14.17 inches).

slightly smaller than that (= 50 kN = 11 kips) obtained from the 3D FE analysis, as shown in Table 4.9. In comparison, the lateral capacity of the pile group is estimated to be 31 kN (7 kips) by using the design method prescribed by AASHTO (2020), which is slightly unconservative for this example. The *p-y* curved used by the AASHTO (2020) method are the API curves shown in Figure 4.19.

5. CONCLUSION

In this report, we explored the response of both single piles and pile groups to lateral loads. We found that pile geometry, soil profile, and load eccentricity have significant impact on the load deflection curve of the pile.

For a single pile, the greater the bending stiffness of the pile is and the smaller the load eccentricity is, the greater the pile lateral capacity is. However, the impact of load eccentricity on *p-y* curves is negligible, so we can use the same *p-y* curves for all values of load eccentricities. We proposed new equations for the *p-y* curves for normally consolidated clay (Equation 2.5) and sand (Equation 2.1), which are extracted directly from the results of finite elements analysis done for the present research. Variables like relative density, effective vertical stress and pile diameter are included in the equation.

We also explored the lateral response of a pile group. The individual piles in the pile group will act differently from a single pile in the same soil profile. We used pile efficiencies to relate the pile capacities of piles in a group to the capacity of an individual pile in the same soil profile. The *p-y* curves for group piles are also different. We used *p*-multipliers to relate the *p-y* curves for a pile at a given location in the pile group to the corresponding *p-y* curves for the single pile. We proposed equations for the pile efficiency (Equation 3.1) and a new set of pile *p*-multipliers and two corresponding design methods.

We found that, contrary to a common design assumption, the moment added on the top of a pile group will not be fully absorbed by axial loads. Part of it will be transferred to individual piles in the pile group. These "residual" moments acting at the heads of individual piles in the pile group significantly weaken the piles. If these moments are ignored, as is often done, the resulting estimated capacity could be greater, perhaps substantially greater, than an estimate that takes the moments into account. Because of this, knowledge of moment distribution between piles is necessary if the design method using *p*-multipliers is used. Since we usually do not know the moment distribution in the pile group, we found that the traditional method using *p*-multipliers to capture group effects must be used with caution, if at all, for large load eccentricities. Because of this, the method proposed here, using the concept of pile efficiency to capture the group effect on individual pile capacity, can be advantageous to use.

Finally, single-row pile groups can be quite vulnerable when loaded in their weak direction in weak soil profiles. We performed several simulations, with results summarized in Section 4.1.1, to explore when soil profiles would be weak in connection with this problem. We suggested that single-row pile group should be avoided when the representative SPT number blow count over a depth of five times the pile diameter depth measured from the pile top is less than 7.

REFERENCES

AASHTO. (2020). *AASHTO LRFD bridge design specifications* (9th ed.). American Association of State Highway and Transportation Officials.

Amar Bouzid, D. (2018). Numerical investigation of large-diameter monopiles in sands: Critical review and evaluation of both API and newly proposed p-y curves. *International Journal of Geomechanics*, *18*(11), 04018141. https://ascelibrary.org/doi/abs/10.1061/%28ASCE%29GM.1943-5622.0001204

Anderson, J. B., Townsend, F. C., & Grajales, B. (2003). Case history evaluation of laterally loaded piles. *Journal of Geotechnical and Geoenvironmental Engineering*, *129*(3), 187–196. https://doi.org/10.1061/(ASCE)1090-0241(2003)129:3(187)

API. (2000, December). *Recommended practice for planning, designing, and constructing fixed offshore platforms–working stress design* (Report RP 2A-WSD, 20th edition). American Petroleum Institute.

Bhattacharya, S., Carrington, T. R. & Aldridge, T. K. (2005). Buckling considerations in pile design. In *Frontiers in Offshore Geotechnics* (pp. 815–821).

Brown, D. A., Morrison, C., & Reese, L. C. (1988, November). Lateral load behavior of pile group in sand. *Journal of Geotechnical Engineering*, *114*(11), 1261–1276.

Burd, H. J., Taborda, D. M. G., Zdravkovicć, L., Abadie, C. N., Byrne, B. W., Houlsby, G. T., Gavin, K. G., Igoe, D. J. P., Jardine, R. J., Martin, C. M., McAdam, R. A., Pedro, A. M. G., & Potts, D. M. (2020, November). PISA design model for monopiles for offshore wind turbines: application to a marine sand. *Géotechnique*, *70*(11), 1048–1066. https://doi.org/10.1680/jgeot.18.P.277

Byrne, B. W., Houlsby, G. T., Burd, H. J., Gavin, K. G., Igoe, D. J. P., Jardine, R. J., Martin, C. M., McAdam, R. A., Potts, D. M., Taborda, D. M., & Zdravković, L. (2020). PISA design model for monopiles for offshore wind turbines: application to a stiff glacial clay till. *Géotechnique*, *70*(11), 1030–1047. https://doi.org/10.1680/jgeot.18.P.255

Carrington, Tim & Bhattacharya, & Subhamoy & Aldridge, Tinika. (2005). Buckling considerations in pile design. https://doi.org/10.1201/NOE0415390637.ch93

Chakraborty, T., Salgado, R., & Loukidis, D. (2013). A two-surface plasticity model for clay. *Computers and Geotechnics*, *49*, 170–190.

Choi, Y. S., Basu, D., Salgado, R., & Prezzi, M. (2014, April). Response of laterally loaded rectangular and circular piles in soils with properties varying with depth. *Journal of Geotechnical and Geoenvironmental Engineering*, *140*(4). https://doi.org/10.1061/(ASCE)GT.1943-5606.0001067

Choobbasti, A. J., & Zahmatkesh, A. (2016, October). Computation of degradation factors of p-y curves in liquefiable soils for analysis of piles using three-dimensional finite-element model. *Soil Dynamics and Earthquake Engineering*, *89*, 61–74. https://www.sciencedirect.com/science/article/pii/S026772611630094X?casa_token=Iirq9mulBj8AAAAA:7F70XKWZjaiEt3xNadWvUO7w5yWppEftovSq41kqtSJm67n-SaPXnX0g2R99r3iOH34JN0GTtA

Davisson, M. T., & Robinson, K. E. (1965). *Bending and buckling of partially embedded piles* [Conference session]. Soil Mechanics and Foundation Engineering Conference, Canada. https://trid.trb.org/view/122242

Dyson, G. J., & Randolph, M. F. (2001, April). Monotonic lateral loading of piles in calcareous sand. *Journal of Geotechnical and Geoenvironmental Engineering*, *127*(4), 346–352. https://doi.org/10.1061/(ASCE)1090-0241(2001)127:4(346)

Han, F., Ganju, E., Salgado, R., & Prezzi, M. (2019). Comparison of the load response of closed-ended and open-ended pipe piles driven in gravelly sand. *Acta Geotechnica*, *14*(6), 1785–1803. https://doi.org/10.1007/s11440-019-00863-1

Han, F., Prezzi, M., & Salgado, R. (2017, November). Energy-based solutions for nondisplacement piles subjected to lateral loads. *International Journal of Geomechanics*, *17*(11). https://doi.org/10.1061/(ASCE)GM.1943-5622.0001012

Han, F., Salgado, R., & Prezzi, M. (2015, October). Nonlinear analyses of laterally loaded piles: A semi-analytical approach. *Computers and Geotechnics*, *70*, 116–129.

Hannigan, P. J., Goble, G. G., Likins, G. E., & Rausche, F. (2006, April). *Design and construction of driven pile foundations: Reference manual – Volume II* (Publication No. FHWA-NHI-05-043). U.S. Department of Transportation Federal Highway Administration.

Haouari, H., & Bouafia, A. (2020). A centrifuge modelling and finite element analysis of laterally loaded single piles in sand with focus on P–Y Curves. *Periodica Polytechnica Civil Engineering*, *64*(4), 1064–1074. https://doi.org/10.3311/PPci.14472

Hu, Q., Han, F., Prezzi, M., Salgado, R., & Zhao, M. (2021). Lateral load response of large-diameter monopiles in sand. *Géotechnique*, *72*(12). https://doi.org/10.1680/jgeot.20.00002

Loukidis, D., & Salgado, R. (2009). Modeling sand response using two-surface plasticity. *Computers and Geotechnics*, *36*, 1–2, 166–186. http://www.sciencedirect.com/science/article/pii/S0266352X08000293

Matlock, H. (1970). Correlation for design of laterally loaded piles in soft clay (Paper No. OTC-1204-MS). *Offshore Technology Conference*. OnePetro. https://doi.org/10.4043/1204-MS

McVay, M., Zhang, L., Molnit, T., & Lai, P. (1998, October). Centrifuge testing of large laterally loaded pile groups in sands. *Journal of Geotechnical and Geoenvironmental Engineering*, *124*(10), 1016–1026. https://doi.org/10.1061/(ASCE)1090-0241(1998)124:10(1016)

Peck, R. B., Hanson, W. E., & Thornburn, T. H. (1974). *Foundation engineering* (2nd ed.). John Willy & Sons.

Prakash, S., & Sharma, H. D. (1991). *Pile foundations in engineering practice*. John Wiley & Sons.

Reese, L. C., Cox, W. R., & Koop, F. D. (1974, May 5–7). Analysis of laterally loaded piles in sand (Paper No. OTC-2080-MS). *Offshore Technology Conference.* OnePetro. https://doi.org/10.4043/2080-MS

Reese, L. C., Cox, W. R., & Koop, F. D. (1975, May 4–7). Field testing and analysis of laterally loaded piles om stiff clay (Paper No. OTC-2312-MS). *Offshore Technology Conference*. OnePetro. https://doi.org/10.4043/2312-MS

Rollins, K. M., Lane, J. D., & Gerber, T. M. (2005). Measured and computed lateral response of a pile group in sand. *Journal of Geotechnical and Geoenvironmental Engineering*, *131*(1), 103–114. https://doi.org/10.1061/(ASCE)1090-0241(2005)131:1(103)

Salgado, R. (2022). *The engineering of foundations, slopes and retaining structures*. CRC Press.

Salgado, R., Woo, S. I., & Kim, D. (2011). *Development of load and resistance factor design for ultimate and serviceability limit states of transportation structure foundations* (Joint Transportation Research Program Publication No. FHWA/IN/JTRP-2011/03). West Lafayette, IN: Purdue University. https://doi.org/10.5703/1288284314618

SIMULIA. (2021). *Abaqus/CAE* [Computer software]. Dassault Systèmes.

Stewart, D. P. (2000). *Program PYGMY version 2.31, p-y analysis of laterally loaded piles under general loading- user manual*. The University of Western Australia, Perth, WA.

Su, D., & Yan, W. M. (2019). Relationship between p-multiplier and force ratio at pile head considering non-linear soil–pile interaction. *Géotechnique*, *69*(11), 1019–1025. https://doi.org/10.1680/jgeot.17.P.069

Suryasentana, S. K., & Lehane, B. M. (2014, March). Numerical derivation of CPT-based p–y curves for piles in sand. *Géotechnique*, *64*(3), 186–194. https://doi.org/10.1680/geot.13.P.026

Welch, R. C. (1972). *Lateral load behavior of drilled shafts* [Doctoral dissertation, The University of Texas at Austin]. https://search.proquest.com/openview/8c296e3fa660945e931ca3ed9dc0e5dd/1?pq-origsite=gscholar&cbl=18750&diss=y&casa_token=ndImawszdPYAAAAA:b2cdh01TXtTmk0kB8CF5xyJ43Z2EnEBQm0A8SLGFR5SxkoRrIk1tZhkg5byS9sapB1E26aSB23Y

Zhou, Y., & Tokimatsu, K. (2018, August). Numerical evaluation of pile group effect of a composite group. *Soils and Foundations*, *58*(4), 1059–1067. https://www.sciencedirect.com/science/article/pii/S0038080618300799

APPENDICES

Appendix A. Implementation

APPENDIX A. IMPLEMENTATION

A.1 Single-Row Pile Group in Weak Soil Profiles

Single-row pile groups loaded laterally in weak soil profiles—those with a top layer thickness greater than 5 times the pile diameter and a representative SPT blow count less than 7—should be avoided if loaded in the weak direction.

A.2 *P-y* Relationships for Sand

Based on the results of the FEA performed for laterally loaded single piles, new *p-y* curves are proposed for use for single piles in sand. The relationship between the unit soil resistance p (with units of force per length) and the pile deflection y (with units of length) is given by

$$p = p_u \tanh\left[\left(b\frac{y}{L_R}\right)^c\right] \qquad \text{(Eq. A.1)}$$

where the limit unit soil resistance p_u (with units of force per length) is given by

$$p_u = \left(\frac{D_R}{100\%}\right)^{1.4} \min\left(46.6, 13.8 + 7.00\left(\frac{p_A}{\sigma'_{v0}}\right)\right)\sigma'_{v0}B \qquad \text{(Eq. A.2)}$$

with

$$b = \frac{32.2}{\left(\frac{p_u}{p_A B}\right)^{0.860}}\exp\left[4.10\left(\frac{D_R}{100\%}\right)^5\right] \qquad \text{(Eq. A.3)}$$

$$c = \exp\left[11.6\left(\frac{D_R}{100\%}\right) - 11.0\right] + 0.598 \qquad \text{(Eq. A.4)}$$

and D_R = relative density of the sand in % ($0\ \% \le D_R \le 100\%$), σ'_{v0} = initial vertical effective stress, B = pile diameter, p_A (= 100 kPa ≈ 1 tsf) = reference stress, and L_R (= 1 m ≈ 3.281 ft or equivalent in other units) = reference length.

A.3 *p-y* Relationships for Clay

Based on the results of the FE analyses performed for laterally loaded single piles, new *p-y* curves are proposed for use for single piles in NC clay. The relationship between the unit soil resistance p (with units of force per length) and the pile deflection y (with units of length) is given by

$$p = p_u \left[\frac{\dfrac{y}{y_c}}{a\left(\dfrac{y}{y_c}\right) + 1 - a} \right] \quad \text{when } y < y_c \qquad \text{(Eq. A.5)}$$

$$p = p_u \qquad \text{when } y \geq y_c$$

where the limit unit soil resistance p_u (with units of force per length) is given by

$$p_u = \min\left[64.0\left(\frac{s_u}{p_A}\right) + \left(1.75\frac{L_R}{B} + 5.05\right), 11.67\right] s_u B \qquad \text{(Eq. A.6)}$$

with

$$y_c = \left(-0.0196\left(\frac{B}{L_R}\right)^{-1} + 0.0775\right) L_R + \left(-0.0192\left(\frac{B}{L_R}\right)^{-2.5} + 0.368\right) \exp\left[\left(-23.0\frac{B}{L_R} - 80.0\right)\frac{s_u}{p_A}\right] L_R \qquad \text{(Eq. A.7)}$$

$$a = 0.96 \qquad \text{(Eq. A.8)}$$

and s_u = undrained shear strength of the clay, B = pile diameter, p_A (= 100 kPa ≈ 1 tsf) = reference stress, and L_R (= 1 m ≈ 3.281 ft or equivalent in other units) = the reference length.

A.4 Method 1: *P-y* Analysis Using *P*-Multipliers

Traditionally, engineers have used *p*-multipliers to capture the group effect when designing piles for lateral loads. The flow chart of method 1 is shown in Figure 4.1.We advise caution in using this method, because it relies on the assumption that all the external moment acting on the pile group will be absorbed by increments of axial force in the piles, thus having no impact on the lateral response of the piles in the pile group. However, we found that this is not the case. Finite element analysis results show that some fraction of the external moment is transferred to the individual piles in the pile group *as moments*. Details about this finding are provided in Chapter 3.3.1. Ignoring the moments transferred to the individual piles in the group as moments will lead to severe over-estimation of pile group capacity, as shown in the design example provided in Chapter 4.2.1. As a result, *p-y* analysis of pile groups requires knowledge of moment distribution among individual piles in the pile group.

AASHTO (2020) provides a table of *p*-multipliers. However, only six values of *p*-multiplier are provided, with the *p*-multipliers being independent of the position of the piles in the row, load eccentricity and soil properties. We provide a more complete table of *p*-multipliers, which should bring more accuracy to this design method. The proposed *p*-multipliers are shown in Table 3.14.

We have also shown how to use this method in the four design examples that we propose in Chapter 4.

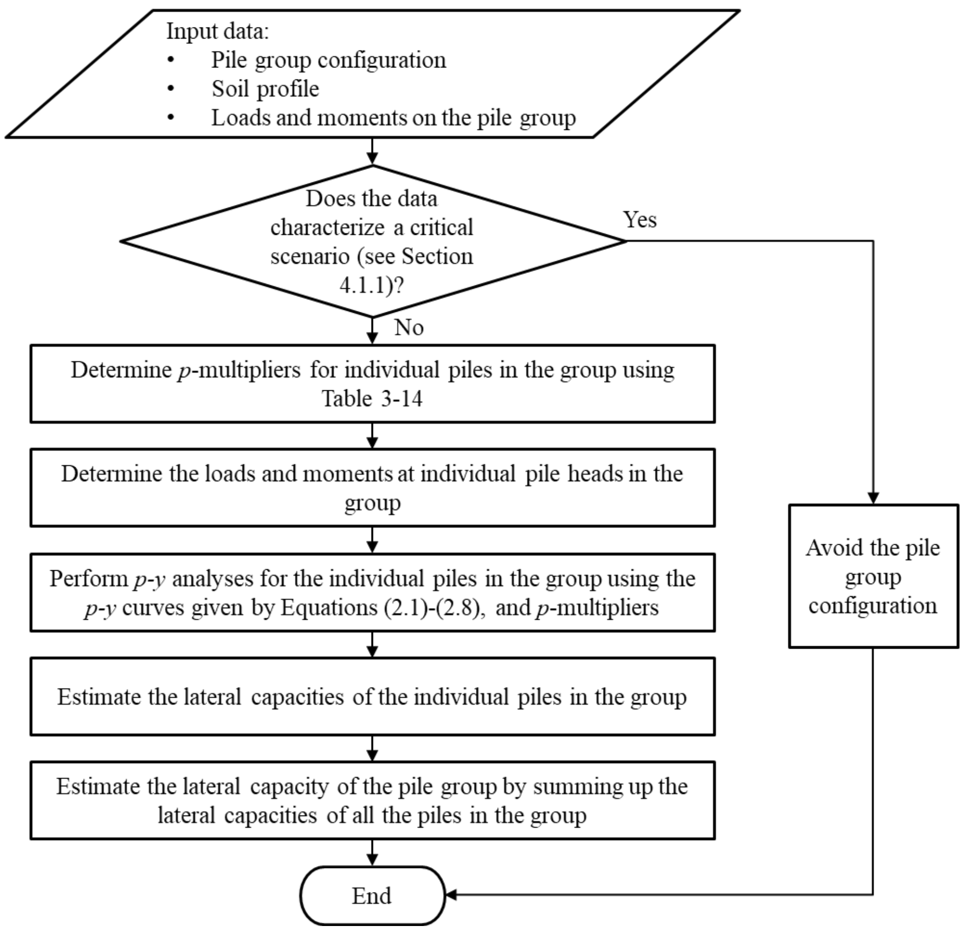

Figure A.1 Flow chart for p-multiplier method.

Table A.1 Proposed *p*-multipliers

Relative Density D_R of Sand	Load Eccentricity *h*	Pile Cap Type	Position	Row 1	Row 2	Row 3
40%	6 m (19.69 ft)	Free-Standing	Edge	0.76	0.33	0.22
			Middle	0.56	0.22	0.16
	10 m (32.81 ft)	Soil-Supported	Edge	0.95	0.25	0.2
			Middle	0.95	0.14	0.14
80%	1 m (3.28 ft)	Free-Standing	Edge	0.62	0.39	0.33
			Middle	0.56	0.32	0.29
	10 m (32.81 ft)	Soil-Supported	Edge	0.86	0.17	0.14
			Middle	0.86	0.1	0.1

A.5 Method 2: *p-y* Analysis Using Pile Efficiencies

The knowledge of moment distribution among piles is usually not available. Thus, we proposed a new method using the concept of pile efficiency to avoid this shortcoming. The flow chart of method 2 is shown in Figure 4.2.

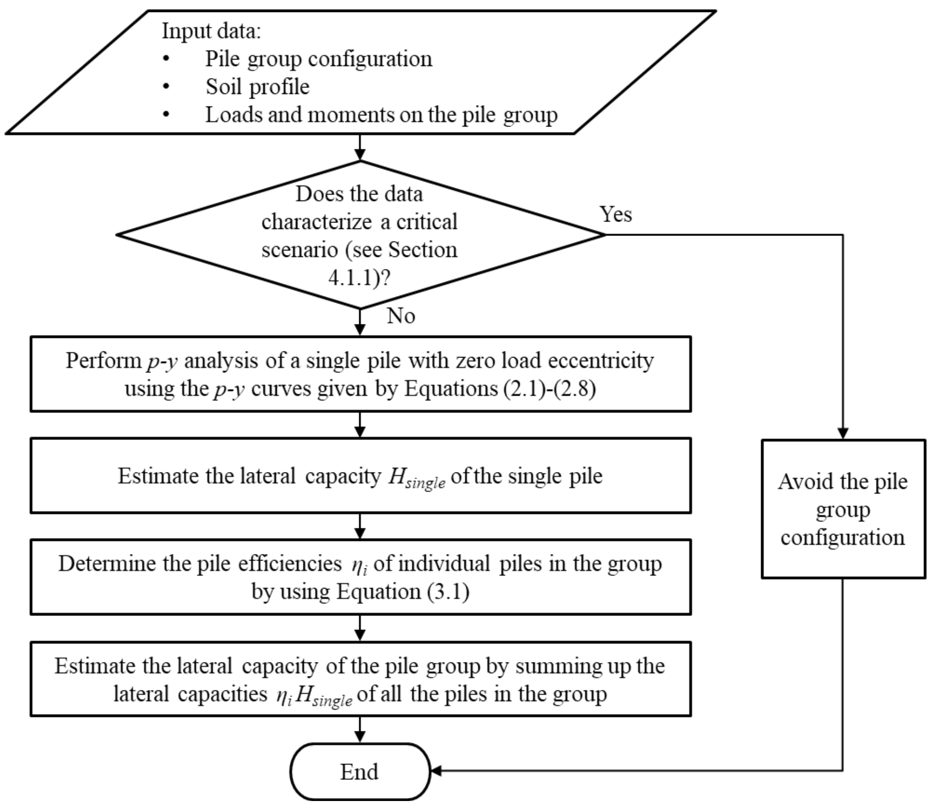

Figure A.2 Flowchart for pile efficiency method.

In this method, we use pile efficiencies to capture group effect. The pile efficiency is defined as the ratio of the lateral capacity of an individual pile in the pile group to the lateral capacity of a single pile in the same soil profile loaded with no load eccentricity. The pile efficiency is a function of load eccentricity, position of the pile in the pile group, as well as the spacing between piles in the pile group. Equation 3.1 can be used to calculate pile efficiency.

$$\eta = -0.020h\left(\frac{x}{B^*}\right)^2 + 0.00053h^2L^{*2} + 0.0062hB^* + 0.63\left(\frac{x}{B^*}\right)^2 - 0.92\frac{x}{B^*} - 0.074\frac{y}{L^*} + 0.16B^* - 0.067h + 0.66 \qquad \text{(Eq. 3.1)}$$

where L_R is the reference length, which is either 1 m for SI units or 3.281 ft for U.S. Customary units. The other factors that are included are explained in Table 3.19, reproduced below. More simulations should be performed in future research in order to increase the range of applicability and reliability of Equation 3.1.

Table A.2 Factors considered in the pile efficiency equation

Factors	Units	Meaning
h	Length	Load eccentricity
x	Length	Distance from the pile center to the center of the nearest pile on the leading edge of the group, as shown in Figure 3.9
y	Length	Distance of the pile center to the center of the nearest pile on an edge of the pile group that is parallel to the load direction, as shown in Figure 3.9
B^*	Length	Distance between the midline of the leading row and the midline of the very last trailing row, as shown in Figure 3.9
L^*	Length	Distance from an edge of the pile group parallel to the load direction to the line passing through the center of all rows, as shown in Figure 3.9

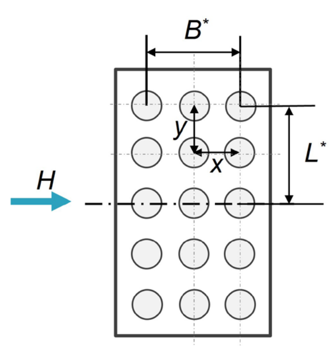

Figure A.3 Factors considered in the pile efficiency equations.

We have also illustrated the use of this method in the four design examples in Chapter 4.

A.6 Lateral Stability Evaluation

There are two different definitions of depth to fixity. One is the difference in length between the free length of the pile above ground and the length of a fixed-ended beam required to have the same deflection at its top as that at the top of the pile. Another one is the depth to the final zero-deflection point. To prevent confusion, it is desirable that design flow processes at INDOT clarify which of the two definitions to use when the critical buckling loads of the laterally loaded piles are estimated. The current design guidance given by AASHTO (2020) is to use depth to fixity equations for sand and clay that depend on the soil stiffness but contain only limited information about how to estimate soil stiffness. The equations suggested by AASHTO (2020) for piles in sand and clay were derived by assuming linear *p-y* relationships. Depending on the estimated soil stiffness and the *p-y* relationship extracted from simulation result, the calculated depth to fixity, and the critical buckling load can vary significantly. However, this report shows that the buckling loads calculated following either AASHTO (2020) or the procedure proposed in this report are much greater than the axial service loads on the piles. This means that buckling is unlikely to be a critical limit state in most cases.

About the Joint Transportation Research Program (JTRP)

On March 11, 1937, the Indiana Legislature passed an act which authorized the Indiana State Highway Commission to cooperate with and assist Purdue University in developing the best methods of improving and maintaining the highways of the state and the respective counties thereof. That collaborative effort was called the Joint Highway Research Project (JHRP). In 1997 the collaborative venture was renamed as the Joint Transportation Research Program (JTRP) to reflect the state and national efforts to integrate the management and operation of various transportation modes.

The first studies of JHRP were concerned with Test Road No. 1—evaluation of the weathering characteristics of stabilized materials. After World War II, the JHRP program grew substantially and was regularly producing technical reports. Over 1,600 technical reports are now available, published as part of the JHRP and subsequently JTRP collaborative venture between Purdue University and what is now the Indiana Department of Transportation.

Free online access to all reports is provided through a unique collaboration between JTRP and Purdue Libraries. These are available at http://docs.lib.purdue.edu/jtrp.

Further information about JTRP and its current research program is available at http://www.purdue.edu/jtrp.

About This Report

An open access version of this publication is available online. See the URL in the citation below.

Wang, Y., Lim, J., Salgado, R., Prezzi, M., & Hunter, J. (2022). *Pile stability analysis in soft or loose soils: Guidance on foundation design assumptions with respect to loose or soft soil effects on pile lateral capacity and stability* (Joint Transportation Research Program Publication No. FHWA/IN/JTRP-2022/24). West Lafayette, IN: Purdue University. https://doi.org/10.5703/1288284317387